DBI Diploma Thesis isys

Integration and analysis of AngII induced neuronal plasticity by means of multi-scale modeling

cand. kyb Dirk Fey,
University of Stuttgart

Supervisors: Rajanikanth Vadigepalli, PhD (DBI)
Research Assistant Professor

Dr.-Ing. Thomas Sauter (ISYS)

Thomas Jefferson University
Daniel Baugh Institute for functional genomics and computational biology (DBI)
Prof. Dr. James Schwaber, Director

University of Stuttgart
Institute for System Dynamics (ISYS)
Prof. Dr.-Ing. Oliver Sawodny

October 2006

Abstract

The fundamental process underlying all brain function is the ability of the neurons to adapt to external inputs in the context of the neuronal state. The adaptive processes span multiple spatial and temporal scales ranging from millisecond dynamics of the ion channels, seconds to minutes time-scale of the signaling pathways, and tens of minutes to hours time-scale of the gene regulation and its feedback onto the signaling pathways and electrophysiology. Mathematical modeling and analysis provides appropriate tools to decipher how the signals are integrated in this complex multi-scale system [Sauter and Bullinger 2004; Kitano 2002]. The present study focuses on integrating two levels of the neuronal adaptation: signaling dynamics elicited by neuropeptide receptors and the consequences on electrophysiology. The particular system considered is the angiotensin II receptor signaling and electrical activity in the cardiorespiratory neurons in the Nucleus Tractus Solitarius (NTS) in the brainstem. The octapeptide Angiotensin II (AngII) is a multifunctional hormone and is involved in stimulation of water and sodium uptake, vasopressin secretion, increased blood pressure and modulation of baroreflexes. Most of the effects are mediated by the activation of the Angiotensin Type 1 Receptor (AT1R) in the NTS neurons. Stimulation of the NTS neurons by AngII has been shown to result in a transient increase in the electrical activity leading to neuronal adaptation. Pharmacological studies have implicated the signaling kinases, PKC and CaMKII, in modulation of the different ion channels [Sumners et al. 2002].

To understand the dynamics of the AT1R mediated neuromodulation and the relative contribution of different kinases, we have developed an integrated

model of AngII induced neuronal firing behavior. This multi-scale model integrates a Hodgkin-Huxley like model of the electrophysiology describing the millisecond dynamics of the ion channels and a detailed kinetic reaction model of the AT1R mediated intracellular signaling pathway. The membrane electrical model includes descriptions of different ion channels in the NTS neurons: sodium, delayed rectifier potassium, calcium activated potassium, high threshold L-type calcium, and leak channel [Rogers et al. 2000; Rybak et al. 1997]. The signaling model was adapted from Mishra and Bhalla [2002] by adding kinetic descriptions of receptor desensitization and the sodium-calcium exchanger. The modified model includes the dynamics of PLC, PKC, CaMKII, DAG, IP3 and intracellular calcium.

The key aspect of integrating the signaling and electrical models is the change in the conductance of different ion channels upon phosphorylation by the kinases PKC and CamKII. The exact kinetics of this phosphorylation are unclear and hence different formulations of kinetic behavior were explored in the simulations. Analysis of the model dynamics revealed distinct regulatory properties corresponding to different ion channels and a novel role for the delayed rectifier potassium channel as a dual regulator. In addition, the simulations indicate that the non-voltage-activated transport dynamics lead to transient inhibition in response to AT1R stimulation. However, phosphorylation of the delayed rectifier potassium channel by PKC counteracts this transient inhibition to result in a net increase in the electrical activity, in concordance with the electrophysiological experimental observations.

The current model forms the basis for developing a multi-scale neuronal adaptation model that integrates electrophysiology, signaling and gene regulation.

Contents

List of Figures

Acknowledgements

My tanks are to my all the people that made this thesis possible:

Rajanikanth Vadigepalli for his great and uncomplicated supervision and his help especially with the modeling part.

Thomas Sauter, without whom this thesis would not have been possible, for his support in all matters.

James Schwaber for inviting me to the DBI, the fruitful discussions (not only) about 'the big picture' and his support and kindness.

Gregory E. Gonye (DBI) for his valuable contribution and enjoyable introductions into the biology-part.

Dionisios G. Vlachos (University of Delaware) for discussing the multi-scale issues.

Introduction

The aim of this work is to clarify the processes of Angiotensin II mediated neuronal behavior, whereat a systems modeling approach is chosen that integrates a Hodgkin-Huxley like model of the membrane behavior and a kinetic reaction model of the intracellular signal transduction pathway. Therefore it is necessary to combine empirical models[1] of the ion channels, which are mainly based on experimental data dictating the functional relations within the model, and a theoretical model[2] of the intracellular substances and proteins, which is derived from the signaling network structure and a fundamental principle of reaction kinetics, the law of mass action.

Changes in neuronal activity or firing rate are controlled through the

[1]Empirical macroscopic models of voltage dependent ion channels describe the overall behavior of a specific voltage dependent transmembrane ion current for the entire cell. It is based on patch clamp studies in the whole cell configuration, and posses mainly two distinct characteristics that are fitted to experimental data. These are activation and inactivation, describing the steady-state values of the channels opening and closing, as well as time variables of activation and inactivation, describing the transient behavior (the time-frame in which the steady-state values are reached). Each of these characteristics is voltage dependent, and modeled through e-functions giving the best fit.

[2]Theoretical kinetic reaction models are based on a 'natural law', the law of mass action, which is in turn applied to the network structure (signaling pathway). Consequently the resulting mathematical description is derived in a systematical manner, and its parameters are finally tuned to fit selected particular time-courses of which experimental data exists.

activity of ion channels. Consequently alterations in neuronal function involve effects on ionic currents, and their underlying channels. Angiotensin II (AngII) mediated effects on neuronal activity involve activation of the AT1 receptor and its intracellular signalling pathway. This includes activation of G-Protein alpha subunit and subsequent Phospholipase-C-beta, which rises the concentrations of the second messengers Ca^{2+} and DAG. These in turn activate the Protein-Kinase-C alpha (PKC), which reduces the fast activating as well as the delayed rectifier potassium currents (I_{Ka} and I_{Kdr} respectively), and activates (probably through inhibition of a negative effect of G-Protein beta-gamma subunit) the total transmembrane calcium current [Sumners et al. 1996]. A rise in intracellular Ca^{2+} also activates the Calcium-Calmodulin-dependent Kinase II (CaMKII), further reducing I_{Kdr}. The potassium channel subtypes involved in this inhibition are Kv2.2 for I_{Kdr} and Kv1.4 for I_{Ka} respectively [Gelband et al. 1999], and their modulation is most probably the effect of direct phosphorylation through the above mentioned kinases (Kv2.2 possesses a highly conserved cytosolic PKC phosphorylation site between the the S4 and S5 transmembrane domains).

Opening and closing of ion channels and the resulting spike formation occurs in milliseconds, whereas changes in receptor phosphorylation or kinase activity occurs in seconds to minutes. To relate the 1000 fold slower signal transduction processes to changes in neuronal activity, a systems modeling approach is suitable. For instance a sharp increase in firing rate is reported at 20 to 30 seconds after onset of AngII application in bulbospinal neurons [Li and Guyenet 1996] and a maximum of frequency after 80 to 100 seconds. This corresponds to modeled increases of the intracellular Ca^{2+} concentration, as well as the active PKC and CaMKII concentrations occurring on similar time-frames [Sauter and Vadigepalli 2005].

Toxicological and patch clamp studies indicate the modulation of firing behavior through phosphorylation of the delayed rectifier potassium channel (Sumners and coworkers). But also regulation of fast potassium and calcium channels has been reported (Sumners and coworkers), as well as modulation of a potassium leak current [Li and Guyenet 1996]. How these channels influence the neuronal behavior and to which extend as well as how the signal-transduction regulates the channels dynamically are questions to pose. A detailed mathematical model as described above should enable us to specify and quantify these questions and thus provide a basis for efficient experiments clarifying inconsistencies and crucial points.

The combination of the signaling model with the electro-physiological model enables us to relate changes of intracellular concentrations, especially of PKC and CaMKII kinase activity, directly to membrane potential, and consequently firing rate and excitability. This allows a quantitative analysis of the system and to reveal possible regulation principles efficiently and quickly. The quantitative predictions arising from the integrated model can help to focus further experiments on crucial points or even allow the setup of new experiments, testing the hypothesis of the revealed regulation principles.

Chapter 1

Biological and modeling background

1.1 Signaling in cell biology

Many different kinds of molecules transmit information between the cells of multicellular organisms. Although all these molecules act as ligands that bind to receptors expressed by their target cells, there is considerable variation in the structure and function of the different types of molecules that serve as signal transmitters. The structure of used signaling molecules range in complexity from simple gases to complex proteins. Some of these molecules carry signals over long distances, whereas others act locally to convey information between neighboring cells. In addition, signaling molecules differ in their mode of action on their target cells. Some signaling molecules are able to cross the plasma membrane and bind to intracellular receptors in the cytoplasm or nucleus, whereas most bind to receptors expressed on the surface of the target cell. [Cooper 2000]

1.1.1 Modes of cell-cell signaling

Cell signaling can result either from the direct interaction of a cell with its neighbor or from the action of secreted signaling molecules. Signaling by direct cell-cell (or cell-matrix) interactions plays a critical role in regulating the behavior of cells in animal tissues. For example, the integrins and cadherins function not only as cell adhesion molecules but also as signaling molecules that regulate cell proliferation and survival in response to cell-cell and cell-matrix contacts. In addition, cells express a variety of cell surface receptors that interact with signaling molecules on the surface of neighboring cells. Signaling via such direct cell-cell interactions plays a crucial role in regulating the various interactions between different types of cells that take place during embryonic development, as well as in the maintenance of adult tissues.

The multiple varieties of signaling by secreted molecules are frequently divided into three general categories based on the distance over which signals are transmitted [Alberts et al. 2002; Cooper 2000].

- In **endocrine signaling**, the signaling molecules (hormones) are secreted by specialized endocrine cells and carried through the circulation to act on target cells at distant body sites. A classic example is provided by the steroid hormone estrogen, which is produced by the ovary and stimulates development and maintenance of the female reproductive system and secondary sex characteristics. In animals, more than 50 different hormones are produced by endocrine glands, including the pituitary, thyroid, parathyroid, pancreas, adrenal glands, and gonads.

In contrast to hormones, some signaling molecules act locally to affect the behavior of nearby cells.

- In **paracrine signaling**, a molecule released by one cell acts on neighboring target cells. An example is provided by the action of neurotransmitters in carrying signals between nerve cells at a synapse.

Finally, some cells respond to signaling molecules that they themselves produce.

- One important example of such **autocrine signaling** is the response of cells of the vertebrate immune system to foreign antigens. Certain types of T lymphocytes respond to antigenic stimulation by synthesizing a growth factor that drives their own proliferation, thereby increasing the number of responsive T lymphocytes and amplifying the immune response. It is also noteworthy that abnormal autocrine signaling frequently contributes to the uncontrolled growth of cancer cells. In this situation, a cancer cell produces a growth factor to which it also responds, thereby continuously driving its own unregulated proliferation.

Neurons, which are the subject of this thesis, do not only receive paracrine signals on the synapses from upstream neurons (see Section 1.3.2), but are also influenced by longer range hormonic signalling by neuropeptides. Neuropeptide signals play a role in information processing that is different to that of conventional neurotransmitters, and many appear to be particularly associated with specific behaviors. For example, oxytocin and vasopressin have striking and specific effects on social behaviors, including maternal behavior and pair bonding. In contrast to classical neurotransmitters as dopamine and glutamate, that trigger fast electrical actions by membrane polarization and depolarization, neuropeptides act more like classical endocrinic hormones, activating biochemical signalling pathways in the neuron altering the intracellular state and gene expression. Examples for neuropeptides are Angiotensin II (subject of this thesis), Bradykinin and Insulin.

1.1.2 Cell surface receptors

As mentioned above, most ligands responsible for cell-cell signaling (including neurotransmitters, peptide hormones, and growth factors) bind to receptors on the surface of their target cells. Consequently, a major challenge in understanding cell-cell signaling is clarifying the mechanisms by which cell surface receptors transmit the signals initiated by ligand binding. Some neurotransmitter receptors are ligand-gated ion channels that directly control ion flux across the plasma membrane (i.e. synaptic transmission, paracrine signalling). Other cell surface receptors, including the receptors for peptide hormones and growth factors, act instead by altering the activity of intracellular proteins (i.e. neuopeptide transmission, endocrine signalling). These proteins then transmit signals from the receptor to a series of additional intracellular targets, frequently including transcription factors. Ligand binding to a receptor on the surface of the cell initiates a chain of intracellular reactions, finally often reaching the target cell nucleus and resulting in programmed changes in gene expression.

The different types of cell-surface receptors that interact with water-soluble ligands are schematically represented in figure 1.1. Binding of ligand to some of these receptors induces second-messenger formation, whereas ligand binding to others does not. For convenience, we can sort these receptors into four classes [Alberts et al. 2002; Lodish et al. 2000]:

- G protein coupled receptors (see Figure 1.1a): Ligand binding activates a G protein, which in turn activates or inhibits an enzyme that generates a specific second messenger or modulates an ion channel, causing a change in membrane potential. The receptors for angiotensin, epinephrine, serotonin, and glucagon are examples.

- Ion-channel receptors (see Figure 1.1b): Ligand binding changes the conformation of the receptor so that specific ions flow through it; the resultant ion movements alter the electric potential across the cell membrane. The glutamate receptor NMDA, which is involved in long-term potentiation and learning, is an example, but also GABA and AMPA.

- Tyrosine kinase linked receptors (see Figure 1.1c): These receptors lack intrinsic catalytic activity, but ligand binding stimulates formation of a dimeric receptor, which then interacts with and activates one or more cytosolic protein-tyrosine kinases. The receptors for many cytokines, the interferons, and human growth factor are of this type. These tyrosine kinase linked receptors sometimes are referred to as the cytokine-receptor superfamily.

- Receptors with intrinsic enzymatic activity (see Figure 1.1d): Several types of receptors have intrinsic catalytic activity, which is activated by binding of ligand. For instance, some activated receptors catalyze conversion of GTP to cGMP; others act as protein phosphatases, removing phosphate groups from phosphotyrosine residues in substrate proteins, thereby modifying their activity. The receptors for insulin and many growth factors are ligand-triggered protein kinases; in most cases, the ligand binds as a dimer, leading to dimerization of the receptor and activation of its kinase activity. These receptors often referred to as receptor serine/threonine kinases or receptor tyrosine kinases autophosphorylate residues in their own cytosolic domain and also can phosphorylate various substrate proteins.

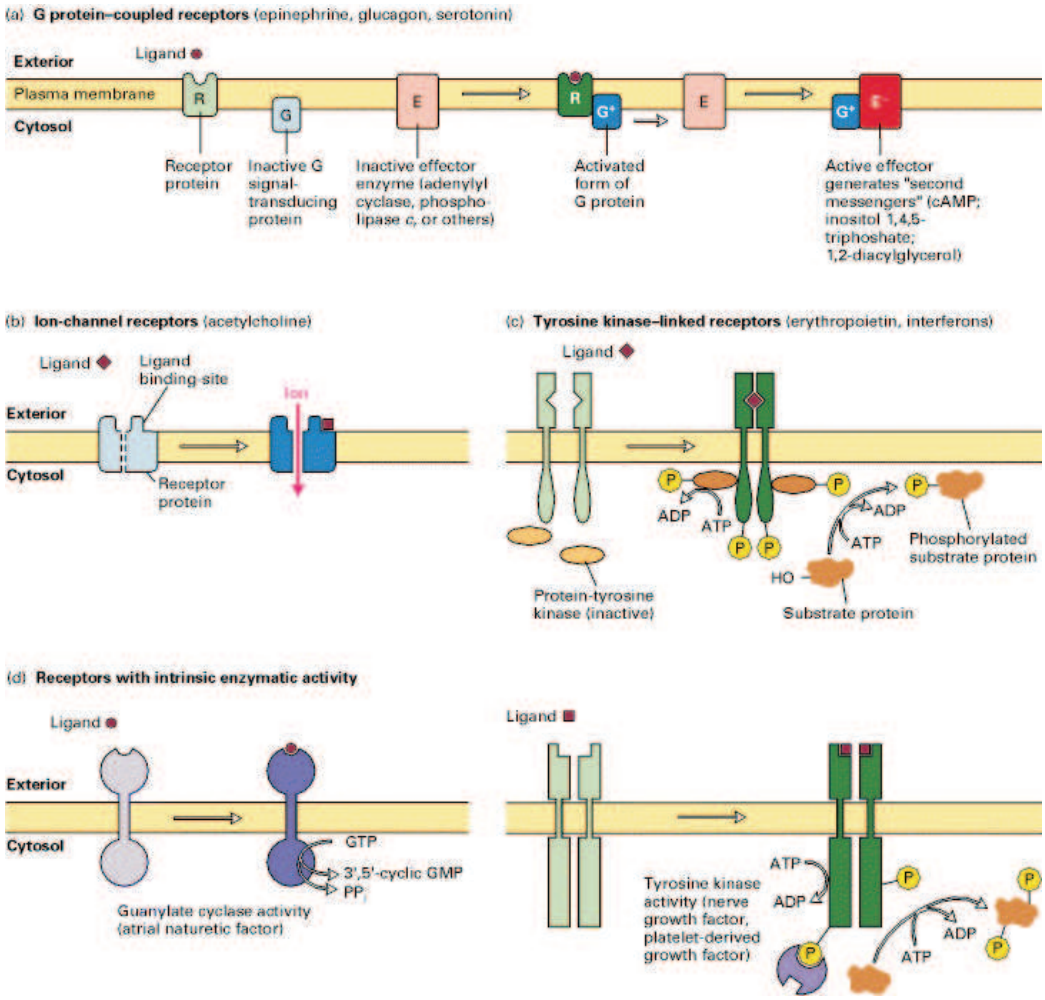

Figure 1.1: Classification of cell-surface (transmembrane) receptors in G protein coupled receptors, ion channels, tyrosine kinase linked receptors and receptors with intrinsic enzymatic activity. Figure taken from [Alberts et al. 2002]

1.1.3 G-proteins

The signal transduction pathway that is investigated in this thesis is mediated by a certain guanine nucleotide binding protein (G-protein) coupled receptor, the Angiotensin type II receptor (AT1R). It modulates the second messengers calcium (Ca_2) and diacylglycerol (DAG) through the G-protein α subunit.

G-proteins are membrane-associated heterotrimeric proteins, consisting of an alpha, beta and gamma subunit. They belong to the GTPases, using the exchange of guanosine diphosphate (GDP, low energy state) for guanosine triphosphate (GTP, high energy state) as a general molecular "switch" function to regulate cell processes. After having performed the effect, the inherent GTPase activity converts GTP back to GDP. This effect is often accelerated by so-called regulators of G-proteins (RGS), which boost the incoming signal by increasing the turnover.

The G-proteins can be divided in five families Gs, Gi, Gt, Gq, and G13, each with a characteristic set of subsequent effectors. The β and γ subunits are closely bound to one another and are referred to as the beta-gamma complex. The $G_{\beta\gamma}$ complex is released from the G_α subunit after its GDP-GTP exchange. The free $G_\beta\gamma$ complex can act as a signaling molecule itself, by activating other second messengers or by gating ion channels directly.

The G-protein involved in the angiotensin pathway considered here is the Gq-protein, which stimulates the phopholipase C (PLC) through its α subunit.

1.1.4 Kinases

A kinase is a type of enzyme that transfers phosphate groups from high-energy donor molecules, such as ATP or GTP, to specific target molecules

(substrates), a process that is called phosphorylation. All kinases require a divalent metal ion such as Mg^{2+} or Mn^{2+} to be present, which stabilizes the high-energy bonds of the donor molecule (usually ATP or ATP derivative) and allows phosphorylation to occur. An enzyme that removes phosphate groups from targets is known as a phosphatase. Phosphorylation by kinases can have different effects:

- Activation of a molecule by increasing its energy, allowing it to participate in a subsequent reaction with a negative free-energy change.
- Inhibition of activity, as for instance in the tyrosine kinase src, which if phosphorylated on a particular tyrosine, folds on itself, and thus masks its own kinase domain, therewith shutting off.
- Docking or binding of proteins, which have recognition domains for a phosphorylated tyrosine, serine or threonine motif. As a result of binding a particular protein, a distinct signaling system may be activated or inhibited.

The largest group of kinases are protein kinases, which act on and/or modify activity of specific proteins. They are used extensively to transmit signals and control complex processes in cells.

Subject of this thesis are the Protein Kinase C α (PKCα) and the Calmodulin-dependent Kinase II (CaMKII), which recently have been shown to be involved in the modulation of neuronal ion channels (see literature review in Chapter 2).

1.2 Modeling of signal transduction pathways

Interactions of cell compartments (functional units like receptors or enzymes, signaling molecules and kinases) are based on several chemical forces and can be described in terms of biochemical reactions. Receptors and most of its adaptor molecules are macro-molecules, largely composed of long amino acid chains. They are folded into a particular three-dimensional structure (often referred to as conformation) which determines its function. The conformation as well as the assembly of several macro molecules and ligands is stabilized by different types of chemical bounds:

- **Covalent bonds** are characterized by the sharing of one or more pairs of electrons between two elements, producing a mutual attraction that holds the resultant molecule together. Atoms tend to share electrons in such a way that their outer electron shells are filled. They most frequently occur between atoms with similar electronegativities.

- An **ionic bond** can be formed after two or more atoms lose or gain electrons to form an ion. Ionic bonds occur between metals, losing electrons, and non-metals, gaining electrons. Ions with opposite charges will attract one another creating an ionic bond. Such bonds are stronger than hydrogen bonds, but similar in strength to covalent bonds.

- Van der Waals interactions refer to intermolecular forces that deal with forces due to the polarization of molecules. Forces that deal with fixed or angle averaged dipoles (Keesom forces) and free or rotation dipoles (Debye forces) as well as shifts in electron cloud distribution (London Forces).

- **Hydrogen bonds** exists between two partial electric charges of oppo-

site polarity. Although stronger than most other intermolecular forces, the typical hydrogen bond is much weaker than both the ionic bond and the covalent bond. Within macromolecules such as proteins and nucleic acids, it can exist between two parts of the same molecule, and figures as an important constraint on such molecules' overall shape.

- **Hydrophobic interactions** are performed by water, which is electrically polarized and able to form hydrogen bonds internally. Non-polarized matter is repelled by water and tends to cluster together since one larger area disturbing the internal structure of water is more energetic favorable than two smaller areas.

- A **disulfide bond**, also called a disulfide bridge, is a strong covalent bond between two sulfhydryl groups (-SH). The presence of disulfide bonds help to maintain the tertiary structure of the protein.

In the above presented processes of ligand binding, conformential change and multi-molecule assembly bounds are broken down and formed new continuously. In consequence all these processes can be regarded as chemical transformations, and described in terms of reaction-kinetic equations. This is an approach very common and widely used in modeling molecular biological processes and results in metabolic and signalling pathways completely described by a network of biochemical reactions. On the molecular level where all involved substances (in Biology often referred to as species) are considered, a mathematical model can be derived by applying the law of mass action.

1.2.1 The law of mass action

The law of mass action is the origin of our quantitative treatment of chemical reactions and their kinetics. In a reaction system, the probability, that two molecules come close enough together to interact and perform a chemical bound does highly depend on the temperature, which is a measure of the nondirectional molecule movement. For reactions occurring in cell biological systems, the temperature is generally assumed to be constant since the changes are relatively small relative to the absolute values measured in Kelvin. Consequently the reactive activity of the molecules does not depend on the temperature. Then the law of mass action can be obtained from a kinetic point of view:

- **Law of mass action**: The rate of a chemical reaction is directly proportional to the active masses (concentrations) of each of the reactants.

The reaction rates describe the flux of substances, which is a measure of how much substrate is converted to product per time, leading to a description of the reaction system in terms of ordinary differential equations. For a general reversible chemical reaction of the form

$$aA + ... + bB \rightleftharpoons cC + ... + dD$$

the reaction rates are

$$\begin{aligned} r_{products} &= k_{products} c_A^a \cdot \ldots \cdot c_B^b \\ r_{substrates} &= k_{substrates} c_C^c \cdot \ldots \cdot c_D^d \end{aligned}$$

The total reaction rate is

$$r_{total} = r_{products} - r_{substrates}$$

To get the change of concentrations in time $\frac{dc_i}{dt}$ the stoichiometric parameters $a, ..., b$ and $c, ..., d$ have to be considered as pre-factors of the reaction rate, which hereby are related to an one molar change. The reaction above, for instance, needs a mole substrate A and thus the ordinary differential equation equation for the change A is

$$\frac{dc_A}{dt} = -ar_{total}$$

Generally the reactions are assumed to direct from the left side (substrates) to the right side (product) of the reaction equation. Consequently the stoichiometric parameters are negative for substrates, and positive for product. If the reaction runs actually vice versa, the net reaction rate becomes negative.

1.2.2 System of reactions

Signal transduction pathways are biological reaction networks with a multitude of substances and reactions connecting them. The changes of concentrations are now described by the sum of all producing and consuming terms, i.e. the sum of all reaction rates multiplied by their stoichiometric coefficient. This finally leads to a system of ordinary differential equations of the form

$$\frac{d\mathbf{c}}{dt} = N\mathbf{c}, \quad N \in \mathbb{R}^{n\times n},\ \mathbf{c} \in \mathbb{R}^{+}$$

where N denotes the stoichiometric matrix and $\mathbf{c}$ the vector of all species concentrations. As we will see in the next subsection, a system of reactions can include direct dependencies, and consequently the stoichiometric matrix N has not full row rank, i.e the number of independent rows ($rowrank(N)$) does not equal the number of rows.

1.2.3 Conserved moieties

Conserved moieties are sums of concentrations which are constant over time. They state linear dependencies within an reaction system, and lead to an inherent model reduction of the ordinary differential equations system. A famous example is the enzyme driven reaction from a substrate S to a product P. The substrate binds to an enzyme E (catalytic unit) reversibly building an enzyme-substrate complex C which triggers the transformation of bound S to the product P, which is irreversible. The reaction scheme is

$$S + E \rightleftharpoons C \rightharpoonup E + P$$

The reaction rates are

$$\begin{aligned} r_1 &= k_{+1} c_S c_E - k_{-1} c_C \\ r_2 &= k_2 c_C \end{aligned}$$

leading to the system of ordinary differential equations

$$\frac{d}{dt} \begin{pmatrix} c_S \\ c_E \\ c_C \\ c_P \end{pmatrix} = \begin{pmatrix} -1 & 0 \\ -1 & 1 \\ 1 & -1 \\ 0 & 1 \end{pmatrix} \begin{pmatrix} r_1 \\ r_2 \end{pmatrix}$$

The rows two and three of the stoichiometric matrix N are linear dependent, and consequently sum of the corresponding equations become zero.

$$\frac{d}{dt} c_E + \frac{d}{dt} c_C = -r_1 + r_2 + r_1 - r_2 = 0 \tag{1.1}$$

Thus the sum $c_E + c_C$ is constant, and denoted as conserved moiety of enzyme. Integration of 1.1 from the starting point $t = 0$ to any time point t gives

$$c_E(t) + c_C(t) = c_E(0) + c_C(0)$$

For convenience we omit the dependence of time in notation and denote the states $c_E(t) = c_E$, $c_C(t) = c_C$ and the initial conditions $c_E(0) = c_{E0}$,

$c_C(0) = c_{C0}$ in the following. Solving the equation for c_E and applying to the system results in elimination of c_E. Accordingly, only three differential equations must be solved, and the concentration of enzyme is determined by the algebraic condition

$$c_E(t) = c_E(0) + c_C(0) - c_C(t) \tag{1.2}$$

Generally reaction systems are of the form $\frac{d}{dt}\mathbf{c} = \mathbf{N}(\mathbf{r})$, where the number of necessary differential equations determining the system is given by the row-rank of the stoichiometric matrix N.

$$N = \begin{pmatrix} N_0 \\ N_D \end{pmatrix}, \qquad \text{with } N \text{ has full row-rank} \tag{1.3}$$

A link matrix L is set up describing the algebraic conditions between the dependent and independent states ($N_D = LN_0$).

$$\frac{d}{dt}\begin{pmatrix} \mathbf{c_{indep}} \\ \mathbf{c_{dep}} \end{pmatrix} = \frac{d}{dt}\begin{pmatrix} N_0 \\ LN_0 \end{pmatrix}\mathbf{r} = \begin{pmatrix} I \\ L \end{pmatrix} N_0\mathbf{r} \tag{1.4}$$

This separation of independent states (c_{indep})and linear dependent states (c_{dep}) allows solving of a $dim(c) - rowrank(N)$ smaller differential system. Note that the reaction rates are functions of the concentrations $r = r(c_{indep}, c_{dep})$. The link matrix is used to reduce the dependencies to the independent states, and only the solving of the following differential equations is necessary.

$$\frac{d}{dt}c_{indep} = N_0 r(c_{indep}, Lc_{indep}) \tag{1.5}$$

The dependent states are algebraically calculated from the independent ones through the link matrix:

$$c_{dep} = L \tag{1.6}$$

Note that the given initial conditions of a real system $c(0)$ have to be consistent according to the dependencies expressed through the link matrix L: $c_{dep}(0) = Lc_{indep}(0)$.

1.2.4 Reaction kinetics

Depending on the level of abstraction, the reaction rate does not necessarily follow the law of mass action. Different assumptions and/or model reduction methods lead to more complex reaction rates as for instance Michaelis-Menten kinetics, Hill kinetics or other, more specialized kinetics describing enzymatic activity and allosteric regulation. Often, the reaction rate is determined experimentally and fitted to special reaction kinetic functions. However, one could state that these complex kinetics can all be traced back to the law of mass action and the Arrhenius equation, if all involved molecules and processes are considered.

1.3 The nervous system

The nervous system of an animal coordinates the activity of the muscles, monitors the organs, constructs and also stops input from the senses, and initiates actions. It controls most of the bodys internal environment as for instance the composition of its extracellular fluid, the supply of oxygen and nutrients to the tissues, and the removal of carbon dioxide and metabolites from the tissues. Changes in the internal environment are monitored by sensory receptors and regulatory action is taken if the changes in the environment exceed the set limits, thereby restoring the equilibrium state due to activation of various effector cells. Cardiac muscle, gland cells, and the smooth muscles of visceral organs and of blood vessels are examples of such effector cells. In more complex organisms, the nervous system is responsible for the ability of learning, exploring and memorizing [Brown 2001].

In vertebrates the nervous system can be divided in the central nervous system (CNS) and the peripheral nervous system (PNS). The CNS consists

Peripheral	Somatic	
	Autonomic	Sympathetic
		Parasympathetic
Central	Brain	
	Spinal cord	

Table 1.1: Organization of the vertebrate nervous system

of the brain and the spinal cord, all other nerves and neurons belong to the PNS [Lodish et al. 2000].

The large majority of what are commonly called nerves (which are actually axonal processes of nerve cells) are considered to be PNS. The peripheral nervous system is divided into the somatic nervous system and the autonomic nervous system. The human brain, for example, is part of the nervous system (see Table 1.1).

The somatic nervous system is responsible for coordinating the body's movements, and also for receiving external stimuli. The autonomic nervous system is the involuntary part of the nervous system where all of the internal maintenance is taken care of.

The autonomic nervous system is then divided into the sympathetic division and parasympathetic division. The sympathetic nervous system responds to impending danger or stress, and is responsible for the increase of the heartbeat and blood pressure, among other physiological changes, along with the sense of excitement caused by the increase of adrenaline in the system. The parasympathetic nervous system, on the other hand, is evident when a person is resting and feels relaxed, and is for instance responsible for the constriction of the pupils, the slowing of the heart rate, the dilation of blood vessels, and the stimulation of digestive and genitourinary systems

(Figure 1.2).

1.3.1 The brain

The brain is composed of two broad classes of cells, neurons and glia both of which contain several different cell types which perform different functions. Interconnected neurons form neural networks (or neural ensembles). These networks are similar to man-made electrical circuits in that they contain circuit elements (neurons) connected by biological wires (nerve fibers). However, these do not form simple one-to-one electrical circuits like many man-made circuits. Typically neurons connect to at least a thousand other neurons. These highly specialized circuits make up systems which are the basis of perception, action, and higher cognitive function.

The human brain contains 30 to 100 billion neurons. Depending on size and weight that are 15000 neurons per square millimeter. By processing sensory information and coordinating complex behavior, it is the most important organ for the integration of vitally important information.

The brain stem forms the bottom part of the brain and contains in- and outgoing nerve fibres (sometimes referred to as white matter) and neurons (grey matter). It circuits and processes incoming sensory information and outgoing motor action and is thereby responsible for elementary control mechanisms and reflexes, controlling various autonomic functions such as respiration and the regulation of heart rhythms.

The **nucleus of the solitary tract** (NTS) is a structure in the **brainstem** located along the medulla and the lower ponds that carries and receives visceral sensation and taste (see also Figure 1.3). It handles information from the carotid and aortic bodies and baroreceptors, thereby controlling blood pressure and volume. For further processing most information goes to the

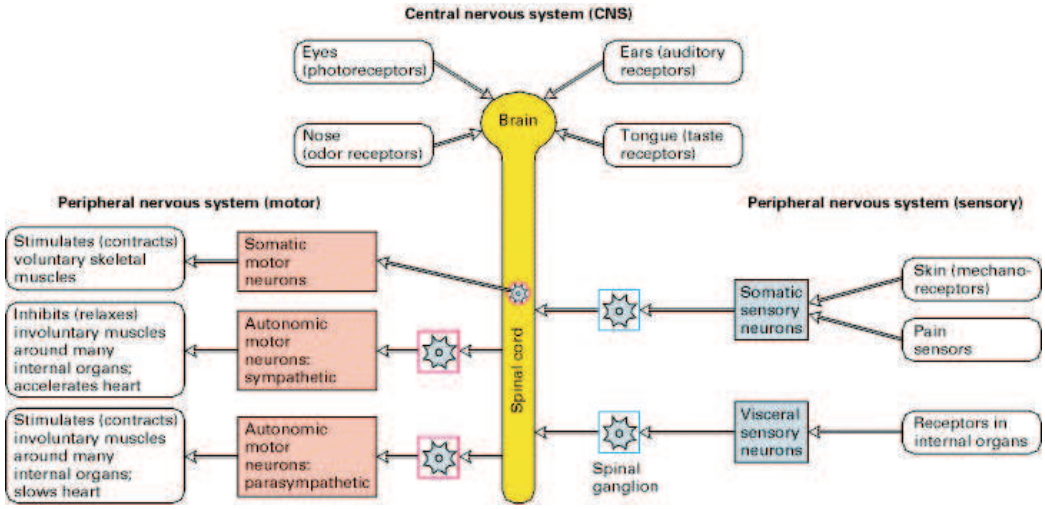

Figure 1.2: A highly schematic diagram of the vertebrate nervous system. The central nervous system (CNS) comprises the brain and spinal cord. It receives direct sensory input from the eyes, nose, tongue, and ears. The peripheral nervous system (PNS) comprises three sets of neurons: (1) somatic and visceral sensory neurons, which relay information to the CNS from receptors in somatic and internal organs; (2) somatic motor neurons, which innervate voluntary skeletal muscles; and (3) autonomic motor neurons, which innervate the heart, the smooth involuntary muscles such as those surrounding the stomach and intestine, and glands such as the liver and pancreas. The sympathetic and parasympathetic autonomic motor neurons frequently cause opposite effects on internal organs. The cell bodies of somatic motor neurons are within the CNS; those of somatic sensory neurons and of autonomic motor neurons are in ganglia adjacent to the CNS. Figure taken from Lodish et al. [2000].

hypothalamus and cingulate gyrus, as well as to other nuclei in the brainstem (such as visceral motor or respiratory centers).

The **hypothalamus** regulates a variety of physiological and psychological processes and is itself neurally and hormonally regulated via the nerve system and blood stream respectively. The hypothalamus is therefore together with the hypophysis or pituitary gland the central connection of the hormone system and the nerve system.

1.3.2 The neuron

Neurons are nerve cells that transmit nerve signals electrically to and from the brain at up to 300 kph. The neuron consists of a cell body (or soma) with branching dendrites (signal receivers) and a projection called axon that conducts the nerve signal (see Figure 1.4). At the end of the axon, the axon terminal transmits the electro-chemical signal across the synapse (the gap between the axon terminal and the receiving cell).

The **axon**, a long extension of a nerve cell, transmits information electrically away from the cell body. Bundles of axons are known as nerves or, within the CNS (central nervous system), as nerve tracts or pathways. The **cell body** (**soma**) contains the neuron's nucleus (with DNA and typical nuclear organelles). **Dendrites** branch from the cell body and receive messages, thereby integrating all synaptic input.

A typical neuron has about 1,000 to 10,000 synapses, meaning it communicates with 1,000-10,000 other neurons, muscle cells, glands, etc. Unlike most other cells, neurons cannot regrow after damage (except neurons from the hippocampus). Fortunately, there are about 100 billion neurons in the brain.

Neurons are very diverse. While they all carry electro-chemical nerve

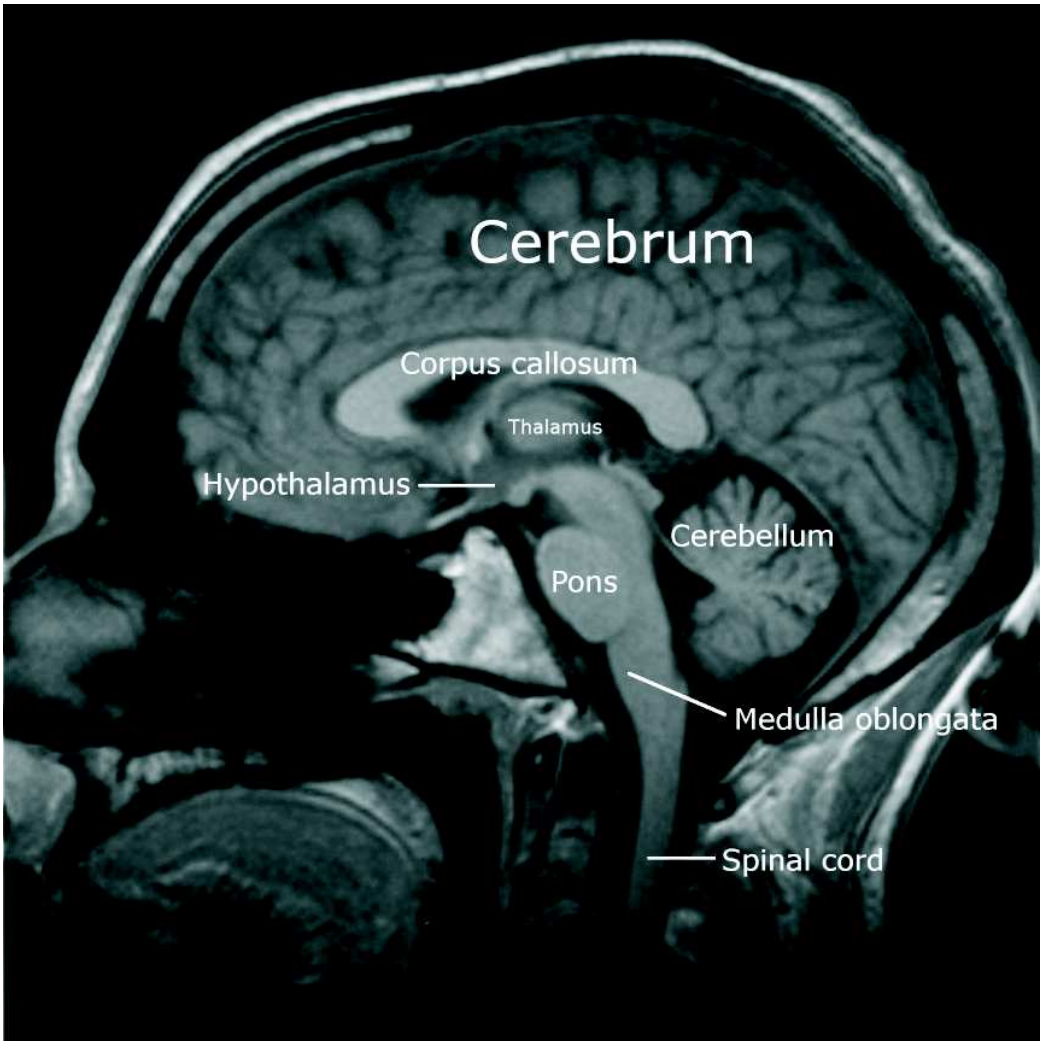

Figure 1.3: The human brain, showing the localization of the brain stem and adjacent brain regions.

signals, they differ in structure (the number of processes, or axons, emanating from the cell body) and are even found in different parts of the body. They vary in size from 4 microns (0.004 mm) to 100 microns (0.1 mm) in diameter, with length varying from a fraction of a centimeter to several decimeters. In general, neurons can be classified into three groups:

- Interneurons or Pseudopolare (Spelling) cells form all the neural wiring within the CNS. They process information in local circuits and possess relay function.

- Motoneurons or Multipolar neurons carry signals from the CNS muscles and glands and are responsible for muscle contraction and hormone release. Motoneurons account for 9% of all neurons. (Examples are spinal motor neurons, pyramidal neurons, Purkinje cells.)

- Sensory neurons or bipolar neurons carry messages from the body's sense receptors (eyes, ears, etc.) to the CNS. Sensory neuron account for 0.9% of all neurons. (Examples are retinal cells, olfactory epithelium cells.)

1.3.3 The neuron function

The neuron receives a synaptic signal biochemically by binding of a neurotransmitter to the postsynaptic ligand activated ion channels of the dendrites and soma. The activated ion channel receptor opens, allowing the exchange of charged ions between the intracellular and extracellular space. This change of the intra- and extracellular proportion of ionic charges results in changes of the neurons membrane potential. If the membrane potential crosses a certain limit, the so called action potential, an electrical pulse is transmitted along the axon. That is an action potential is fired by integrating all

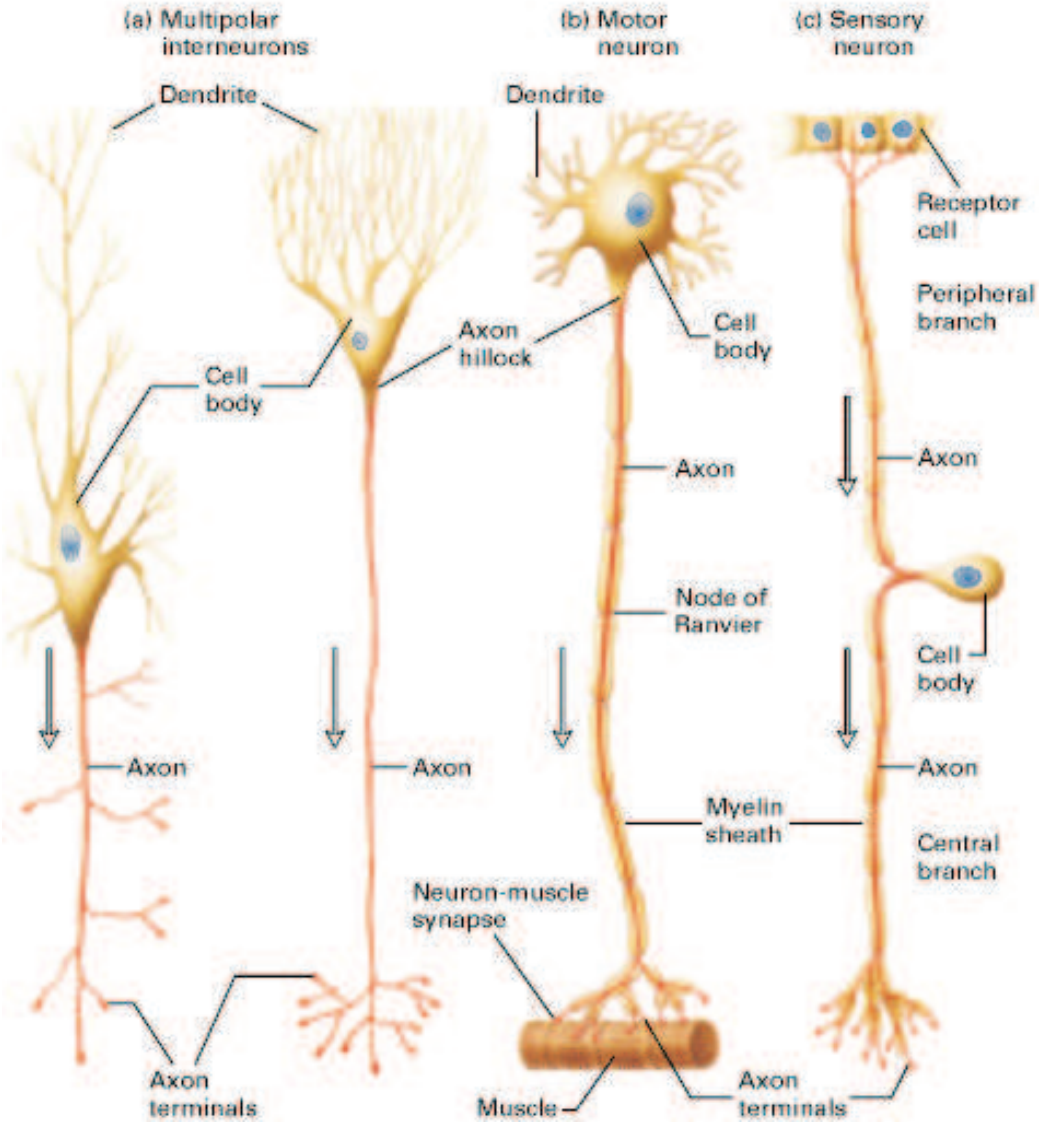

Figure 1.4: Structure of typical mammalian neurons. Arrows indicate the direction of conduction of action potentials in axons (red). (a) Multipolar interneurons. (b) A motor neuron that innervates a muscle cell. (c) A sensory neuron in which the axon branches just after it leaves the cell body. Figure taken from Lodish et al. [2000]

excitatory (depolarizing) and inhibitory (polarizing) input. The closer the synapse is to the soma, the stronger is its (de-)polarizing influence. The greater the distance between two simultaneously stimulated synapses, the more linear the inputs are summarized. Little depolarization due to firing of upstream (presynaptic) neurons and synaptic stimulation are often referred to as excitatory postsynaptic potentials (EPSPs).

The propagation of an action potential can be explained by the combination of two voltage-activated channels, the sodium (Na) channel and the potassium (K) channel [Brown 2001].

1. Transmitters at excitatory synapses cause an increase of the membrane potential.

2. Rising membrane potential leads to a sudden loss of impermeability against Na+ ions. Compared to the state of equilibrium more Na^+ ions can enter the cell, resulting in further increase of the membrane potential.

3. Na^+ ions enter the cell until the Na^+ equilibrium of around +50 mV is almost reached.

4. The positive membrane potential of the cell causes adjacent Na^+ gates to open so that an impulse can propagate along the axon.

5. The membrane loses its impermeability against K^+ ions leading to an e.ux of K^+ ions. Additionally, Na^+ channels inactivate decreasing the influx of Na^+. Both e.ects help restore the resting membrane potential of the cell.

6. K^+ channels inactivate leading to reduced e.ux of K^+ ions.

7. After the occurrence of a single action potential, the cell has gained a small amount of Na^+ ions and lost a small amount of K^+ ions. These changes are compensated for by the activity of the Na^+-K^+ pump.

The action potential creates a peak-to-peak amplitude of about 100-120 mV. The frequency of action potential generation is limited. The period that is needed for restoring the cells equilibrium is called absolute refractory period. During that period, further action potentials can not be produced. The so called relative refractory period is the period after the absolute refractory period, in which action potentials can be initiated. However, during the relative refractory period the strength of the current required to initiate an impulse is larger than normal [Wu 2001].

The amplitude of the action potential does not vary with different currents injected. The action potential is an all or nothing event, i.e. it either does occur or it does not occur. If it does occur, its shape is always the same. Information can therefore not be transmitted by varying the amplitude of the potentials. It is rather the frequency of the signal that contains information [Brown 2001].

1.4 Ion Transporters

The generation of electrical signals in neurons requires both selective membrane permeability and specific ion concentration gradients across the plasma membrane. The membrane proteins that give rise to selective permeability are called ion channels, whereas other proteins called active transporters create and maintain ion gradients. From the perspective of electrical signaling, active transporters and ion channels are complementary: Transporters create the concentration gradients that, in turn, drive ions through open ion

channels, therewith generating electrical signals.

The concentration difference of ions across the membrane causes a potential gradient, which is usually negative inside the cell with respect to the outside. The membrane is said to be polarized. The potential difference across the membrane at rest is called the resting potential and is approximately -70 mV in neurons. (The negative sign indicates that the inside of the cell is negative with respect to the outside.)

1.4.1 Active transport

In contrast to the functions of ion channels, active transporters are membrane proteins that produce and maintain ion concentration gradients. The most important of these is the sodium-potassium pump (Na^+-K^+ATPase), which hydrolyzes ATP to regulate the intracellular concentrations of both Na^+ and K^+. Other active transporters produce concentration gradients for the full range of physiologically important ions, including $Cl^{\cdot}$, Ca^{2+}, and H^+.

The active transport of potassium and sodium ions into and out of the cell, respectively, is accomplished by a number of sodium-potassium pumps scattered across the cell membrane. Each pump transports two ions of potassium into the cell for every three ions of sodium pumped out. This establishes a particular distribution of positively charged ions across the cell membrane, with more sodium present outside the cell than inside, and more potassium inside the cell than outside.

The Na-Ca exchanger

The Na^+-Ca^{2+} exchanger is involved in the Angiotensin II pathway, playing a crucial role in regulating intracellular Ca^{2+}. Normally, the concentrations of intracellular Na and Ca are higher than extracellular. The Na+-Ca^{2+}

exchanger uses the potential energy of the negative Na+ gradient to 'pump' Ca^{2+} ions against their gradient outwards by exchanging three Na^{+} ions inwards for one Ca^{2+} ion outwards. Three valences charge are let in, to push one out, resulting in a net charge flux of one positive valence across the membrane, polarizing it. Not using high energetic molecules (as ATP) provided by the cell directly but rather the resulting Na^{+} gradient of the Na^{+}-K^{+}ATPase, this exchange is referred to as secondary active transport. Further, because of the oppositely directed flux of this exchanger, it is an example for an antiport.

The Na^{+}-Ca^{2+} exchanger is crucial for maintaining the intracellular Ca^{2+} homeostasis. A strong raise of this concentration however, causes the exchanger to switch and go into revers mode, transporting Na^{+} out and Ca^{2+} into the cell [Philipson et al. 2002].

1.4.2 Ion channels

An ion channel is an integral membrane protein or more typically an assembly of several proteins. Such multi-subunit assemblies involve usually a circular arrangement of identical or homologous proteins, closely packed together, forming a water-filled pore through the membrane (see Figure 1.5). These pore-forming subunits are called principal- or α-subunits. They often attach auxiliary subunits, which are then referred to as β-subunits [Coetzee et al. 1999].

While some channels permit the passage of ions based solely on charge, the typal channel pore is just one or two atoms wide at its narrowest point. It conducts a specific species of ion, such as sodium or potassium, and conveys them through the membrane lipid bilayer nearly as quickly as the ions move through free fluid. In some ion channels, passage through the pore is governed

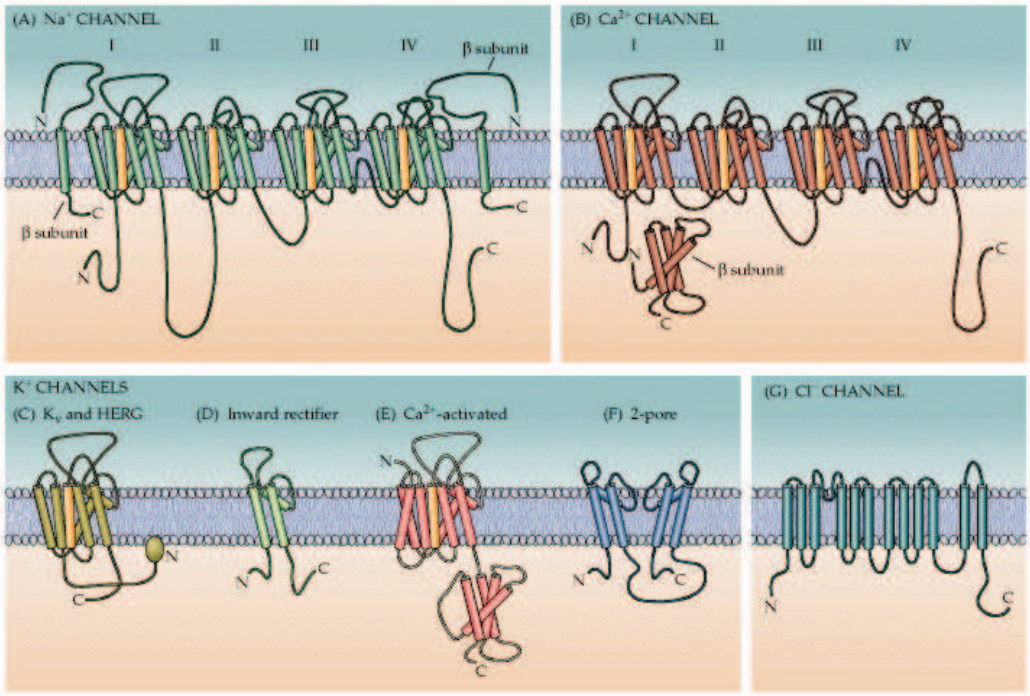

Figure 1.5: Molecular diversity of ion channels. A common theme is, that they all form an aqueous pore surrounded by protein helices, where the ion passes through. Figure taken from [Purves et al. 2001]

by a gate, which may be opened or closed by chemical or electrical signals, temperature, or mechanical force, depending on the variety of channel. Many types of ion channels have now been identified at the molecular level, and this diversity generates a wide spectrum of electrical characteristics among neuron types and even among different neuron parts (dentrites, soma, axon).

Channels are especially prominent components of the nervous system, where voltage-gated channels underlie the generation and propagation of the nerve impulse and transmitter-gated channels mediate conduction across the synapses.

1.4.3 Potassium channels

Potassium channels, which form potassium-selective pores that span through the cell membrane, are the most common type of ion channel. They are found in most cells, controlling the electrical excitability of the cell membrane. In neurons, they shape action potentials and set the resting membrane potential.

There are several types of potassium channels, which can be grouped by their number of transmembrane domains (TMDs) passing through the neurons lipid bilayer.

- Voltage- and Ca-activated K channels possessing six TDMs are denoted Kv and K_{Ca} (or sometimes BK) respectively.
- Leak K channels possess four TDMs forming two pores, which is why they are often referred to as 2-pore channels, are denoted K_{2P}
- inward rectifier K channels possessing two TDMs are denoted K_{ir}.

These (genetically) different channel types have different electrophysiological properties as well. Voltage gated channels open due to membrane depo-

larization, as do Ca^{2+} activated channels due to increased Ca^{2+} concentration. Leak channels are insensitive to changes in membrane potential or ligand concentrations, but,for instance, change activity according to pH. Inward rectifier channels are reversed to voltage gated channels in that they increase conduction with hyperpolarization of the membrane. Some important electro-physiological properties of ion different channels are illustrated in Figure 1.6.

1.4.4 Voltage gated potassium channel

A special feature of voltage activated channels is a sensor that detects the electrical potential across the membrane. This sensor is a transmembrane domain that contains positive charges. The domain is a helical structure with charged amino acids along one face of the helix. Evidently, membrane depolarization influences the charged amino acids such that the helix rotates, thereby allowing the channel pore to open (see Figure 1.7). Similarly, channels that inactivate as a function of membrane voltage also have sequences of amino acids that plug the channel pore during prolonged depolarization.

Voltage gated potassium channels (Kv) form an exceedingly diverse group, much more so than one would predict simply based on the number of distinct genes that encode them (Figure 1.8). This diversity arises from several factors.

- Heteromultimerization. Each Kv gene encodes a peptide subunit, four of which are required to form a functional channel. Kv channels may be homotetramers but may also be heterotetramers formed between different subunits within the same family (in the case of the Kv1, Kv7, and Kv10 families), and these diverse heterotetramers express properties

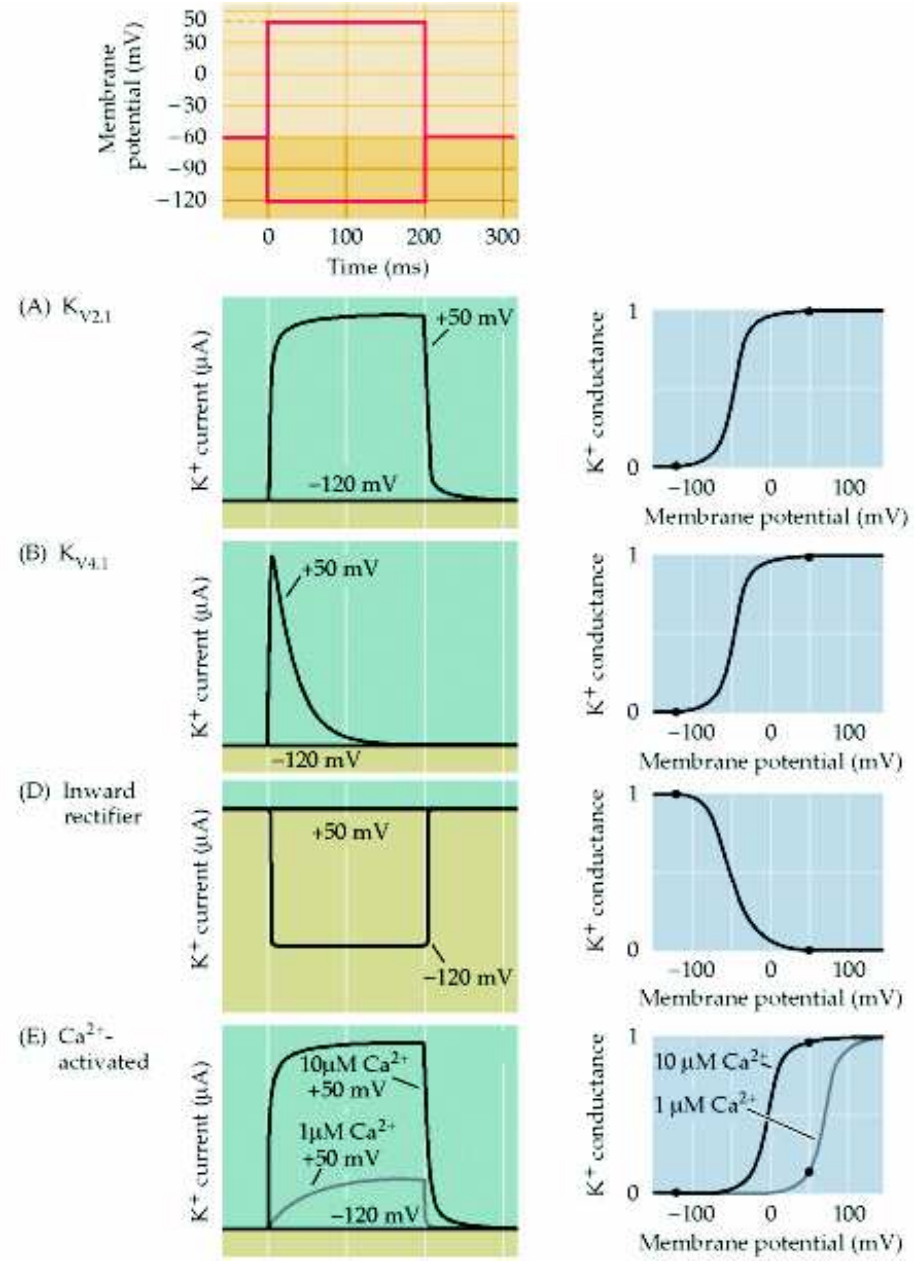

Figure 1.6: Some important ion channel types and their electro-physiological properties. Figure taken from [Purves et al. 2001].

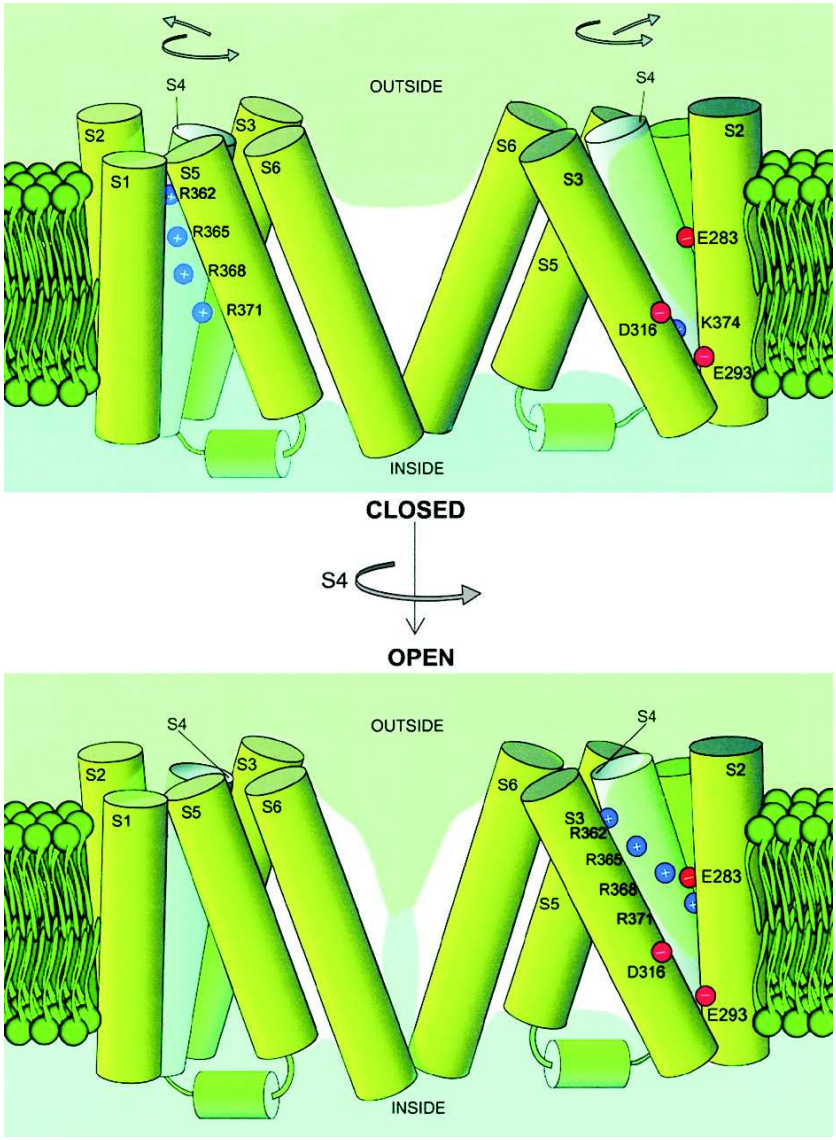

Figure 1.7: Molecular function of the Shaker K channel (delayed rectifier K current related). Under influence of the membrane potential, the voltage sensor (S4 domain) rotates, thus gating the channel pore. [Jiang et al. 2003a,b]

that may be considerably different from those of any of the homotetramers.

- Modifier subunits. Four of the Kv families (Kv5, 6, 8, and 9) encode subunits that act as modifiers. Although these do not produce functional channels on their own, they form heterotetramers with Kv2 family subunits, increasing the functional diversity within this family.

- Accessory proteins. A variety of other peptides has also been shown to associate with Kv tetramers and modify their properties, including several β-subunits (which associate with Kv1 and Kv2 channels).

- Alternate mRNA splicing. Various members of the Kv3, 4, 6, 7, 9, 10, and 11 gene families have coding regions made up of several exons (gene parts that encode for parts of mature proteins) that are alternately spliced (differently combined for translation, resulting in different mature proteins).

- Post-translational modification. Many Kv channels can be post-translationally modified by phosphorylation [Jerng et al. 2004], ubiquitinylation [Henke et al. 2004], and palmitoylation [Gubitosi-Klug et al. 2005], therewith altering the channel's function.

Of special importance for this thesis is the Kv2.2 channel, which is the α-subtype involved in the delayed rectifier potassium current in the here considered NTS neurons, and the Kv1.4 channel, which is involved in generation of the fast activating potassium current. Both channel proteins are regulated by Angiotensin II due to post-translational modification, most probably phosphorylation [Sumners et al. 2002; Pan et al. 2000; Wang et al. 1997b].

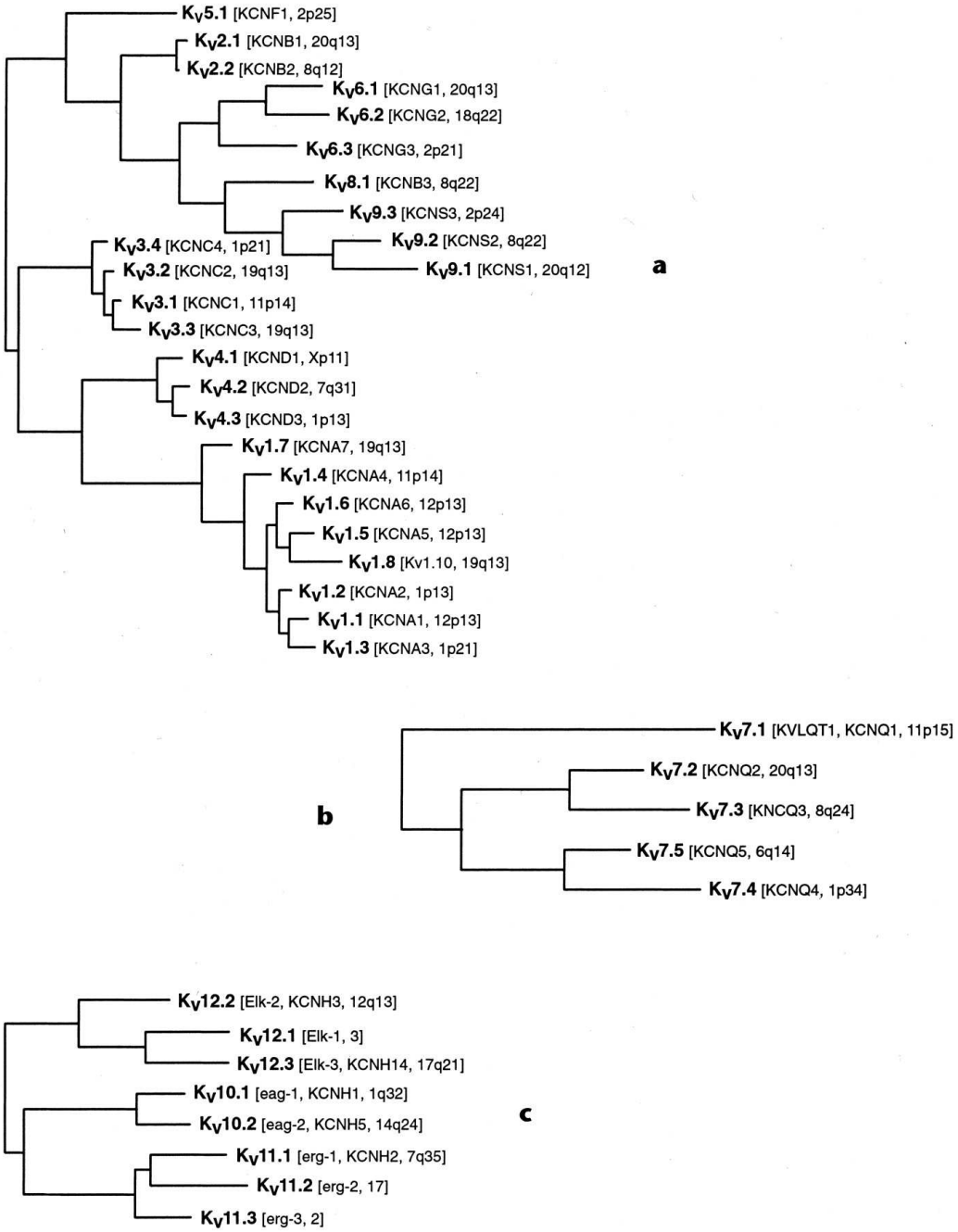

Figure 1.8: Genealogical tree of the different potassium channel subtypes. Figure taken from Coetzee et al. [1999]

1.5 The Hodgkin-Huxley model of a neuron

Hodgkin-Huxley like (HH) models simulate neurons and their spiking behavior close to the biological processes. In the original work of [HODGKIN and HUXLEY 1952] , the spike formation of an action potential is explained by the interaction of the Na and the K ion channel, modelled by different time and voltage dependent conductances, and the capacity of the neurons outer membrane, modelled by a capacitor (see Figure 1.9). This view of a neuron as an electrical circuit is the principle of all HH-models. Newer models however include a variety of different ionic conductances often related to specific ion channels. The basic mathematical description consists of a differential equation of the membranes potential (V) and the activation (m_i) and inactivation (h_i) variables of the different ionic conductances, and is described in more detail below.

Membrane potential

In the non-partial case, the ordinary differential equation for the membrane potential is

$$C_m \frac{d}{dt} V = \sum_i g_i (E_i - V)$$

where

- C_m is the capacity of the neurons membrane
- g_i are different time and voltage dependent ionic conductances
- E_i is the equilibrium potential of the conductance i

The term $g_i(E_i - V)$ represents the ionic current $I_i = g_i(E_i - V)$ of the channel i. At the equilibrium potential E_i of the channel i, chemical and

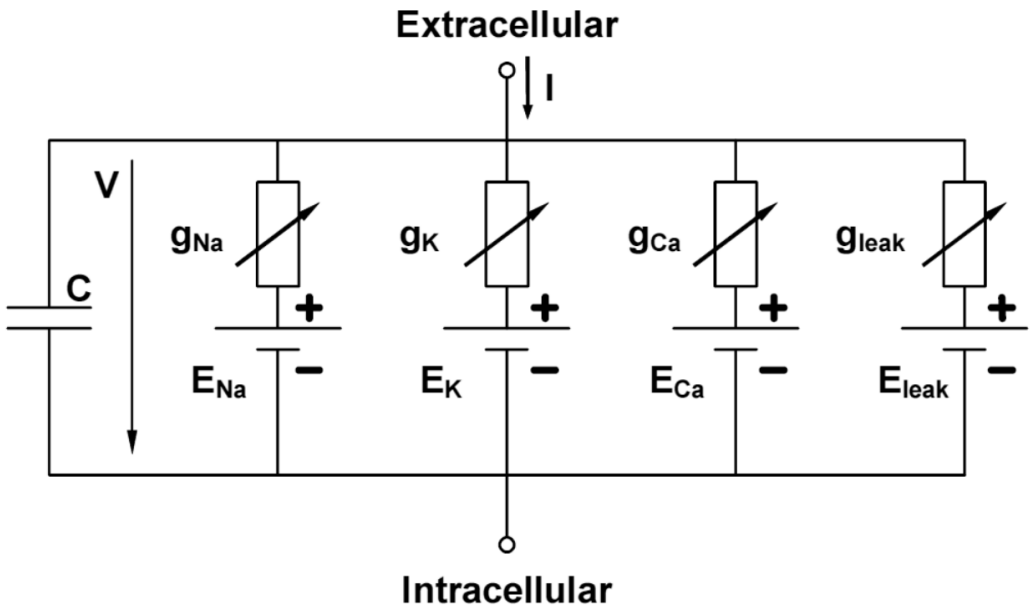

Figure 1.9: Model of the electrical activity of a neuron as an electrical circuit. The membrane is considered as capacitor, the ion channels as voltage dependent conductors.

electrical forces cancel each other, and there is no net flux of ions through this channel and consequently no current.

Ionic conductances

The ionic conductances are of the form

$$g_i = \bar{g}_i m_i^{M_i} h_i^{H_i}$$

where

- $\bar{g}_i$ is the maximal conductance
- m_i and h_i are the activation and inactivation variables respectively
- M_i and H_i the order of activation and inactivation respectively

The activation and inactivation variables, m_i and h_i respectively, are described with the ordinary differential equations

$$\begin{aligned} \tau_{m,i} \frac{d}{dt} m_i &= m_{\infty,i} - m_i \\ \tau_{h,i} \frac{d}{dt} h_i &= h_{\infty,i} - h_i \end{aligned}$$

where $m_{\infty,i}$ and $h_{\infty,i}$ are the voltage dependent steady state activation and inactivation respectively and τ the corresponding time variable. Generally they have sigmoidal form, running depending on the membrane potential from 0 to 1 for activation and 1 to 0 for inactivation.

The steady state activation and inactivation variables and their corresponding time variables (τ) can be described in reaction kinetic (Hodgkin Huxley) or parameterized (Bolzmann) form. They are parameterized by time-course measurements of the ionic currents for different membrane potentials V.

Reaction kinetic form: HH-like

In their original work, HODGKIN and HUXLEY [1952] assumed that the active channel opens and closes according to rates depending on the membrane potential $\alpha(V)$ and $\beta(V)$ respectively:

$$open \underset{\beta(V)}{\overset{\alpha(V)}{\rightleftharpoons}} closed$$

The activation variable is the normalized number of open channels $\frac{[open]}{[open]+[close]} \leq 1$, where $[open]$ and $[close]$ denotes the number (or concentration) of the opened and closed channel, respectively. Consequently the steady state activation $m_{\infty,i}$ and the corresponding time constant $\tau_{m,i}$ is calculated to:

$$\begin{aligned} m_{\infty,i} &= \frac{\alpha_i}{\alpha_i + \beta_i} \\ \tau_{m,i} &= \frac{1}{\alpha_i + \beta_i} \end{aligned}$$

To fit the model to data on specific ion channels obtained by patch-clamb experiments, often e-functions of the membrane potential describing the rates α and β are utilized. The inactivation is described in exactly the same manor.

Parameterized form: Bolzmann-like

The steady state activation and inactivation variables are often characterized by their half-activation/half-inactivation value (V_{12}) and a so called slope factor k after a fitting a Bolzmann function to the data:

$$\begin{aligned} m_{\infty,i} &= \left(1 + exp(-\frac{V - V_{1/2,m,i}}{k_{m,i}})\right)^{-1} \\ h_{\infty,i} &= \left(1 + exp(\frac{V - V_{1/2,h,i}}{k_{h,i}})\right)^{-1} \end{aligned}$$

Notes

For a more detailed derivation of the Hodgkin-Huxley model principle, I refer to a previous study thesis of the NTS neuron model (Ferrari). For a detailed derivation according to experimental data, I refer to the original work of HODGKIN and HUXLEY [1952].

1.6 Modulation of voltage-gated ion channels

Prosttranslational modifications, particularly protein phosphorylation and dephosphorylation, are known to underlie modulation of ion channel activity. For instance, phosphoaminoacid analysis showed significant differences in phosphorylation of Kv2.1 and a truncation mutant, which in combination of whole-cell patch clamb studies, demonstrated that phosphorylation of Kv2.1 shifts the voltage-dependency of activation to more negative potentials, without altering its time constants [Murakoshy97]. Immunocytochemical, biochemical, and biophysical analysis of chimeric Kv channels, consisting in chunks of Kv2.1, Kv2.2 and Kv1.5, showed that the Kv2.1 cytoplasmic C-terminal domain can act as autonomous domain, sufficient to transfer Kv2.1 like clustering, voltage-dependent activation and cholinergic regulation to diverse Kv channels.

1.6.1 Phosphorylation of voltage-gated ion channels

Phosphorylation of voltage-activated ion channels is a widely observed for nearly all known channel subtypes, and can change gating properties as opening and closing probability. From a macroscopic (whole cell) point of view its effects are alterations in activation and/or inactivation variables and their kinetics as well as the modulations of the channel's maximal conductance.

Since the focus of this thesis were potassium current modulations mediated by PKC and CaMKII, some related experimental results are reviewed briefly in the following. A more detailed review also involving other channel types can be found in Appendix A.

1.6.2 Phosphorylation of the K_a channel

An inhibition of 85% of a fast activating potassium current in the brain has been shown due to the direct phosphorylation of the Kv1.4 alpha subunit on PKC and CaMKII related sites[1] [Hagiwara 2003]. Src[2] binding and tyrosine phosphorylation have also been shown to modulate Kv1.4 and Kv1.5 currents and/or inactivation kinetics [Nitabach et al. 2002].

1.6.3 Phosphorylation of the K_{dr} channel

A brain delayed rectifier potassium channel, the Kv1.1 (also known as RCK1), is up to 90% down-regulated by PKC, involving an N-terminus related process [Boland and Jackson 1999, Peretz et al. 1996]. Another brain delayed rectifier channel, the Kv2.1, has been shown to be modulated by phosphorylation in various ways [Misonou et al. 2005, Tiran et al. 2003, Peretz et al.1999, Murakoshy et. al. 1997] Boland and Jackson 1999, Peretz et al. 1996]. Also variety of additional beta subunits have been shown to assemble complexes with the Kv2.1 and the closely related Kv2.2 alpha subunit [3],

[1]Reduction of the Kv1.4 current involving PKC activation is an observed AngII response (see Chapter 2).

[2]Src is a protein kinases similar to PKC or CaMKII. In contrast to PKC and CaMKII, that modify proteins by attaching a phosphate group on a serine or threonine amino-acid residue, it modifies tyrosine residues.

[3]Reduction of the Kv2.2 current is an observed AngII response. The channel subtype genetically related to Kv2.2 most closely is Kv2.1.

regulating their gating properties [Coetzee].

Chapter 2

Summary of experimental data: AngII on neurons

It is well established that the brain angiotensin system exerts regulatory influences in the control of blood pressure and plays a key role in the development and establishment of hypertension. The cardiovascular actions of Angiotensin II (AngII) within the brain involve increases of vasopressin release, dampening of baroreflexes and stimulation of sympathetic pathways via Angiotensin Type 1 (AT1) receptor activation in the hypothalamus and brain stem, particularly in the Nucleus Tractus Solitarius (NTS). The significance of the brain AngII system in blood pressure control and hypertension is further supported by studies with spontaneously hypertensive rats (SHR), which show increased AT1 receptor protein as well as altered K_a channel expression [Sun et al. 2003b; Sundaram et al. 1997].

AngII mediated effects on neuronal activity involve activation of the AT1 receptor and its intracellular signaling pathway (see also Figure 2.1) [Sumners et al. 2002, 1996]. This includes activation of G-Protein-α subunit and subsequent Phospholipase-C-β (PLC), which rises the concentrations of the

second messengers Ca^{2+} and DAG, activating the Protein-Kinase-C α (PKC) and the Calcium-Calmodulin-dependent Kinase II (CaMKII). PKC reduces the fast activating as well as the delayed rectifier potassium current (I_{Ka} and I_{Kdr} respectively), and activates (probably through inhibition of a negative effect of G-Protein β-γ subunit[1]) the total transmembrane calcium current [Pan et al. 2001; Zhu et al. 1997]. I_{Kdr} is further reduced by CaMKII [Zhu et al. 1999]. The potassium channel subtypes involved in this inhibition are Kv2.2 for I_{Kdr} and Kv1.4 for I_{Ka} respectively [Pan et al. 2000; Gelband et al. 1999]. Their modulation is most probably the effect of direct phosphorylation through the above mentioned kinases.

2.1 AngII effects on firing

AngII has shown to increase the neuronal firing rate of rat brain neurons in the hypothalamus and brain stem, particularly in the nucleus of the solitary tract (see Figure 2.2 and Table 2.1). This effect is mediated by the AT1 receptor and involves activation of PKC and CaMKII. [Wang et al. 1997b; Sun et al. 2002; Sumners et al. 2002; Li and Guyenet 1996]. An increase from a basal firing rate of 1.9 Hz to 4.8 was reported after application of 1 uM AngII for one minute in rat bulbospinal neurons of the C1 area due to a proposed K^+ leak channel reduction [Li and Guyenet 1996], showing a peak after approximately 100 sec (see Figure 2.1). The pace of this modulation indicates rather post-translational modification than altered gene expression. A comparison of blood pressure healthy Wistar-Kyoto (WKY) and SHR rats showed the special role of the phosphatidylinositol 3 (IP3) kinase in SHR rats, where the two to three fold higher AngII effects could be reduced to the WKY

[1]Mentioned in Sumners et al. [2002]

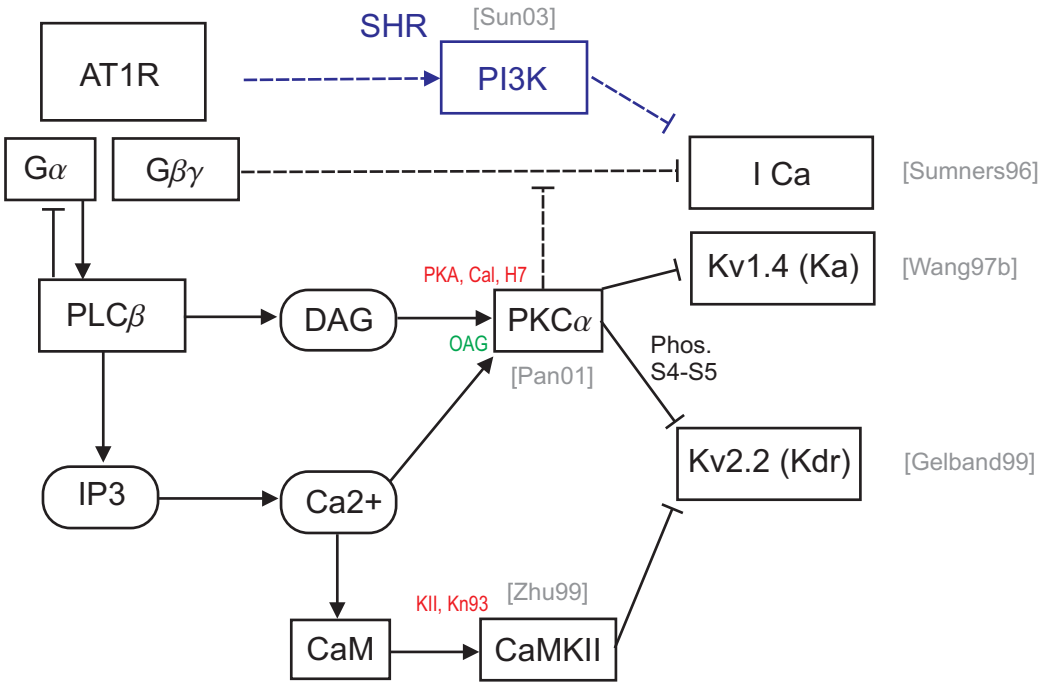

Figure 2.1: Simplified sketch of the AT1R signaling. Arrows are activating influence, bars inhibiting. (Red: inhibitors; Green: activator; Blue: only in SHR)

level by IP3 kinase inhibitors (10 uM LY 294002 or 100 nM wortmannin) [Sun et al. 2003b; Kubo 2005].

Neurons	Nominal	AngII	Dosis	
Bulpospinal C1 neurons [Li and Guyenet 1996]	1.9 Hz	5.4 Hz	1 uM	for 1 min
Hypothalamus and brain stem neurons [Sun et al. 2003a]	0.43 ± 0.07Hz	+97 ± 17 %	10 nM	WKY
		+324 ± 65 %	100 nM	
	0.49 ± 0.06 Hz	+268 ± 45 %	10 nM	SHR
		+556 ± 64 %	100 nM	
[Wang et al. 1997a]	0.8 ± 0.3 Hz	1.3 ± 0.4 Hz	100 nM	

Table 2.1: Overview of experimental data on AngII effects on firing frequency mediated by AT1R.

2.2 Involvement of different channels ($\mathbf{K}_{dr}$, $\mathbf{K}_{a}$, $\mathbf{Ca}^{2+}$)

Changes in neuronal activity or firing rate are controlled through the activity of membrane ionic channels. Consequently alterations in neuronal function involve effects on ionic currents, and their underlying channels. Angiotensin II mediated effects on neuronal currents due to activation of the AT1 receptor are reduction of the Kdr and Ka current and activation of the total Ca^{2+} current. This has been shown through studies of neuronal cultures of rat hypothalamus and brain stem neurons, whereby the injection of AngII (1 to 100

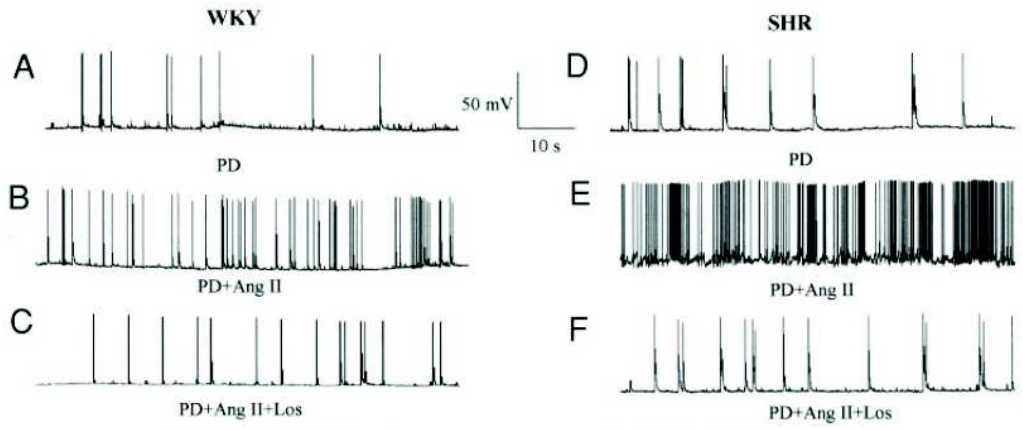

Figure 2.2: AngII produces an AT1 receptor mediated increase in firing rate in spontaneous hypertensive rat (SHR) and Wiskar-Kyoto (WYK) rat neurons. A-C: representative tracings, showing the action potentials (APs) recorded from a single WYK rat neuron under the following sequential treatment conditions: A: Control with superfusion of 1 μM PD123319 for 5 min to block AT2 receptors; B: Superfusion of 100 nM AngII in the presence of PD for 5 min; C: Control with addition of 1 μM Losartan (Los) in the superfusion to block the AT1 receptors. Figure taken from Sun et al. [2003b].

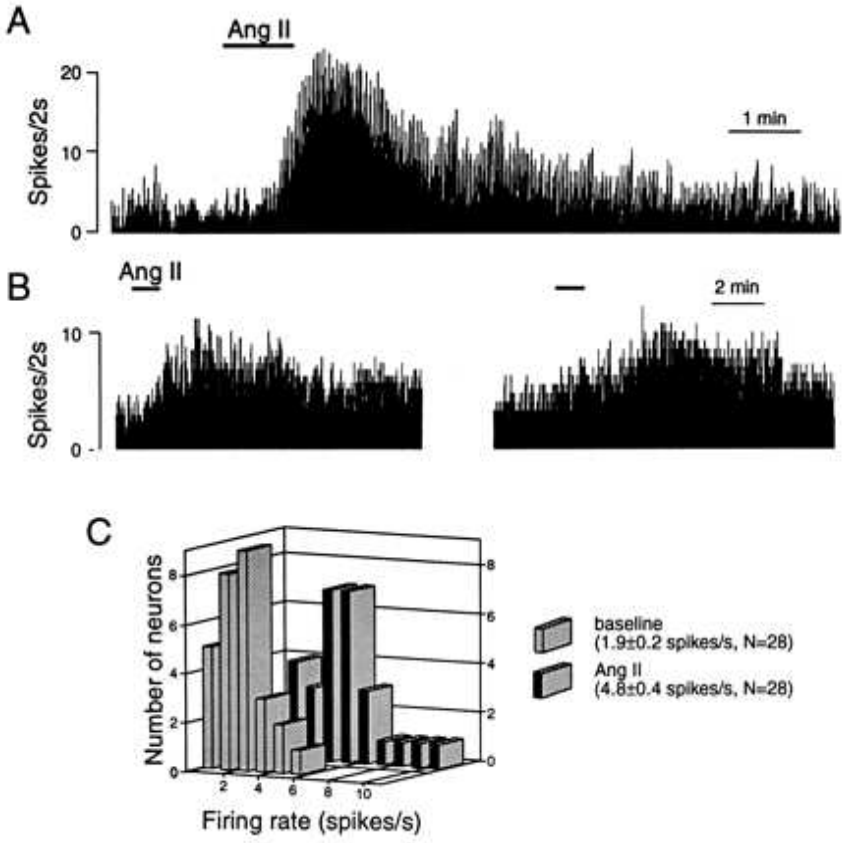

Figure 2.3: Response of one bulbospinal cell to bath application of 1 μmol/L Ang II (at bar). Unit activity (recorded extracellularly in cell-attached mode) is displayed as an integrated rate histogram. B, Different single unit showing reproducibility of excitation by 1 μmol/L Ang II (applied at bar). The interval between the two excerpts was 10 minutes. C, Spontaneous discharge rate of Ang II–sensitive bulbospinal neurons of the RVLM recorded extracellularly in cell-attached mode before and during application of Ang II (1 μmol/L). Figure taken from Li and Guyenet [1996].

nM) - in the presence of a constant superfusion of the AT2 receptor blocker PD 123 319(1 uM) - caused current alterations whose dynamic transitions were completed after approximately 300 seconds [Sumners et al. 1996].

2.2.1 Fast activating potassium current

Patch-clamb studies of the fast activating potassium (Ka) channel from neonatal rat hypothalamus and brain stem neurons have shown a threshold activation at potentials between -30 to -20 mV and a steady state inactivation starting between -80 and -70 mV with a half inactivation of -52.2 mV. AngII (100nM) reduced the Ka current peak by 20% during a voltage step to +20 mV and reduced the single channel activity due to decreased opening probability [Wang et al. 1997b] (see Figure 2.4). The channel subtype underlying this Ka current is Kv1.4 [Pan et al. 2000].

2.2.2 Kdr channel

Similar patch-clamb studies, also of Angg II responsive rat hypothalamus and brain stem neurons, concerned the delayed rectifying potassium (K_{dr}) current, and showed half activations between 0 and 2.3 mV [Gelband et al. 1999].

Pharmacological and biophysical studies suggested Kv2.2 and Kv3.1b as candidates for the AngII responsive Kdr current in these neurons. Reverse transcriptase-polymerase chain reaction analysis confirmed the presence of Kv2.2 and Kv3.1b mRNA, but only Kv2.2 protein was demonstrated by Western blot analysis (see Figure 2.5). Using the Xenopus oocytes expression system and coexpression of Kv2.2 and AT1R, the AngII induced inhibition of the Kv2.2 current has been confirmed [Gelband et al. 1999].

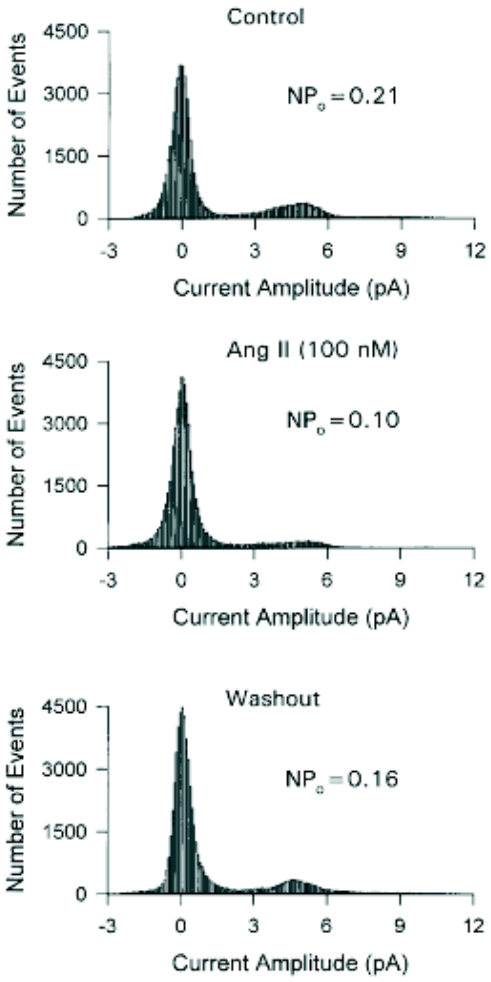

Figure 2.4: Ang II (100nM) decreases open probability (NPo) of A-type K channels. Single-channel analysis was performed on recordings from cell-attached patches. Currents were activated by driving force of 100 mV ($V_{pipete} - V_{membrane} = 100$ mV). NPo in control, in presence of Ang II (100 nM) , and after washout was 0.21, 0.10, and 0.16, respectively. It is to note that Ang II did not alter the single-channel-current amplitude of A-type K channels. Figure taken from Wang et al. [1997b].

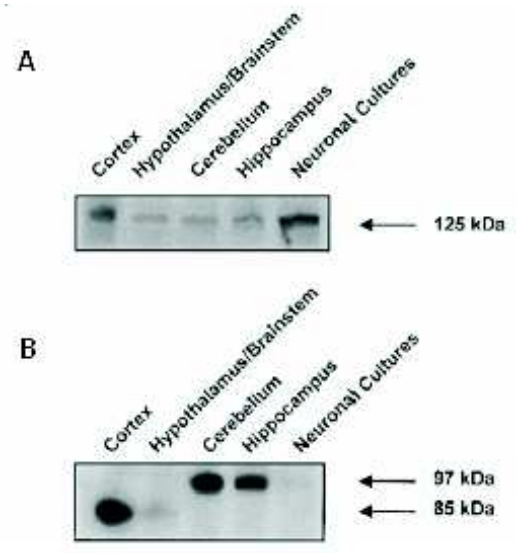

Figure 2.5: A: Representative Western blot analysis showing the presence of Kv2.2 in hypothalamus and brain stem neuronal cultures and rat brain regions. B: Representative Western blot analysis showing the presence of Kv3.1b in selective rat brain regions but not in cultured neurons. All electrophysiological data concerning K_{dr} currents was obtained from these cultured neurons. Figure taken from Gelband et al. [1999].

2.3 Involvement of different kinases (PKC, CamKII)

The AngII pathway activated by the AT1R receptor leads finally to the activation of the Protein Kinase C (PKC) and the Calmodulin dependent Kinase II (CaMKII). PKC is involved in activation of the total Ca^{2+} current and inhibition of the K_{dr} and K_a current. Further inhibition of the K_{dr} involves CaMKII (see Figure 2.1). All studies were performed under the presence of Angiotensin II receptor blockers, that have been shown not to effect the results.

2.3.1 Protein Kinase C

IP3 production as well as PKC activity is highly increased after 100nM Ang II application (about three fold), an effect that is abolished by the AT1 receptor blocker losartan (LOS) [Sumners et al. 1996]. The responsible PKC isoenzyme modulating the potassium currents has been identified as PKC-alpha through antisense studies using western plot analysis (injection of antisense RNA prevents expression of the corresponding gene) [Pan et al. 2001] (see Figure 2.6).

Further it has been shown that both, Ca and DAG are necessary for activation of PKC, and that the AngII mediated effect can be mimicked by the DAG analogous OAG and the PKC activator PMA [Pan et al. 2001] (see Figure 2.7).

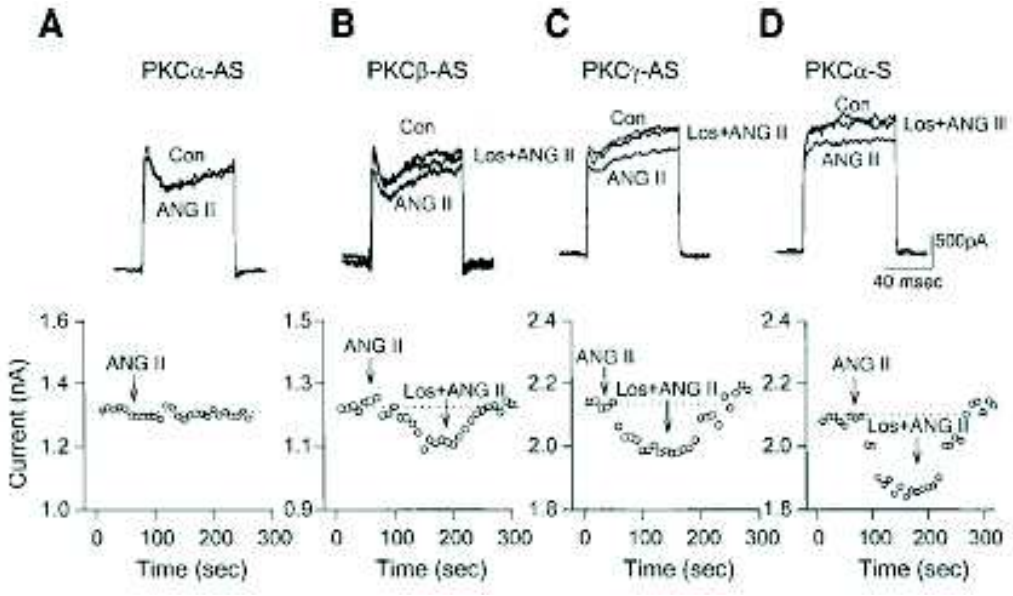

Figure 2.6: Effects of the PCAα, -β and -γ antisense RNA (AS) injection inhibiting the corresponding PKC isoenzymes on AT1 receptor-mediated inhibition of neuronal Kv current. A: representative current traces (top) and time course (bottom) showing effect of ANG II (100 nmol/l) on Kv current after PKC-α-AS pretreatment (voltage step 280 to 110 mV). B, C, and D: representative current traces and time course showing effects of ANG II (100 nmol/l) and Los (1 mmol/l, an AT1R blocker) on Kv current after pretreatment with PKC-β-AS, PKC-γ-AS, and PKC-α-Sense (resulting in functional PKC-α-protein), respectively. Figure taken from Pan et al. [2001].

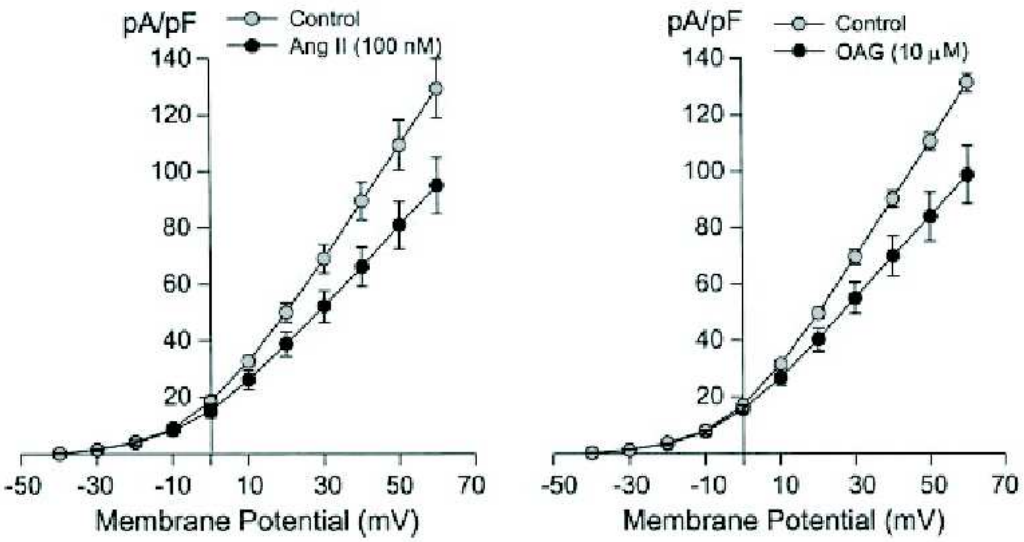

Figure 2.7: Current-voltage relationship for the AngII- or OAG-mediated inhibition of neuronal Kv current. Each point represents ≥ 6 experiments. Figure taken from Pan et al. [2001].

2.3.2 Calmodulin dependent Kinase II

Selective inhibition of CaMKII or CaM has shown to attenuate AngII caused reduction of the Kdr current in cultured rat hypothalamus and brain stem neurons (see Figure 2.8), and the complete abolishment by concurrent inhibition with PKC. Intracellular application of autophosphorylated CaMKII-alpha mimicked AngII induced effects. Increased CaMKII activity due to autophosphorylation has been shown, as well as the presence of messenger RNA corresponding to the AT1R, the CaMKII-α and the PKC-α (single cell reverse transcriptase analysis) [Zhu et al. 1999].

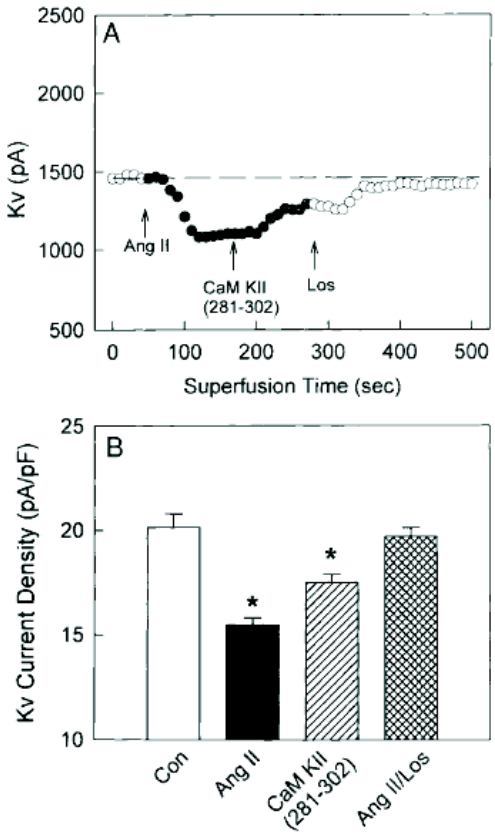

Figure 2.8: Effects of treatment with CaMKII inhibitor CaMKII(281302) on Ang IIinduced decreases in neuronal Kv current. A: representative time course showing the effects of intracellular application of 2 mM CaMKII(281302) on the reduction of Kv current produced by superfusion of 100 nM Ang II. Once the effects of CaMKII(281302) had stabilized, 1 mM Los (an AT1R blocker) was added to the superfusate. B: bar graphs are means ± SE of Kv current densities recorded from 3 neurons during the application of Ang II, CaMKII(281302) and Los. Figure taken from Zhu et al. [1999].

Chapter 3

Modeling membrane electrical activity

The final model of the membrane electrical activity is based on a NTS neuron model from Rybak et al. [1997] consisting of five voltage gated channels and a leakage channel, which had been used to capture unmodeled effects and to tune the membrane resting potential. A feature of this model is that shows frequency adaptation, i.e. an initially high firing frequency after synaptic excitation that decays with time until a steady frequency is reached. We started with the original model, and performed simulations in which we altered conductances according to experimental observations regarding AngII treatment. These theoretical studies included sensitivity analyses, and finally resulted in modifications of the original model, necessary in order to emulate the behavior observed in reality.

Model tuning approach

The model set-up and tuning can be structured in three essential parts:

1. The maximal conductances of the different channel types were taken from Rybak et al. [1997]. This ensures a NTS neuron model exhibiting the desired firing pattern, since this pattern is determined by the actual values of the maximal conductances.

2. The activation variables of the K_{dr} and K_a currents are chosen to provide a good fit to whole cell patch-clamb current data of Sumners and coworkers Wang et al. [1997b]; Gelband et al. [1999].

3. The change of the maximal conductance (K_{dr} and K_a) and the change of the activation variable (only K_a) due to AngII treatment was determined by fitting the channel models to corresponding experimental data of Sumners and coworkers [Wang et al. 1997b; Pan et al. 2001]

3.1 Starting point with Rybak model

The NTS neuron model was taken from Rybak et al. [1997] and consists of a sodium channel (Na), a delayed rectifier (K_{dr}), a fast activating (K_a) and a calcium activated potassium (K_{ahp}) channel, a high threshold L-type calcium (Ca_L) and a leak channel. Sensory integration is realized with variable excitatory and inhibitory synaptic input conductances. The K_a current is composed of two different subtypes in the following referred to as K_a 1 and K_a 2. The mathematical channel descriptions are mainly based on patch-clamb studies of hypothalamic relay neurons [Huguenard and McCormick 1992; Huguenard and Prince 1991; McCormick and Huguenard 1992] and are given in the Appendix B .

The model explains frequency adaptation, which has been observed in blood pressure related neurons of the NTS, after step input of either current

injection or synaptic excitation due to a K_{ahp} Ca_L related process. It shows no firing activity in the unstimulated state.

3.2 Simulations of AngII effects

There is a variety of cellular responses due to AT1 receptor activation by AngII, including increased free Ca^{2+} concentration, activation of the total Ca^{2+} current and inhibition of K_{dr} and K_a currents (see Chapter 2 or Sumners et al. [2002]; Pan et al. [2001]).

In Wang et al. [1997a] and Sumners et al. [2002], K_{dr} channel down-regulation was proposed to cause AngII related frequency modulation. In addition, AngII doubles the intracellular Ca^{2+} concentration. In order to clarify which of these processes effect the neuronal activity and to which extend, simulation studies were performed. The parameters were altered once at a time according to experimental data and the frequency input relationships were obtained by simulation.

Effect of K_{dr} reduction

The performed analysis did not present the expected results, as had been indicated in literature. For example, Sumners and friends proposed that the observed rise of firing frequency is caused by deactivation of the K_{dr} current. However, the Rybak model did not exhibit this effect, but predicted the opposite. In simulations, reduction of the maximal K_{dr} conductance by 30% shifted the frequency-input curve slightly down (see Figure 3.1).

Effect of intracellular Ca^{2+} increase

Intracellular Ca^{2+} responses to AngII with a sharp transient peak and approximately doubled concentration in steady state. Since the effect of this Ca^{2+} mobilization on the firing behavior is not clear, simulations were performed with increased Ca^{2+} levels, predicting inhibition of initial neuronal firing and even immense inhibition after decay of the transient behavior (steady frequency). For a wide range of injected currents, the model predicts initial firing with high frequencies, but a quick and finally elapsing decay. high frequency initially, but decaying quickly and finally elapsing. (see Figure 3.1). This effect can be explained by the Ca^{2+} increase that strongly activates K_{ahp} , hereby polarizing the membrane. As a consequence, higher stimulus is necessary for repetitive firing.

Interestingly, this result indicates that Ca^{2+} sensing of the K_{ahp} should rather be independent (for the most part) from the average intracellular Ca^{2+} concentration, but be determined by Ca^{2+} concentrations directly underneath the cell membrane. This seems reasonable since it has been shown, that K_{ahp} and Ca_L channels form close clusters [**?**]Raj, have a reference?). Further, the principle of distinct Ca^{2+} signal coding has recently been presented elsewhere [Naoki et al. 2005], even though in another context. As the interplay of the K_{ahp} and Ca_L channel is responsible for frequency adaptation in the Rybak model, it is not suitable to exclude the K_{ahp} channel from the model in order to preserve this feature.

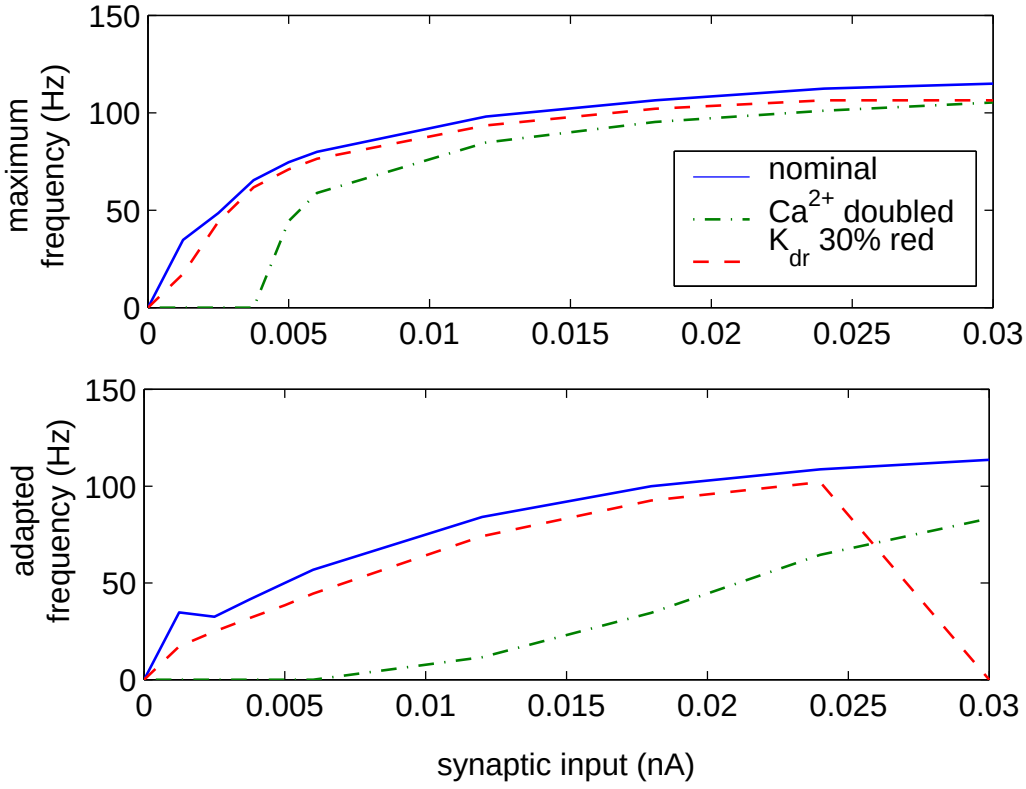

Figure 3.1: Simulation of AngII effects with the Rybak model. The frequency-input relationship was obtained by stimulation with excitatory synaptic input. Parameters were altered according to the literature: reduction of K_{dr} conductance (g_{Kdr}) about 30% and increase of intracellular Ca^{2+} about 100% (in steady state). The model showed not the expected results, since an increase of firing has been observed for very low frequencies (<5Hz).

3.3 Modification needed based on experimental data

The intent of the Rybak-model was to model the (high) frequency response to synaptic input. The resting membrane potential was tuned to a level not showing firing in the unstimulated state by varying the equilibrium potential of the leak channel. With synaptic excitation exceeding a certain threshold, firing is exhibited with high frequencies. However, the experimental data on the AngII response, as it is currently available, regards basal NTS activity only (see Table 2.1). Thus modifications of the original model were considered, in order to achieve a sound NTS model not only for high, but also for low firing frequencies. Three weak points of the Rybak model were identified, and eliminated.

First, the K_{dr} activation of the Rybak model did not correspond well to reported half activation constants of Kv2.2 and time constants of rat brain hypothalamic neurons. To facilitate parametrization and to preserve fourth order kinetics, the K_{dr} activation was modeled with a fourth order Bolzmann function based on experimental data on rat brain thalamic relay neurons [Huguenard and Prince 1991].

$$I = g_{max} \cdot \left(1 + (2^{1/n} - 1) \cdot e^{\frac{V_{12}-V}{k}}\right)^n$$

The factor $(2^{1/n} - 1)$ was included, so that V_{12} reflects the half activated current directly instead of the activation variable $m = e^{\frac{V_{12}-V}{k}}$ as in Huguenard and Prince [1991]. g_{max} presents the maximal conductance, n the channel-order and k the slope factor. V denotes the membrane potential and I the current after the channels transient activation is completed. The half activation was set to 2.3 mV and the slope factor to 17 according to a quinine sensitive K_{dr} current in cultured hypothalamic and brain stem neurons, re-

flecting the AngII responsive Kv2.2 current [Gelband et al. 1999]. The time constant function was adopted from Huguenard and Prince [1991], but scaled by multiplication to a maximum of 20 seconds, a value reported for the rat brain Kv2.2 channel [Hwang et al. 1992]. A quantitative comparison of the resulting K_{dr} model and the K_{dr} model used in Rybak et al. [1997] is shown in Figure 3.3.

Second, the K_a current in the Rybak model is composed of two channel subtypes K_a 1 and K_a 2, possessing half activation constants of -60 mV and -30 mV respectively (see Appendix B). However, in the neurons considered considered in this study, the first subtype ($V_{12} = -60$) impairs the fit of the model to whole-cell patch-clamb current data of Wang et al. [1997b]. This data can be reproduced well by simulation of the K_a 2 ($V_{12} = -36$) component only (see Figure 3.3). Hence, we concluded that the K_a 1 channel is not present in this neurons, and excluded it from the model.

Finally, the Rybak-model did not show any firing without stimulation by excitatory synaptic input or direct current injection mimicking patch-clamb experiments (see Figure 3.1). However, the considered neurons in the hypothalamus and brain stem, where the AngII related experimental data was obtained from, showed basal (unstimulated) activity of 0.5 to 1.9 Hz (see Table 2.1). Hence, the model was adjusted to exhibit repetitive firing of approximately 1 Hz by varying the equilibrium potential of the leak channel. The model shows, as the original Rybak model, frequency adaptation after stimulus (see Figure 3.4).

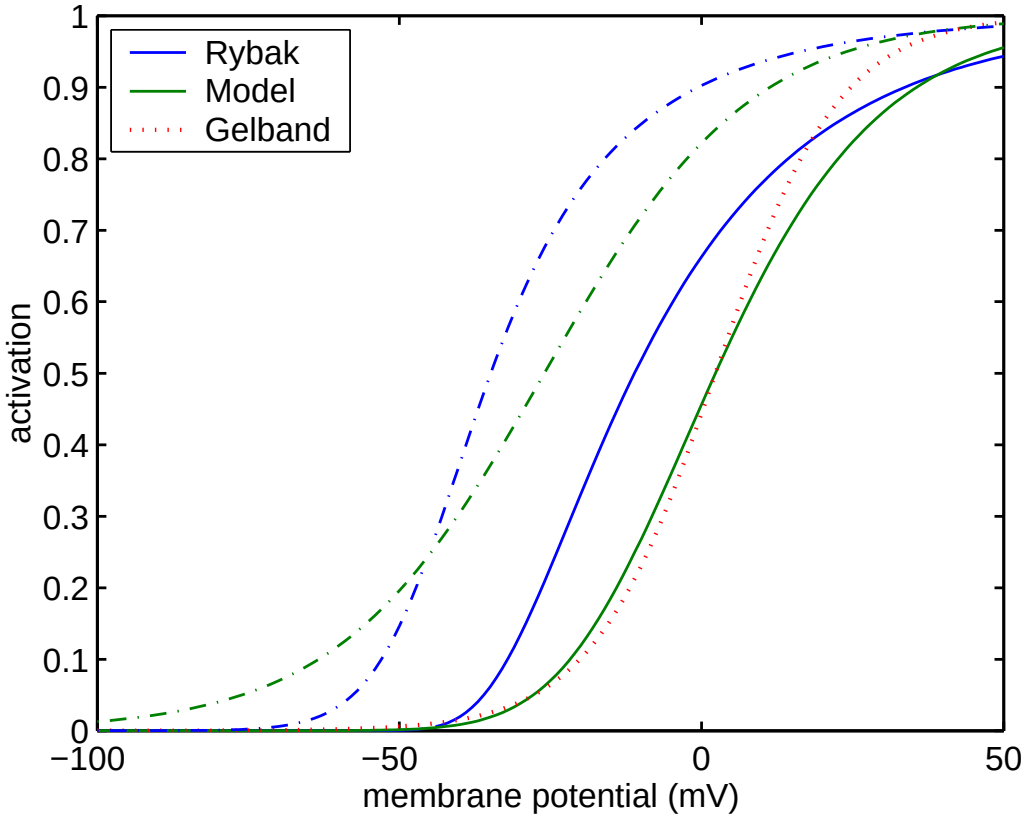

Figure 3.2: K_{dr} activation of the modified model. The red dotted line presents the experimental data reference (a very good first order Bolzmann fit to whole cell currents as performed in Gelband et al. [1999], that would however not be applicable for dynamic simulation since it only leads to first order transient behavior). The used forth order Bolzmann model fits the actual K_{dr} activation much better than the [Rybak et al. 1997] model. The dash-dotted lines present the activation variable m_{Kdr}, the solid lines m^4_{Kdr}, which is a straighter representation of the resulting current.

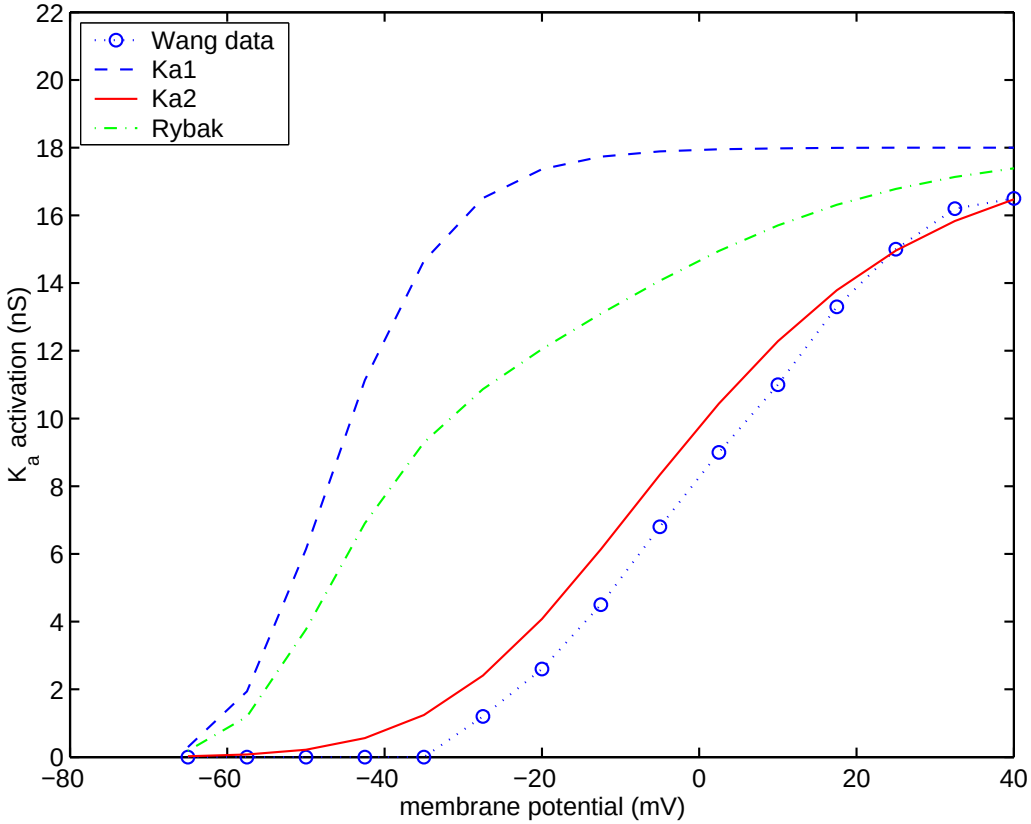

Figure 3.3: K_a activation of the modified model. The K_a 1 component of the Rybak model impairs the fit of whole cell K_a patch clamb data on the conductance as obtained in [Wang et al. 1997b]. To fit the normalized activation variable $m(V)$, the activation variable is taken to the fourth order so that it reflects the conductance (K_a channel models are fourth order: $g \sim m^4$):

$$\text{Rybak model:} \quad g = g_{max} \cdot (0.6 m_{Ka1}^4 + 0.4 m_{Ka2}^4)$$

$$\text{Modified model:} \quad g = g_{max} \cdot 0.4 m_{Ka2}^4$$

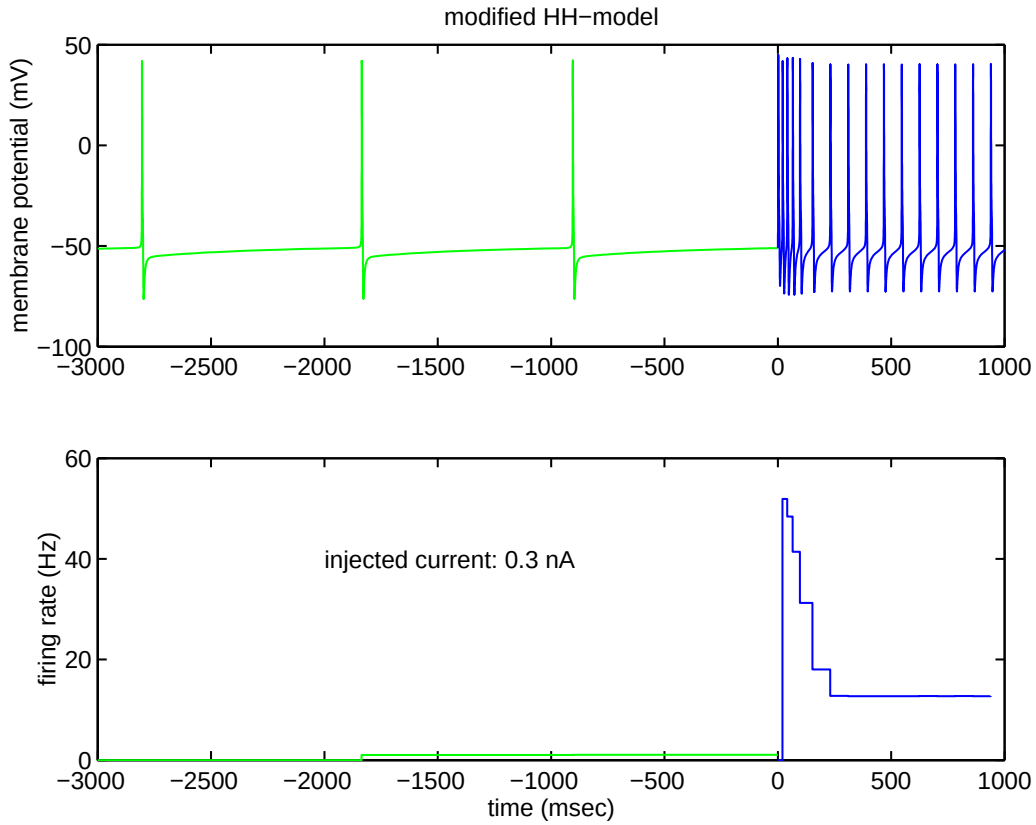

Figure 3.4: The modified model was tuned to a basal activity of 1 Hz. As the original Rybak model, it shows frequency adaptation. Simulation was performed with an injected current step from 0 to 0.3 nA at 0 ms.

3.4 Simulations with Kdr inhibition

In order to determine the participation of different ion channel modifications on the firing frequency and the influence of the tuning parameter (which is the equilibrium potential of the leak channel E_{leak}) different AngII treatment related conditions were simulated. Therefore, the K_{dr} , K_a and Ca_L currents were altered according to experimental observations by either changing the maximal conductance (about 20%) or the half activation constant (about 4 mV) of the corresponding channel. Despite the different molecular principle of these two modification types, there is no significant difference in the outcome concerning the firing frequency. Both have similar effects, indicating that it's modulation is in principle determined by the channel type itself (see Figure 3.5).

Activation of K_{dr} reduces the onset of repetitive firing, thus stimulating neurons that have not been firing before. Neurons that are just above this onset fire with low frequencies and are stimulated by K_{dr} reduction. However, for high frequencies the effect is opposite. This reveals an interesting two modal effect of the K_{dr} conductance that is stimulatory for low firing frequencies ($< 3Hz$) and inhibitory for high frequencies. Considering the response at high frequencies, this result is in accordance with the first simulations of the Rybak model presented at the beginning of this chapter (Section 3.2). Simulation studies performed with an equally tuned model but comprising the original Rybak K_{dr} description, showed the same bimodal K_{dr} effect.

Inhibiting the K_a channel has no visible effect. This can be explained due to its inactivity during interspike potentials and the removal of the K_a 1 compartment, which is the only compartment active at such low potentials (half activation of $-60mV$). In principle, the firing rate at low frequencies is

determined by the height of the current inbetween the spikes, since it is this current, that drives the potential slowly across the threshold, thus generating a new spike (mainly due to opening of the Na channel). The K_a 2 component however, is not active at this potentials (half activation of $-36mV$), and does not contribute to the interspike current nor to the firing frequency. Note that in simulations with the original Rybak model inhibition of K_a 1 resulted in uniformly higher frequencies over the entire spectrum of varied E_{leak}, indeed exactly due to its uniform contribution to the interspike current, whereas the K_a 2 compartment had no effect (Figure in Appendix B).

Activating Ca_L merely has inhibitory effect, since it increases intracellular Ca^{2+} and hence activates K_{ahp} subsequently . This indicates that the increase of neuronal firing by activation of the total Ca^{2+} current proposed in [Wang et al. 1997a; Sumners et al. 2002] is not due to CaL activation, but rather caused by a different Ca^{2+} channel subtype, which is probably involved in synaptic transmission and/or neurotransmitter release. Note that presynaptic augmentation of sensory transmission by AngII has been reported in NTS neurons (in addition to its postsynaptic effects) [Barnes et al. 2003].

3.5 Parameter exploration for different channel parameters

We wanted to determine which parameters of the channel models are responsible for AngII related current modulation. Because there is variation in the data from experiment to experiment, the applied K_{dr} and K_a model is fitted to particular experiments, by adjusting their maximal conductance and half activation constant. However, this is only done to identify the necessary parameter changes. The original maximal conductances of the Rybak model

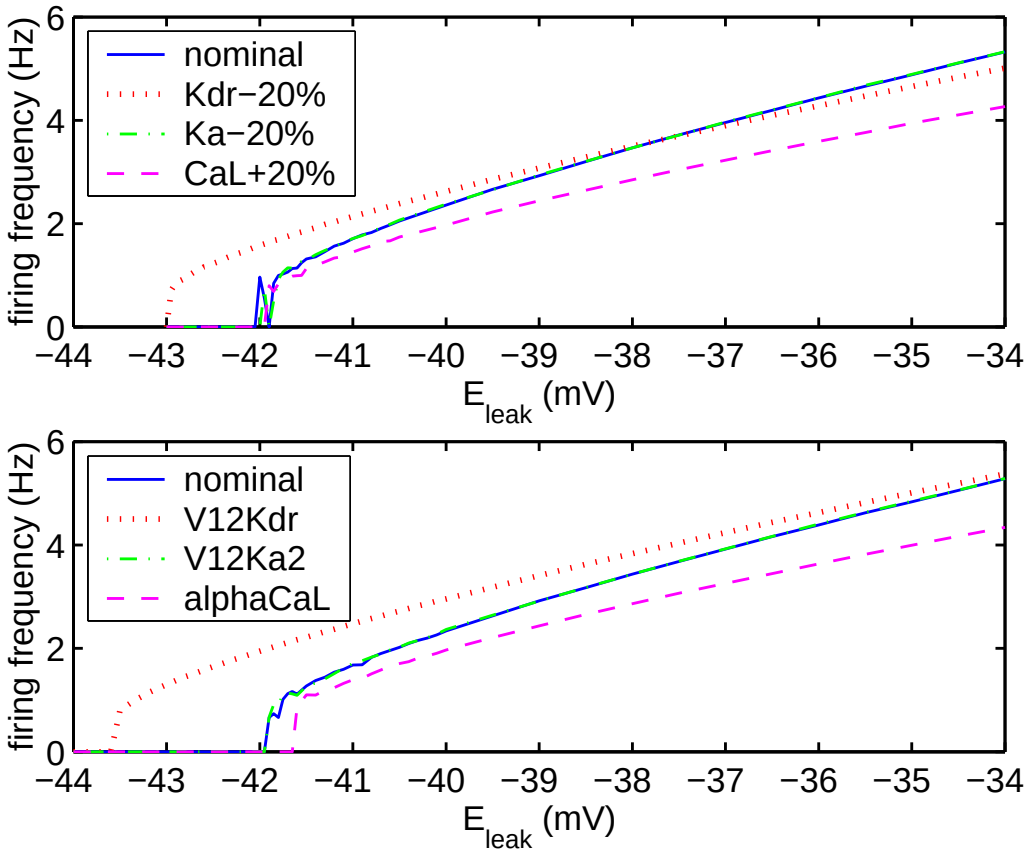

Figure 3.5: Influence of channel parameters on firing frequency. Firing frequency in response to changes of Top: the maximal conductance g or Bottom: the activation characteristics $V_1 2$ (half activation) or α (activation rate).

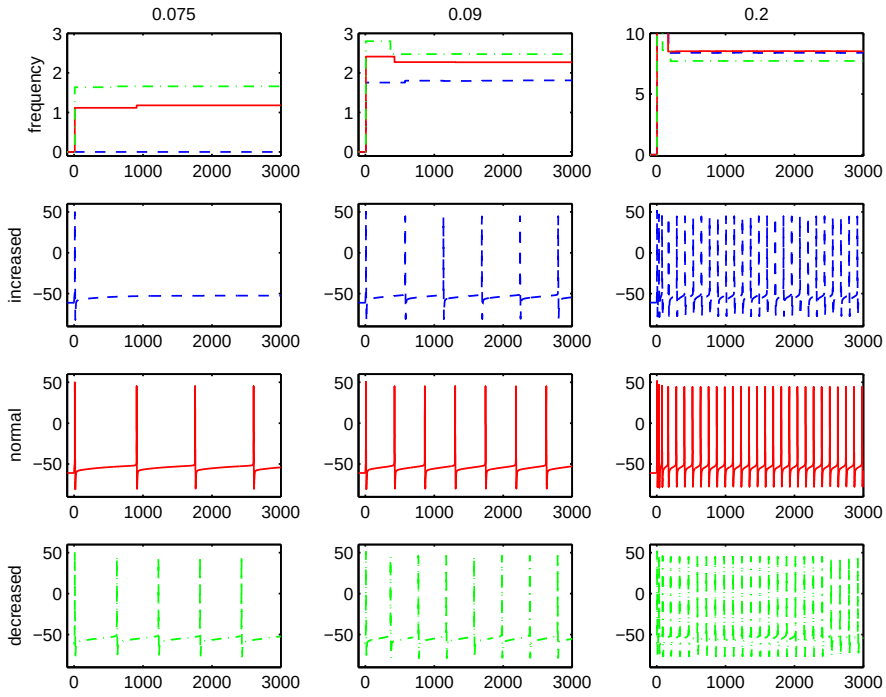

Figure 3.6: Step response of different synaptic excitation in conjunction with different K_{dr} modulations.

were used as nominal (no AngII treatment) maximal conductances of the integrated model.

As can be seen in Figures 3.7 and 3.8, reducing the maximal conductance of K_{dr} and K_a by 25% and 20% respectively can well explain the changes in ionic currents after 100 nM AngII treatment. However, the fit of the K_a model is significantly improved, if the half activation constant is shifted of about 4 mV towards higher potential. The result is in good accordance to single channel studies of K_a showing a decreased opening probability in addition to the reduced maximal conductance [Wang et al. 1997b]. Note that a decreased opening probability corresponds to a decreased opening rate, and finally to an increase of the half activation constant.

The K_{dr} channel activation fits whole cell current data of Pan et al. [2001] best with a with half activation of 12.3 mV (shifted about +10 mV compared to the modified Rybak model). The equilibrium potential of potassium was set to -80 mV (a typical value) and the nominal maximal conductance to 0.9 pA/pF. Using this parameters, the model shows that a conductance reduction of about 25% is sufficient to explain AngII mediated modulation of the K_{dr} current (see Figure 3.7).

The K_a channel is fitted to conductance measurements of [Wang et al. 1997b] with a nominal half activation constant of -29 mV (shifted about +7 mV compared to the modified Rybak model) and a nominal maximal conductance of 18 nS. To be consistent, the equilibrium potential of potassium has been set to -80mV as for K_{dr} parameter tuning. Using this parameters, AngII treatment leads to reduction of the maximal conductance about 20% and a shift in half activation of +4mV (see Figure 3.8).

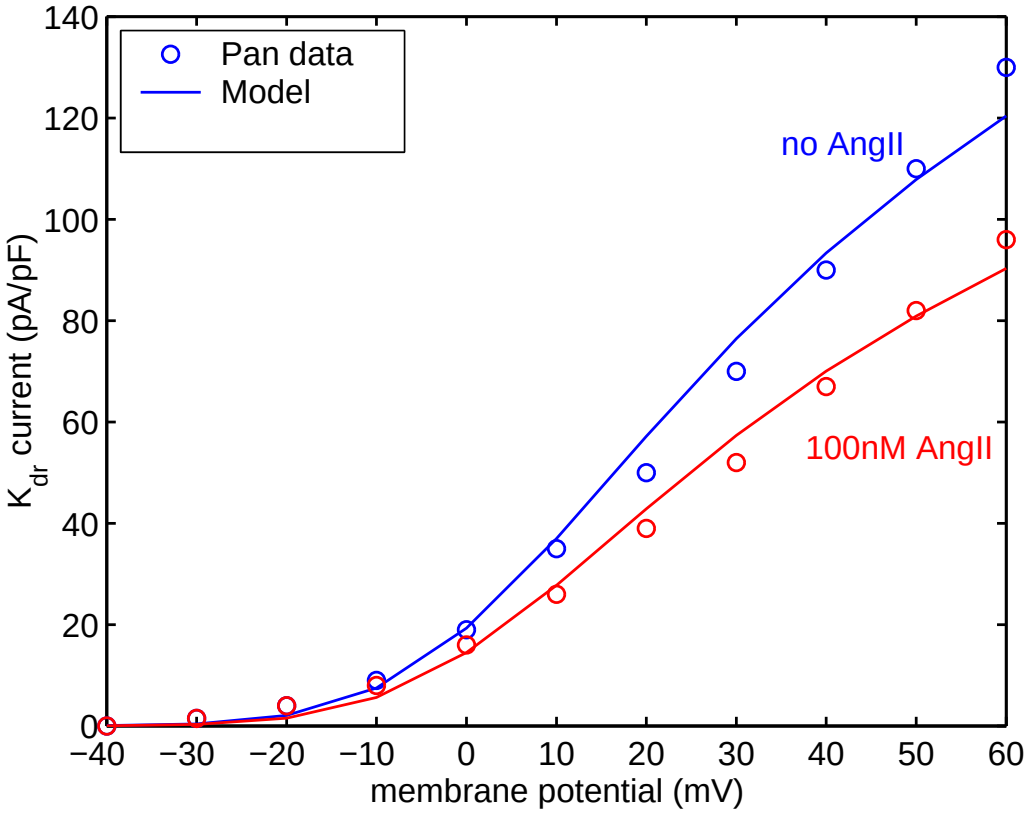

Figure 3.7: Reduction of the maximal conductance is sufficient to explain K_{dr} current modulation. A forth order Bolzmann model with a half activation of 12.3 mV, a slope factor of 17, a nominal maximal conductance of 0.9 pA/pF and an equilibrium potential of -80 mV predicts a g_{Kdr} reduction of 25% if fitted to experimental current data obtained in Pan et al. [2001].

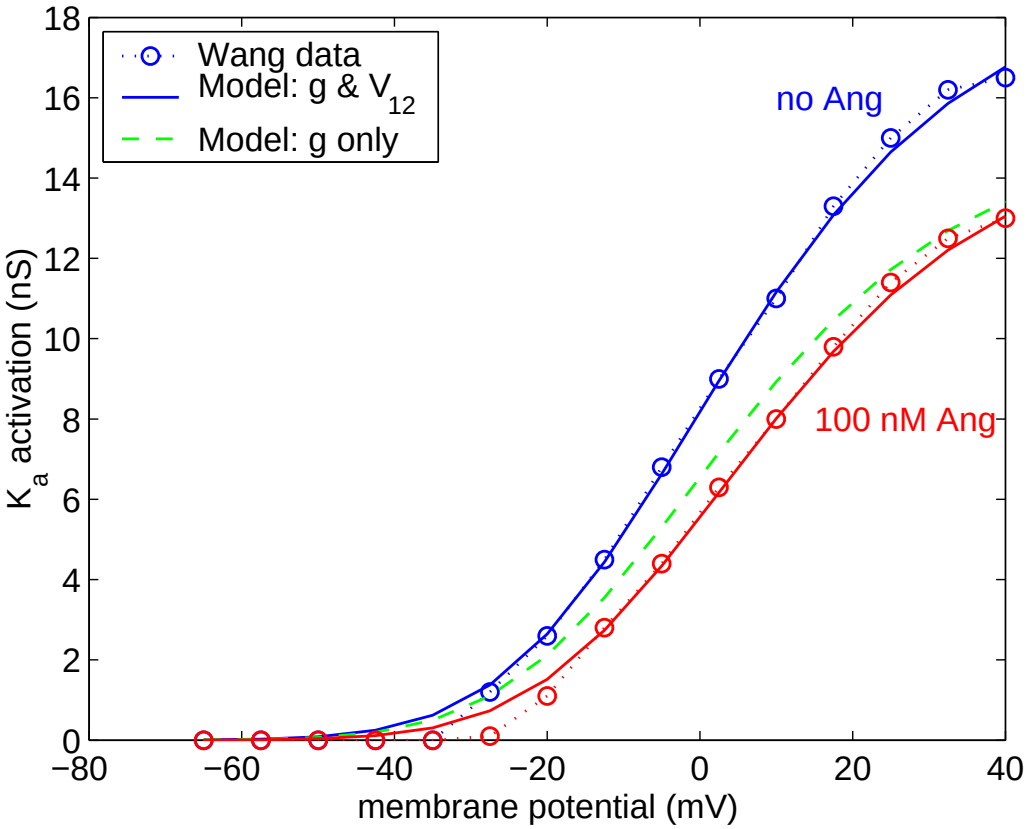

Figure 3.8: K_a channel modulation involves maximal conductance and half activation. Using experimental conductance data of [Wang et al. 1997b] An forth order Bolzmann model with a nominal half activation of -29 mV, a slope factor of 8.5, a nominal maximal conductance of 18 nS and an equilibrium potential of -80 mV predicts an g_{Ka} reduction of 20% and a +4 mV shift of the half activation constant. Only reducing g_{Ka} (green line) fits the data slightly worse.

Original Rybak versus modified model

The qualitative results of both models were similar. Regardless of the channel modifications, activation and inhibition of the K_{dr} and Ca_L respectively had the same effect on the firing rate in both models. The only exception represents activation of the total K_a conductance, that has shown to stimulate firing in the Rybak model but had no effect in the modified model. This is due the removal of the K_a 1 component, which is responsible for this frequency modulation. Activating only the second component K_a 2 in both, the original Rybak model and the modified model had no effect on the firing frequency.

In addition to the presented results, different channel activation variables and kinetics have been investigated. These include different combinations of the activation variables and time-constants of the HH-like channel of the Rybak model and first, second and fourth order Bolzmann activation variables as described in [Gelband et al. 1999], [McCormick and Huguenard 1992] and [Huguenard and Prince 1991] respectively. In principle, they all showed the here described bimodal effect (data not shown).

It was also tried to identify the maximal conductances from available data in the literature that regards AngII responsive NTS neurons (mainly from Sumners and friends). However, there is no data on the Na or K_{ahp} channel. Data that was available on K_{dr} and K_a conductances varied from experiment to experiment and is, in addition, probably strongly biased by the different channel blocking agents used. As a consequence, the therewith constructed model produced peaks whose shape did not match experimental data well in respect to peak durations and after hyperpolarization (data not shown). For this reason, the maximal conductances actually used in the modified model are these of the original Rybak model.

3.6 Comments on whether Kdr inhibition results in observed experimental data

We have shown that, K_{dr} channel inhibition can explain experimental observations concerning AngII mediated activation of neuronal firing, whereas K_a channel inhibition had minor to no effects on the frequency. In contrast, activation of the Ca_L channel results in reduction of firing in our simulations due to subsequent K_{ahp} activation. In order to quantify the different effects of the considered ion channels, relating them to each other and analyzing possible cooperative effects, a detailed sensitivity analysis was performed.

The sensitivity analysis of the modified model considered the AngII responsive K_{dr} and K_a , the Ca_L as possible agent of total Ca^{2+} current activation and a K leak channel (In Li and Guyenet [1996] K leak channel inhibitions was proposed as cause of AngII mediated reduction of firing in Bulpospinal C1 neurons). Note, that this simulations were done before the model was tuned to later used basal activity of 1 Hz[1], and that two leak channels, one K selective and one Ca^{2+} selective, were used. The input resistance was tuned to 120 MOhm and the resting potential to 61 mV (according to NTS neuron data in [Sundaram et al. 1997]), by adjusting the conductances of these leak channels. For the analyses, the maximal conductances were regulated either 20% up- or down, and the corresponding frequency-input relationships were obtained by simulations with different injected currents. Clusters that may emanate in the frequency-input plot due to modification of the one or other channel are then corresponding to dominating effects that are robust in respect to the other channel perturbations. For exam-

[1]This explains that in Figure 3.9 a positive input is necessary to stimulate the neuron to exhibit repetitive firing.

ple, up-regulation of Ca_L clearly separates the frequency-input curves for high injected currents ($> 0.1nA$), revealing a strong inhibitory effect of Ca_L activation (see Figure 3.9). The second significant regulatory property corresponds to K_{dr} inhibition. Though the inhibitory effect of K_{dr} inhibition for high frequencies is dominated by Ca_L related inhibition, its activating effect for low frequencies is dominant. As can be seen in Figure 3.9, K_{dr} inhibition reduces the onset of repetative firing, thus stimulating silent neurons beforehand, an effect that exceeds all other channel modifications. The K leak and the K_a channel have only minor influence on the firing frequency, and are not subject to any clustering.

Summarizing, these results suggest that the K_{dr} plays a major role in AngII induced neuromodulation, and is a crucial factor for firing frequency modulation mediated by voltage-activated ion channels.

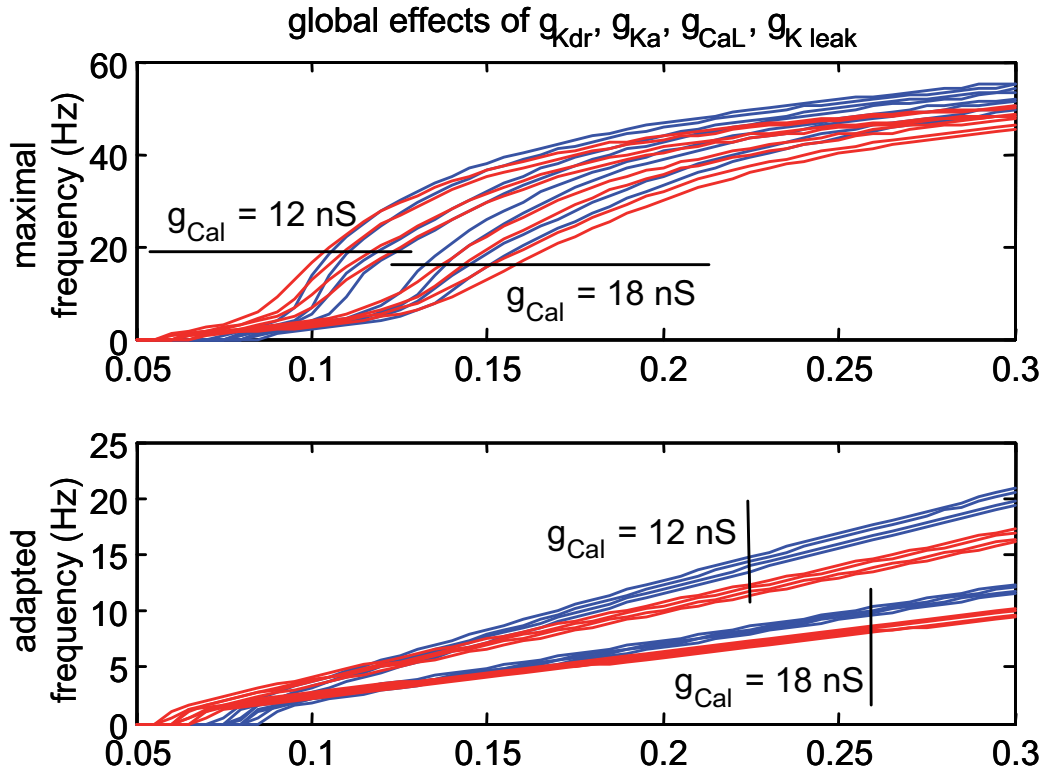

Figure 3.9: NTS neuron model according to [Sundaram et al. 1997] data, with an input resistance of 120 MOhm and a resting potential of -61 mV. The leak channel was divided into a K^+ selective and a Ca^{2+} selective component, using the corresponding equilibrium potentials E_K and E_Ca. The different frequency curves correspond to up- and down-regulated channel conductances of the K_{dr} , K_a , K_{leak} and Ca_L about 20% in different combinations. Down-regulated K_{dr} is colored red, up-regulated K_{dr} is colored blue.

Chapter 4

Signal transduction model

The Signaling model explains the intracellular Ca^{2+} response of neurons to AngII treatment by means of a kinetic reaction model. The model is mainly based on two earlier works of Mishra and Bhalla [2002] and Sauter and Vadigepalli [2005].

Model tuning approach

The model set-up and tuning can be structured in three essential parts:

1. The model structure and kinetics are based on detailed experimental reaction kinetic data of single reaction. Thereby the reaction rates, orders and constants and/or Michaelis Menten constants were determined experimentally (see DOQCS database).

2. The model of Mishra and Bhalla [2002] was extended by AT1 receptor activation and Na^{+}-Ca^{2+} exchange. The parameters for that were chosen to fit time-course data of the Ca^{2+} response in neurons.

3. Extension to include the dependency of transmembrane transport on the membrane potential were added. The parameters were chosen to

equal the rates of the unextended model at resting potential.

4.1 Starting point

The model of the AT1 receptor (AT1R) mediated intracellular signaling pathway includes Gq-protein and phospholipase C (PLC) stimulation, phosphoinostide (PI) hydrolysis and the mobilization of the second messengers Ca^{2+} and diacylglycerol (DAG) and the subsequent activation of protein kinase C (PKC) and calmodulin-dependent kinase II (CaMKII) (see Figure 4.1). It is based on a detailed model of the Ins(145)P3 metabolism integrated with GPCR mediated PLC-beta activation and Ca^{2+} release by the InsP3 receptor [Mishra and Bhalla 2002] (available as accession #31 in the DOQCS database, http;//doqcs.ncbs.res.in), and has been modified for AT1 receptor activation and extended by the NaCa exchanger as has been published earlier [Sauter and Vadigepalli 2005]. It is very detailed in respect to the calcium buffering and explains the highly nonlinear response for low and high Ca^{2+} baseline due to an intracellular Ca^{2+} switch. The dynamics of a few important substances in response to AngII are shown in Figure 4.2. The model has been tuned to match time-course data on the intracellular Ca^{2+} concentration [Fernandez et al. 2003; Monck et al. 1990]. It was therefore our intent to preserve the model's internal structure, kinetics and parameters as far as possible. However, as we will see in Section 4.4 modifications were necessary to integrate the dynamic dependence of trans-membrane ion transport on the membrane potential.

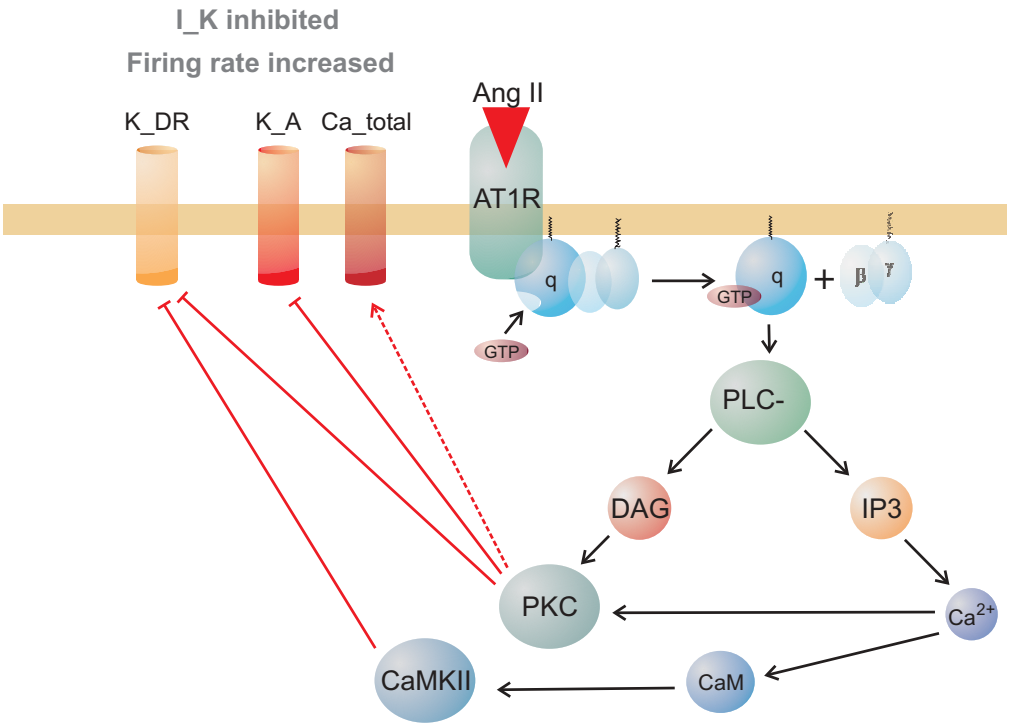

Figure 4.1: Simplified sketch of the AT1R signalling.

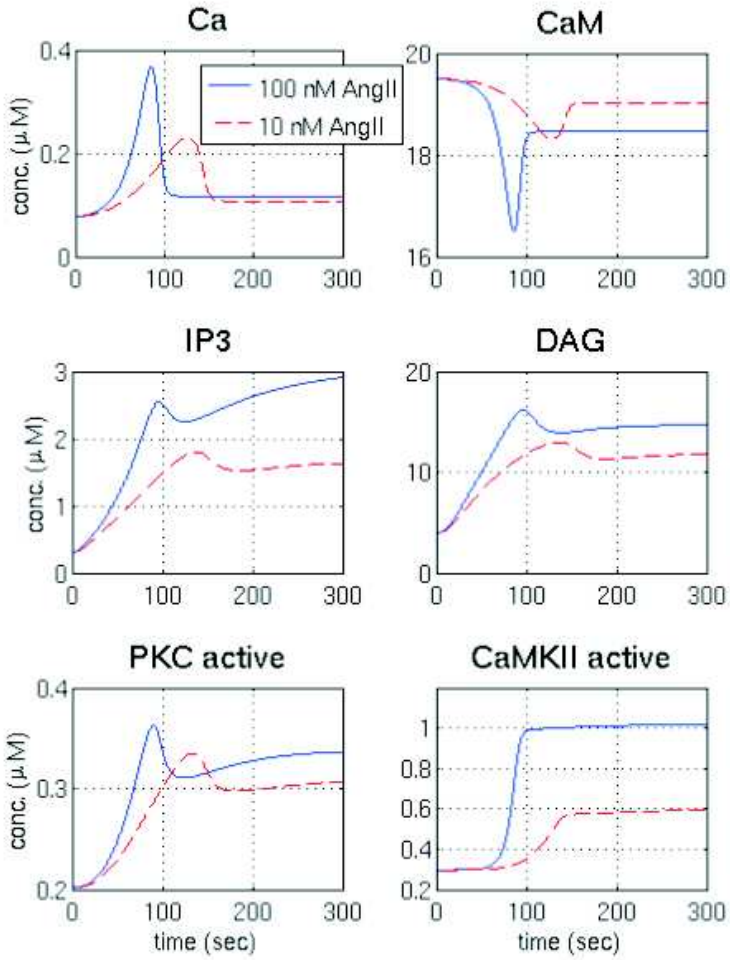

Figure 4.2: Response of the signaling model after an AngII step of 100 and 10 nM. The Ca^{2+} and CaM transients show high peaks, the concentrations of the second messengers IP3 and DAG are highly increased in steady state, as are the active forms of PKC and CaMKII. AngII dosages higher than 50 nM saturate the receptor, leading to faster transient dynamics, but not significantly higher PKC and CaMKII activation in steady state.

4.2 Model output: Active kinases PKC and CaMKII

To determine the total kinase activity of the model, one has to account for different active kinase forms. Both, PKC and CaMKII can form complexes with different activators as for instance Ca^{2+} and DAG or be phosphorylated at several binding sites (see Figures 4.3 and 4.4). We assumed that all active species present in the signaling model have similar catalytic activity. This means that the reaction constants describing subsequent protein modifications that are catalyzed by PKC and CaMKII respectively, as for instance ion channel phosphorylation, are equal. Then the active concentration of PKC and CaMKII can be calculated by building the sum of all active species (proof Appendix C):

$$\begin{aligned} PKC_{active} &= PKC\text{-}Ca\text{-}AA^* + PKC\text{-}AA^* + PKC\text{-}DAG\text{-}AA^* + \cdots \\ &\quad + PKC\text{-}DAG\text{-}memb^* + PKC\text{-}Ca\text{-}memb^* \\ CaMKII_{active} &= CaMKII^{***} + CaMKII\text{-}thr306 \end{aligned}$$

4.3 Analysis and response to AngII

4.4 Modifications (NaCa exchanger, ICa)

Since the electrophysiological membrane dynamics were of particular interest for the presented approach, it was necessary to extend the transmembrane processes of the signaling model by the therein neglected membrane potential. Generally, the actual rate of ion transport through the membrane is determined by the balance of electrical and chemical gradient forces,

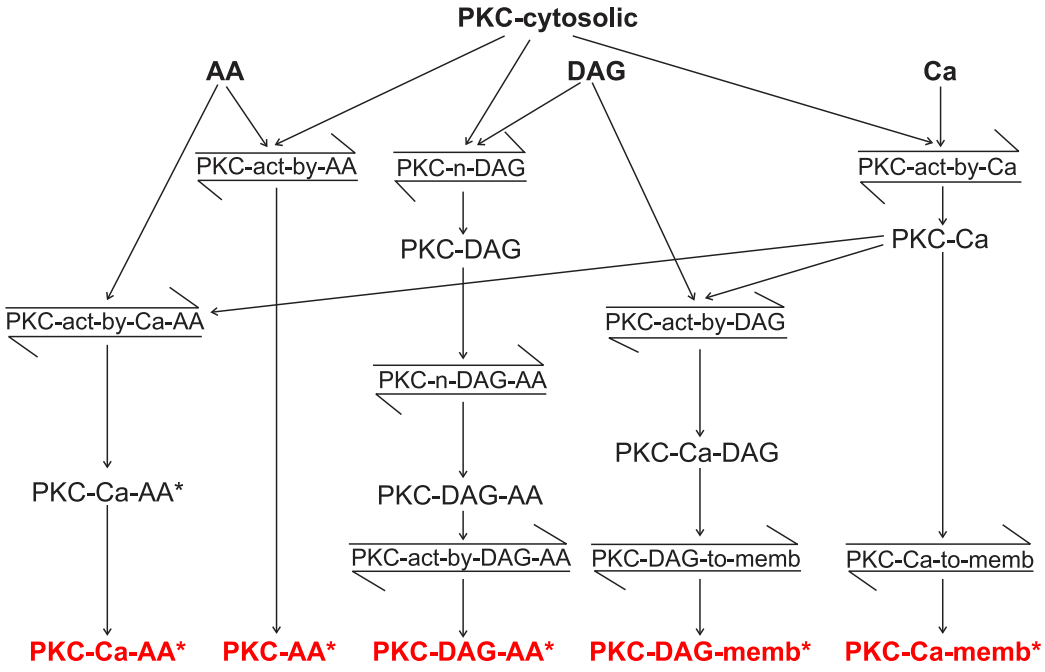

Figure 4.3: Reaction scheme of PKC activation. In addition to some basal PKC activity, PKC can be activated by binding Ca^{2+} , AA or DAG. However, it has to be translocated to the membrane in addition. These active (and membrane adhesive) species are marked red.

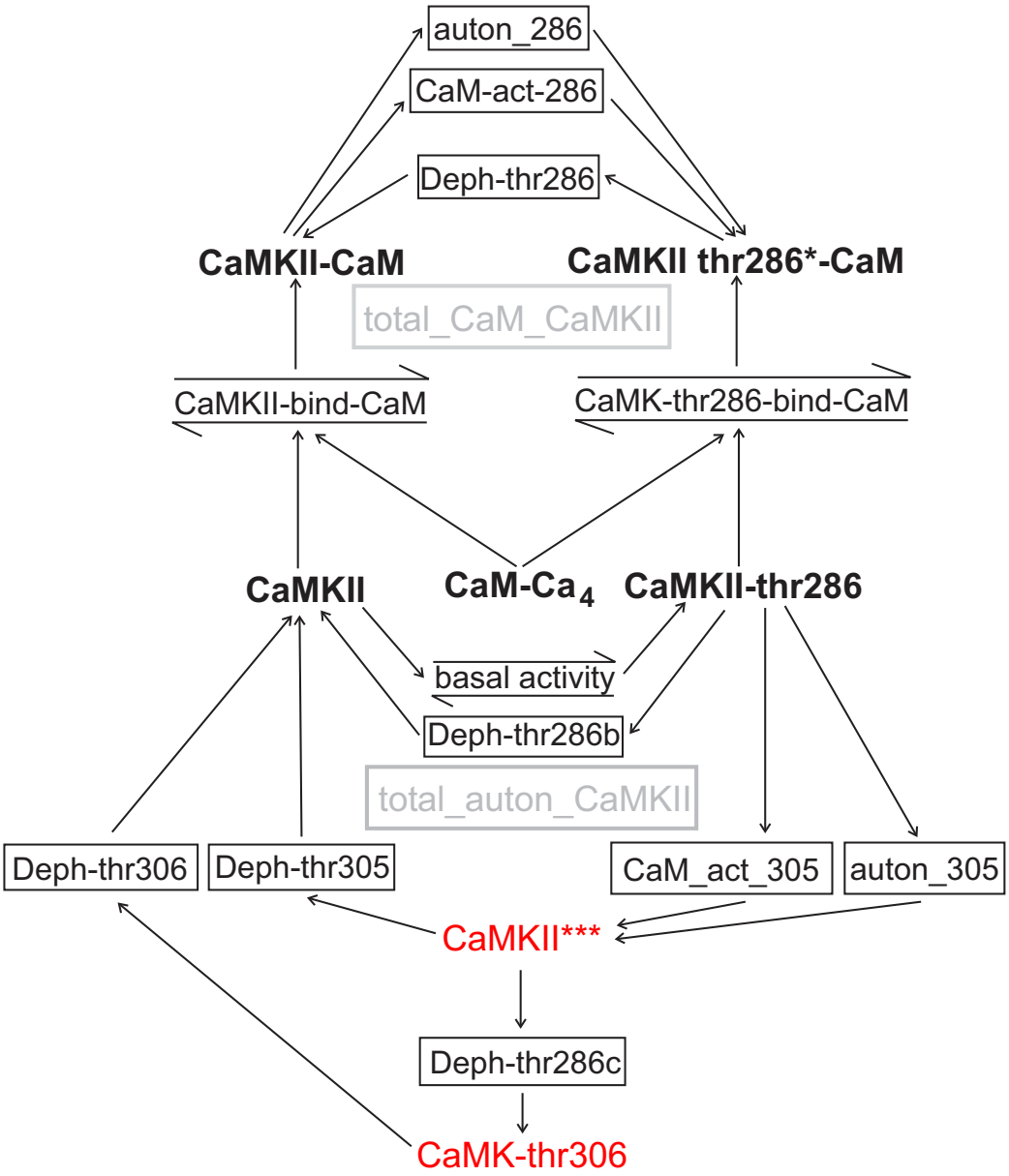

Figure 4.4: Reaction scheme of CaMKII activation. CaMKII can bind CaM, and be phosphorylated at the threonine (thr) residues number 286 and 305 or 306. It is catalytically active, if thr305 or thr306 are phosphorylated (indicated by red coloring).

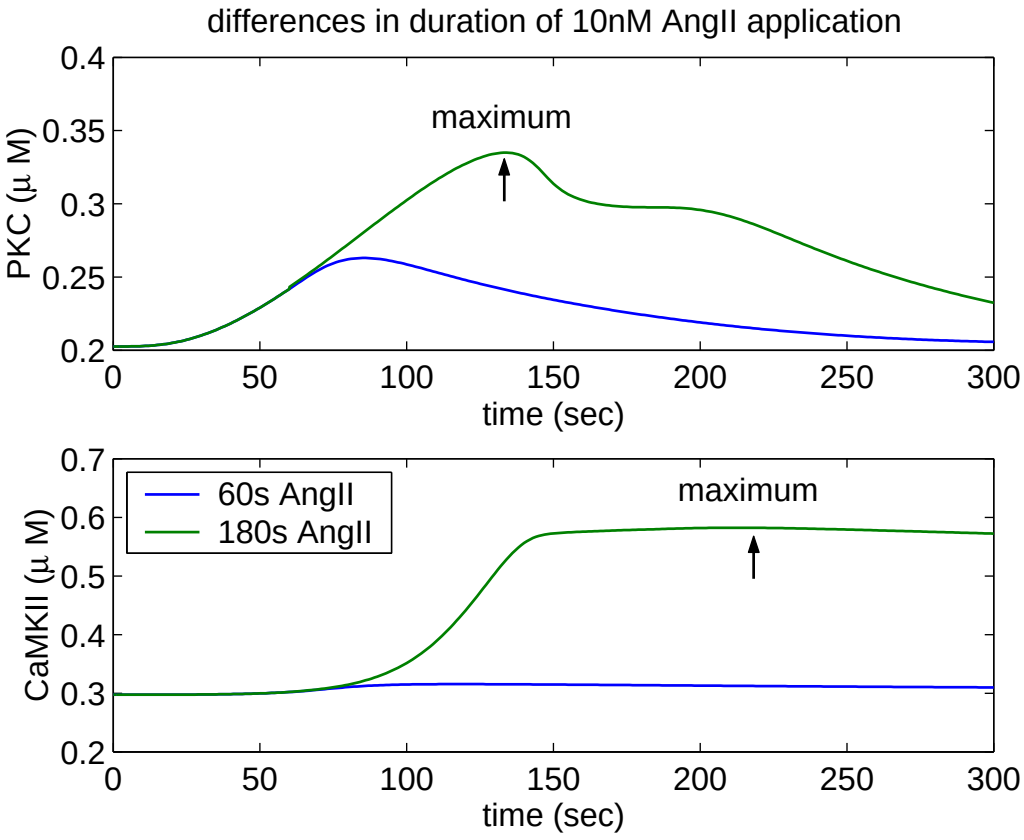

Figure 4.5: Comparison of 10 nM AngII application for 60 and 180 s. Active CaMKII shows practically no response to 60s AngII application, whereas active PKC concentration raises significantly. Consequently the duration of AngII treatment may be crucial, and lead to distinct responses of the CaMKII and PKC activity.

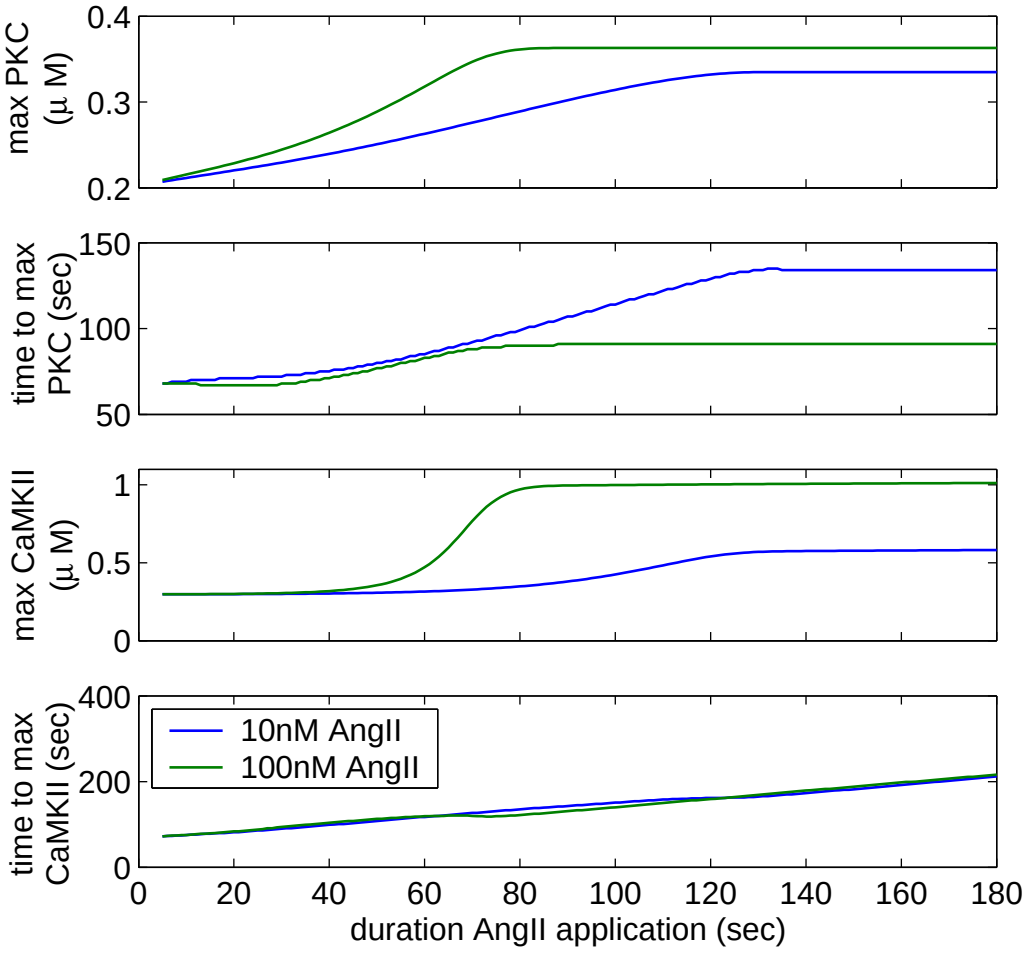

Figure 4.6: Characterization of the duration dependent responses of kinases activity due to application of 10 and 100 nM AngII for 1 to 180 seconds. PKC is linear dependent from AngII treatment duration until a dose dependent threshold is reached (The higher the dose, the higher the slope). For sufficiently high durations, the time at which the maximum is reached, depends only on the dose. In contrast CaMKII does not or barely activate for small durations, and the time at which its maximum is reached is not dose-dependent.

therefore additional factors based on energy barrier models were added to the biochemical rates of the calcium leak channels and the sodium-calcium-exchanger. Since the active transport performed by the calcium-pump is rather a chemical-ATP-driven than an electro-diffusion process, we assumed voltage independency in naccordance with models in literature [Schild et al. 1993].

The mathematical descriptions of the electro-diffusion processes were taken from Athanasiades et al. [2000] and present common Goldman-Hodgkin-Katz (GHK) models. The total leak flux is composed of two channels (see Mishra and Bhalla [2002]) and depends bilinear on the concentration gradient and a GHK term (Equation (4.1)).

$$r_{Ca,leak} = \left(-P_{leak1}c_{leak1} + \frac{P_{leak2}}{15}c_{leak2}\right)\zeta(Ca_{cyt} - Ca_{ex}e^{\zeta})\frac{1}{1-e^{\zeta}}$$

Where c_i denotes the channel concentration and P_i its permeability. Ca_{cyt} and Ca_{ex} denote the cytosolic and extracellular Ca^{2+} concentration respectively. The term $\zeta = \frac{zVF}{RT}$ introduces the connection to the membrane potential V, where $z = 2$ is the valency of calcium, F the Faraday constant, R the gas constant and T the temperature.

The electro-diffusion of the Na^{+}-Ca^{2+} exchanger is influenced by its stoichiometry of three Na ions inwards and one Ca^{2+} ion outwards, assessing the stoichiometry exponent in the influx and outflux terms DF_{in} and DF_{out} to r = 3. The chemical flux-component consists of a PKC-dependent regulatory part [Iwamoto et al. 1996, 1995], a Michaelis-Menten factor corresponding to allosteric activation by Ca^{2+} and a Michaelis-Menten term to capture the Ca^{2+} dependency at high concentrations [Philipson et al. 2002] (see Sauter

and Vadigepalli [2005]).

$$m_{chem} = -\left(1 + \frac{K_{PKCmod}}{1 + e^{\frac{K_{PKC} - 100[PKC] - 3}{D_{PKC}}}}\right) \frac{Ca_{cyt}}{k_m + Ca_{cyt}} \frac{Ca_{cyt}}{NaCa_{act} + Ca_{cyt}}$$

$$\begin{aligned} DF_{in} &= Ca_{ex} Na_{cyt}^r e^{\gamma\zeta} \\ DF_{out} &= Ca_{cyt} Na_{ex}^r e^{(\gamma-1)\zeta} \\ S &= 1 + D(Ca_{cyt} Na_{ex}^r - Ca_{ex} Na_{cyt}^r) \\ m_{GHK} &= -\frac{DF_{in} - DF_{out}}{S} \\ r_{NaCa} &= r_{nominal}\, m_{chem}\, m_{GHK} \end{aligned}$$

The PKC regulatory term rises from 1 to $(1 + K_{PKCmod})$ with increasing active PKC concentration [PKC]. The terms DF_{in} and DF_{out} correspond to electro-diffusion forces directed in- and outwards of the cell according to an energy barrier, which was here assumed to be symmetric: $\gamma = 0.5$. Notations are analogous to the previous equation, with Na_{cyt} and Na_{ex} denoting the cytosolic and extracellular sodium concentration.

Under normal conditions (at low frequencies), the membrane potential is most of the time approximately constant, waiting the next spike to be generated. In the following this potential is referred to as interspike potential. The nominal transport rate of the Na-Ca^{2+} exchanger r_{NaCa} and the permeabilities of the two transmembrane Ca^{2+} leak channels P_{leak1} and P_{leak2} were tuned in order to preserve the fluxes of the original model at the interspike membrane potential of the extended model. The such extended signalling model shows the same Ca^{2+} response to AngII stimulation as the original model.

Chapter 5

Model of ion-channel phosphorylation

5.1 PKC alone: equations for phosphorylated channel level and conductance

The total macroscopic (whole cell) conductance of a specific ion channel is determined by (1) its phosphorylation level and (2) the effect of phosphorylation on the channel's conductance. In a first step the phosphorylation of a channel (Kv) by only one kinase (PKC) is discussed, since it allows the explicit formulation of a quantitative relationship between kinase activity and channel conductance. Phosphorylation and dephosphorylation are considered as distinct processes mediated by the kinase and phophatase respectively. Consequently they are modeled as irreversible biochemical reactions

$$\begin{aligned} K\acute{v}^* + PKC &\xrightarrow{k_p} K\acute{v} + PKC \\ K\acute{v} &\xrightarrow{k_{dp}} K\acute{v}^* \end{aligned}$$

Since the electrophysiological processes of the HH model are approximately 1000 fold slower than the biochemical signaling reactions, a special mathematical interest of this phosphorylation lies in its steady state. Taking into account that the total concentration of channel protein remains unchanged $Kv = Kv_0 - Kv^*$, the quasi steady-state is calculated to:

$$Kv^* = \frac{Kv_0}{1 + K_{PKC} \cdot PKC} \quad \text{with } K_{PKC} = \frac{k_p}{k_{dp}} \tag{5.1}$$

To map the phosphorylation to the conductance, a weighted sum of the channel species by their corresponding normalized single channel conductance is used:

$$\bar{g} = Kv^* g^* + Kv\, g$$

This finally leads to an explicit formula for the total conductance:

$$\bar{g} = (x + y(1 - x))\, Kv_0 g \qquad \text{with } x = \frac{g^*}{g},\ y = \frac{1}{1 + K_{PKC}}$$

where y is a measure for the phosphorylation level, as is x for the single conductance change. K_{PKC} is the half activation constant of the phosphorylation process similar to the Michaelis-Menten constant. In fact this becomes the Michaelis-Menten kinetic for $x \mapsto 0$, meaning that phosphorylation switches the single channel conductance to zero. Since voltage gated potassium channels consist of four subunits, higher order kinetics (Hill kinetics) are likely and even necessary to achieve the required sensitivity needed to fit experimental data within a reasonable parameter range.

$$y = (1 + K_{PKC}^n PKC^n)^{-1} \tag{5.2}$$

We have chosen n = 4, which was intuitively considered natural given the fourfold structure of potassium channels. In principle this means, that all four subunits have to be phosphorylated, in order to significantly alter the channels conductance.

5.2 PKC and CaMKII: equations for phosphorylated channel level and conductance

If phosphorylation by two kinases is considered, the reaction scheme becomes more complex possessing four channel species and eight reactions, thus, preventing the derivation of a simple quasi steady state kinetic. The general reaction scheme for phosphorylation by PKC and CaMKII is given below, possessing the order n, meaning n sites have to be phosphorylated to complete the conductance switch.

$$\begin{array}{rcl@{\qquad}rcl}
Kv^* + n\ PKC & \xrightarrow{k_1} & Kv^1 + PKC & Kv^1 & \xrightarrow{k_{-1}} & Kv^* \\
Kv^* + n\ CaMKII & \xrightarrow{k_2} & Kv^2 + CaMKII & Kv^2 & \xrightarrow{k_{-2}} & Kv^* \\
Kv^1 + n\ CaMKII & \xrightarrow{k_2} & Kv^{1,2} + CaMKII & Kv^{1,2} & \xrightarrow{k_{-2}} & Kv^1 \\
Kv^2 + n\ PKC & \xrightarrow{k_1} & Kv^{1,2} + PKC & Kv^{1,2} & \xrightarrow{k_{-1}} & Kv^2
\end{array}$$

Different phosphorylation processes are assumed to be independent. Therefore both phosphorylation reactions mediated by PKC and CaMKII are described with a single reaction constant $k1$ and $k2$ respectively. The same concept applies for dephosphorylation. Consequently the system is parameterized by the two half phosphorylation constants

$$K_{PKC} = (k_1/k_{-1})^n \text{ and } K_{CaMKII} = (k_2/k_{-2})^n$$

For the potassium channels here, we propose $n = 4$, meaning that all four subunits have to be phosphorylated to switch the channel's conductance. This is a simplified model, regarding the channel phosphorylation as a single process, but taking its multi-step nature into account. This allows a parameterization that results in a low basal phosphorylation level (see Section 5.3). The dynamic description of this process consists of three ordinary differential equations, since the sum of all phosphorylation species has to equal the total

amount of channel concentration ($Kv^* + Kv1 + Kv2 + Kv12 = Kv_0$).

$$\begin{aligned}
\frac{d}{dt}Kv^* &= -k_1 Kv^* PKC^n - k_2 Kv^* CaMKII^n + k_{-1} Kv^1 + k_{-2} Kv^2 \qquad (5.3)\\
\frac{d}{dt}Kv^1 &= +k_{-1} Kv^* PKC^n - k_2 Kv^1 CaMKII^n \ldots \\
&\quad -k_{-1} Kv^1 + k_{-2}(Kv_0 - Kv^* - Kv^1 - Kv^2) \\
\frac{d}{dt}Kv^2 &= -k_1 Kv^2 PKC^n + k_2 Kv^* CaMKII^n \ldots \\
&\quad +k_{-1}(Kv_0 - Kv^* - Kv^1 - Kv^2) - k_{-2} Kv^2
\end{aligned}$$

In total, the active maximal conductance of the channel is then calculated as the sum of the different channel phosphorylation species weighted by their corresponding conductance.

$$\bar{g} = g^* Kv^* + g_1 Kv^1 + g_2 Kv^2 + g_{1,2}(Kv_0 - Kv^* - Kv^1 - Kv^2) \qquad (5.4)$$

As outlined in the introduction, PKC/CaMKII modulation of the delayed rectifier current is not necessarily due to the direct phosphorylation of the alpha subunit. However, this is not of crucial importance for our modeling purposes, since the kinases are simply regarded as mediators. From this point of view, it makes no difference if the phosphorylation site is located on the α subunit directly, or on an attached auxiliary subunit of the channel.

5.3 Parameter exploration (figures)

A comparison of the first and forth order phosphorylation model was performed, showing much higher sensitivity to changes in active PKC and CaMKII concentrations in the interesting area. This area of high sensitivity can be moved by changing the half phosphorylation constants. However, the basal and stimulated phosphorylation level can not be tuned independently, so that for the given basal kinase activity and a desired phosphorylation level the

change of phosphorylation due to AngII treatment is already assessed or vice versa. This is exemplified in Figure 5.1, where the model was tuned to a phosphorylation level of 70% in response to 100 nM AngII. This forces the basal phosphorylation of the first order model to a much higher value than for the fourth order model, thereby assessing a phosphorylation change of 12.5% and 27.7% respectively.

To explore reasonable parameters, the system was stimulated by 100 nM AngII and the normalized change of channel phosphorylation was determined as $(K\hat{v}^*_{Ang} - K\hat{v}^*_{noAng})/K\hat{v}^*_{noAng}$ and plotted via K_{PKC} and K_{CaMKII}. Since both kinases have shown to have an effect, the gradient of this surface must possess a nonzero value either direction (see Figure 5.2).

The transient behavior of the phosphorylation model is determined by the actual height of the phosphorylation and dephosphorylation constants (k_p, k_{dp}). Increasing k_p and k_{dp} such that the half activation remains unchanged, speeds up the process. To illustrate this behavior, a 1uM AngII pulse with 1 min duration (experiment in [Li and Guyenet 1996]) is applied on the system. The resulting peak of the phosphorylation level forms earlier and is of higher value (see Figure 5.3).

5.4 Matching the experimental data, Model tuning

Treatment with PKC or CaMKII inhibiting agents without AngII application barely has an effect on the K_{dr} current [Pan et al. 2001; Sun et al. 2002; Zhu et al. 1999]. This indicates a low basal channel phosphorylation, i.e. for normal kinase concentrations in the unstimulated state. A maximum of 10% basal channel phosphorylation for the unstimulated system has been

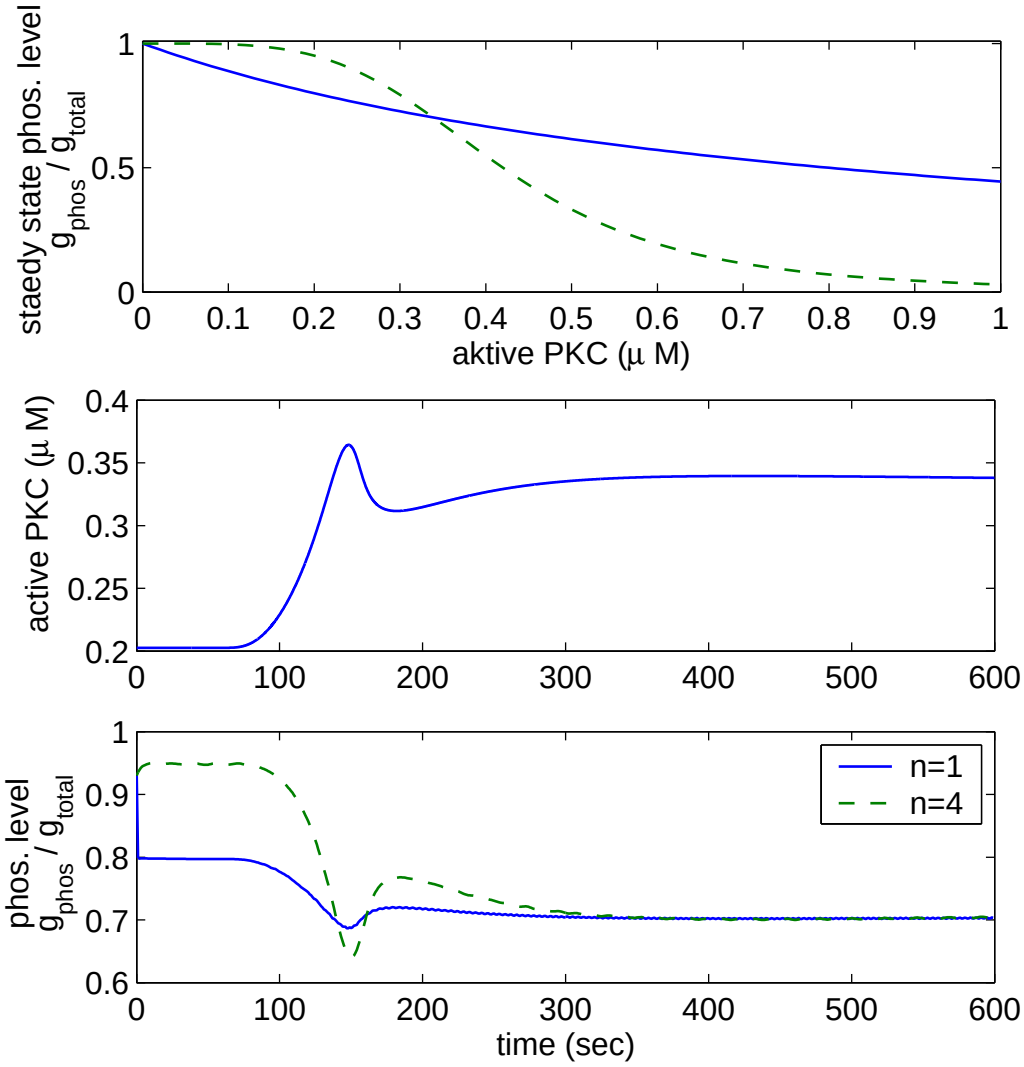

Figure 5.1: Comparison of the first and fourth order channel phosphorylation model. The fourth order model is much more sensitive than the first order model (uppermost plot, steeper slope). Tuning the models to a phosphorylation level of 70% after 100 nM AngII treatment, forces the basal phosphorylation of the first order model to a much higher value than the fourth order model. K_{PKC} was 0.8 for the 1. order model and 0.8 for the 4. order model.

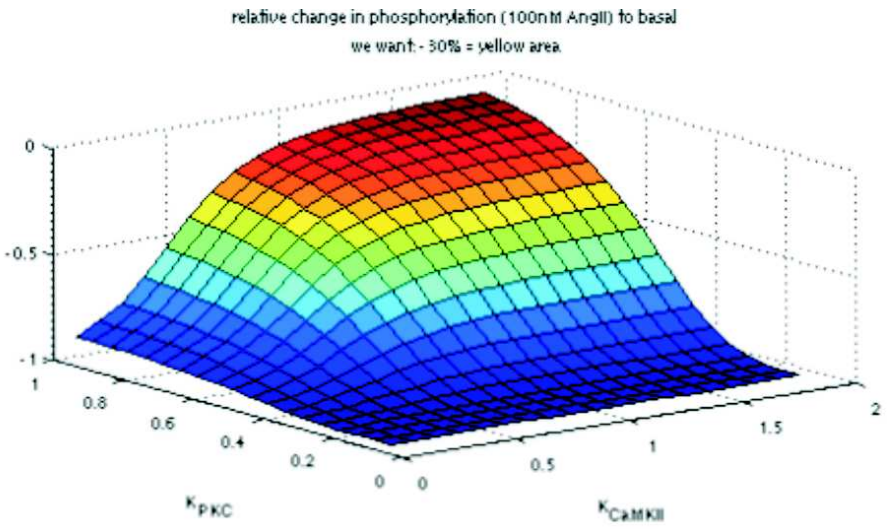

Figure 5.2: Parameter exploration to determine the region of reasonable PKC and CaMKII half phosphorylation constants (K_{PKC}, K_{CaMKII}). The signaling model was stimulated with an AngII step of 100 nM, and simulated for different K_{PKC} and K_{CaMKII}. The lower plot shows the timecourse of the active PKC and CaMKII concentration, which act as 'input' for the phosphorylation kinetic. The gradient of the surface has to have a nonzero value in PKC and CaMKII direction, since both kinases had an effect in experiments.

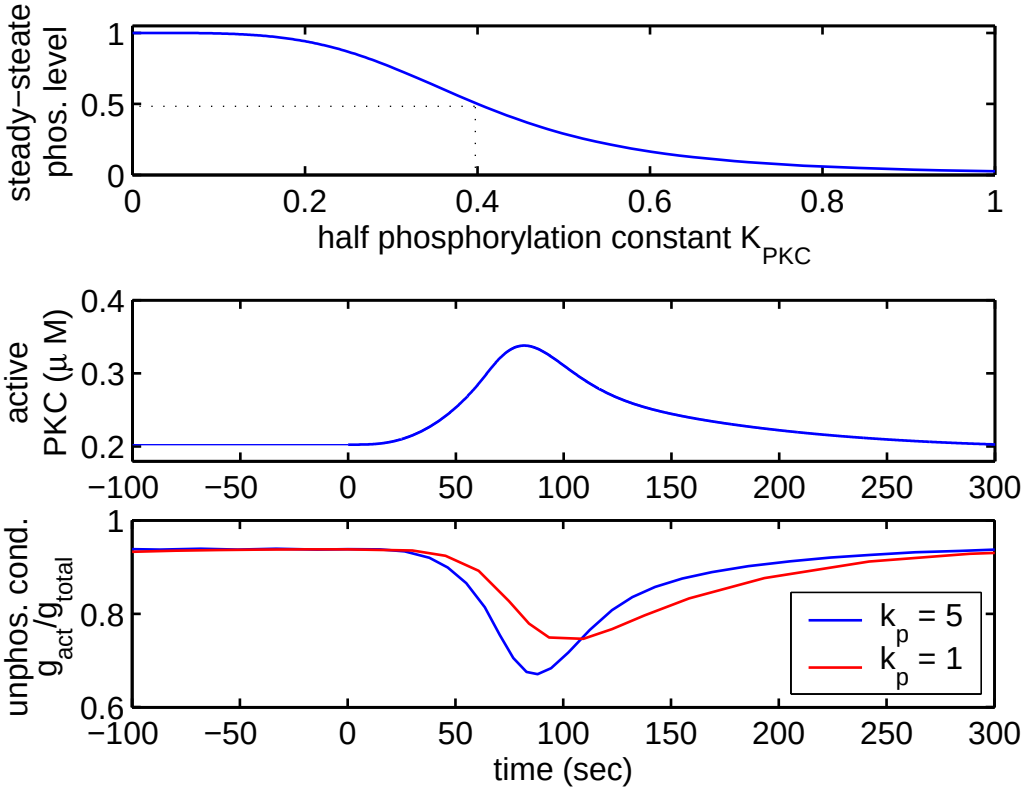

Figure 5.3: Analysis of the phosphorylation kinetics. Upper plot: For active PKC $\mapsto \infty$ the active channel $\mapsto 0$; Middle and lower plot: Time series simulation with 1 uM AngII at 0 sec for 60 sec showing the effect of increased the phosphorylation and dephosphorylation rates. Decreasing the rates of phosphorylation and dephosphorylation such that the steady-state remains unchanged, slows the phosphorylaton process down. Consequently the maximum is delayed and decreased.

assumed, to prevent considerable changes of ionic currents.

Further, the single channel conductance of the phosphorylated channel was assumed to be very small, so that it can be neglected ($x \mapsto 0$). This assumption is reasonable considering the effects of phosphorylation on K_{dr} related channel types mentioned in the introduction. For example, Kv1.1, a brain K_{dr} channel, was downregulated up to 90% due to phosphorylatoin by PKC.

With this limitations, first order kinetics were not able to reproduce experimentally observed conductance changes up to thirty percent, and give additional support for the proposed forth order kinetic. This hypothesis is insofar of biological relevance, as from a microscopic (single channel) point of view, completing the phosphorylation of the fourth subunit would possess the dominant effect on the channels conductance.

The model's predictions concerning the time-course of K_{dr} reduction were in good accordance with experimental data. Time-course data taken from [Pan et al. 2001] concerning a single experiment with 100 nM AngII application showed a change from a nominal value of 1.3 to a reduced value of 0.8 nA, and was fitted well by the model with a K_{PKC} and K_{CaMKII} constant of 0.475 and 1.4 respectively. Sufficiently high rates resulting in fast phosphorylation (here $k_p = 10$ and $k_p = 0.1$ respectively) were chosen (see Figure 5.4).

In the previous Chapter, the mean of maximal K_{dr} conductance reduction was identified to be between 25% and 30%. Based on this estimate and the assumption of fast phosphorylation, the parameters of the phosphorylation model were set to $K_{PKC} = 0.5$, $K_{CaMKII} = 1.5$, $k_1 = 10$ and $k_2 = 10$. The response of this model to 100 nM AngII is presented in Figure 5.5.

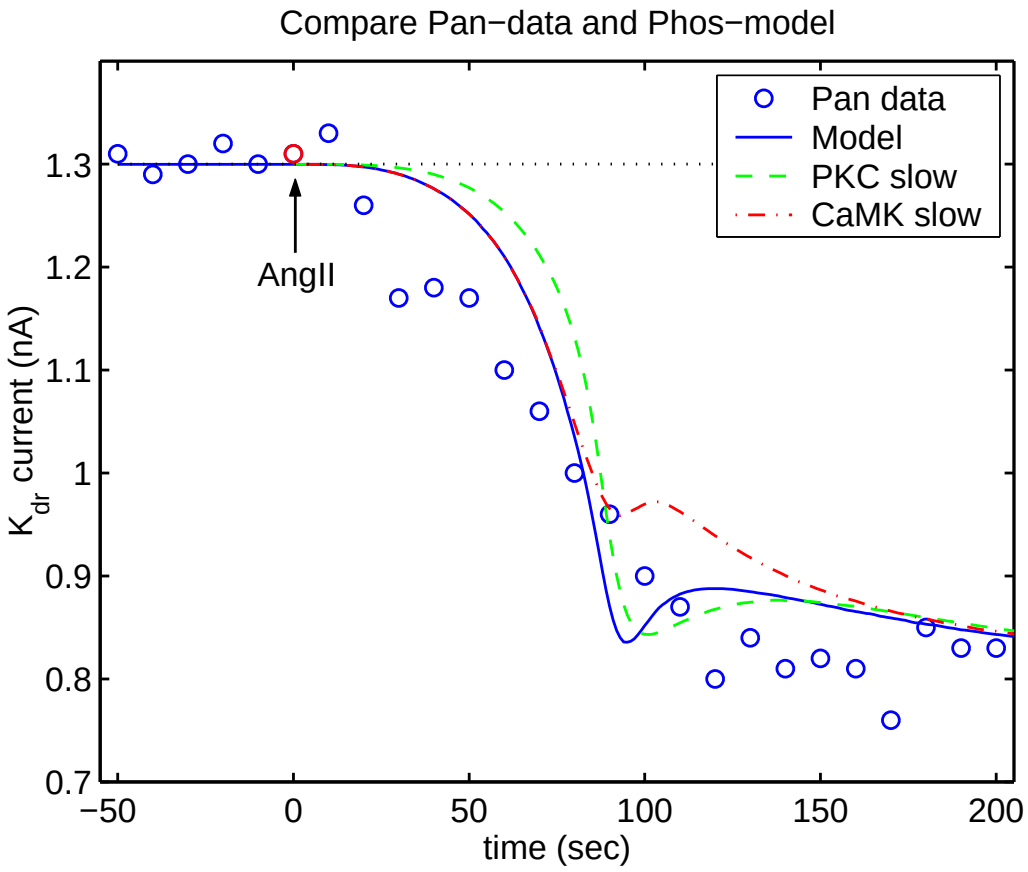

Figure 5.4: Time-course comparison of the phosphorylation model and Pan et al. [2001] data. The half phosphorylation constants K_{PKC} and K_{CaMKII} were set to 0.475 and 1.4 to result in the desired steady-state current reduction. k_1 and k_2 were chosen high: 10 and 0.1 respectively (this is close to the quasi steady state for the phosphorylation level). Slowing the PKC phosphorylation ($k_1 = 1$) delays the beginning of reduction, whereas slowing the CaMKII phosphorylation ($k_2 = 0.01$) flattens the transition close to its steady state.

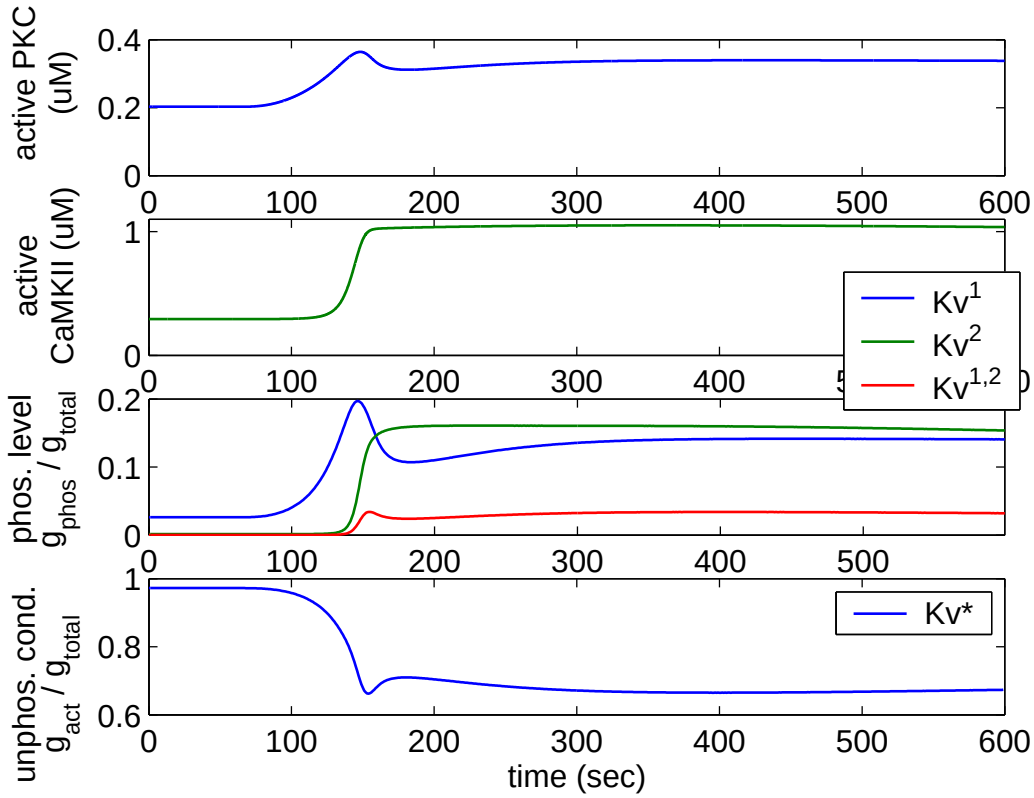

Figure 5.5: Response of the phosphorylation model as used in the combined model in the next chapter to 100 nM Ang II application. The total reduction of K_{dr} is approximately caused to half parts by PKC and CaMKII phosphorylation.

Chapter 6

Integrated signaling and membrane electrical model

To couple the above description of the phosphorylation to the signaling model, one has to account for different active kinase forms, since PKC and CaMKII can form complex formations with different activators as for instance Ca^{2+} and DAG or be phosphorylated at several binding sites. We assumed that all active species present in the signaling model possess similar catalytic activity, and the active concentration of PKC and CaMKII respectively as used in the Equations (5.1), (5.2) or (5.4) can be calculated by building the sum of all active species (proof in Appendix C).

6.1 Approximate approach: Signaling simulated first, use the results in HH model

The original signaling model neglects the dynamics of the membrane potential (see Chapter 4). Thereby, it is possible to connect it to the HH-model solely through the voltage-activated ion channel phosphorylation, using the

conductance mapping in Equation (5.4) as input or time-varying parameter for the HH-model. This approach allows it first to simulate the signalling model, and plug in the results in a second simulation of the HH-model. In the following, this approximate approach is referred to as the 'combined model'.

As mentioned in the previous chapter, phosphorylation at either site changes the conductance to zero. Therewith Equation (5.4) simplifies to

$$\bar{g} = g^* \cdot Kv^*$$

with $g^* = \frac{g_{max,Kdr}}{\bar{g}_{basal}} = \frac{0.9nA}{\bar{g}_{basal}}$, so that at the basal phosphorylation level (if no AngII is applied) the maximal conductance of the original HH-model is preserved.

6.1.1 AngII effect on firing frequency (figures)

We show now a simulation of the coupled model with stimulation of a 1 μM AngII pulse of 60 seconds duration, mimicking an experiment in Li and Guyenet [1996]. The model reproduces the experimental results very well, showing a fast peak after approximately 100 seconds, and a slow decay afterwards (compare Figure 2.1 on page 46 (Experiment) and Figure 6.1 (combined Model)).

6.2 A Rigorous approach: Accounting for Ca2+ balance, NaCa exchanger etc

The above presented coupled model, and the therewith performed simulations can only present preliminary results, since there are two inconsistencies. First, the membrane potential was neglected in the signaling model, but its dynamics are a basic feature of the HH-model. Second, ionic currents caused

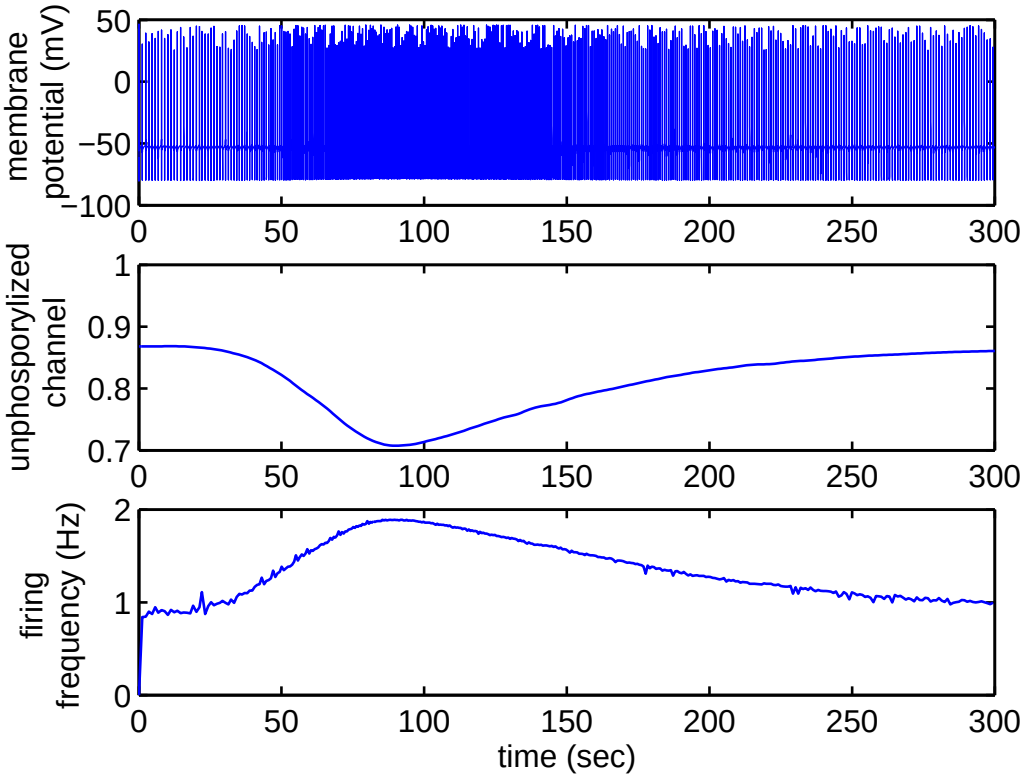

Figure 6.1: Using the phosphorylation level (normalized active channel) obtained by simulation of the signaling model (1 uM AngII from 0 to 60 s) as input or time varying parameter in the HH model relates the intracellular AngII response in a time dependent manor to the electrical membrane behavior and the firing frequency.

by non-voltage-gated ion transporters that are part of the signaling model are neglected in the HH-model. To result in a sound model that integrates the firing behavior and its intracellular modulation, both model-parts have to be set on the same basis with consistent assumptions.

Incorporation of the membrane dynamics into the signaling model was achieved by extending the existent Na-Ca^{2+} exchange and Ca^{2+} leak descriptions with terms based on energy barrier models for the electro-diffusion as described in Chapter 4 on page 76.

Including currents caused by ion transport of the signaling model in the HH-Model

Each ion flux through the outer cell membrane produces an ionic current, contributing to intracellular ion concentrations and the membrane potential, and can be described in chemical or electrical form. In an integrated model it is therefore of fundamental importance to model transport rates and currents consistently according to cytosolic volume and membrane surface.

Since neurons show a huge variability in cell size, we calculated the cytosolic volume based on assumptions about the membrane surface that underlie the HH-model, and supposed a perfectly spherical soma. In consistence with original assumptions of Bhalla, a correction of 16% was considered additionally, accounting for the space claimed by the endoplasmatic reticulum (ER). The molar transport-rates (normalized in respect to the cytosolic volume) are converted into whole-cell currents using the factor $I/r = zv_{cyt}F10^3$, where v_{cyt} is the cytosolic volume $[m^3]$, 10^3 is a unit conversion factor (HH-model: I [nA]; Sig-model: r $[\frac{\mu M}{sec}]$), z the valency of the transported ion and F the Faraday constant $[\frac{secA}{mol}]$. Here, the current is counted in direction of the Ca^{2+} flux, thus for pure Ca^{2+} transport, as for instance leak channels and pumps,

the valency number z is 2. The stoichiometry of the Na-Ca^{2+} exchange is 3:1; for each extruded Ca^{2+} ion three Na ions enter the cell. Consequently, the net valence flux is one positive charge per ion in opposite direction to the Ca^{2+} flux: $z = -1$. The cytosolic volume v_{cyt} is calculated based on the estimated membrane surface used in the HH-model and the assumption of a perfectly spherical soma (see Appendix D).

The correct modeling of the calcium dynamics was crucial for the expected changes in firing behavior and overall performance of the model. The calcium concentration activating the K_{ahp} has to be modeled separately from the free cytosolic calcium, since otherwise the immense increase in cytosolic concentration activates the polarizing potassium current of K_{ahp} far beyond saturation and prevents the neuron from firing. The interplay between K_{ahp} and Ca_L is however responsible for frequency adaptation. In order to not lose this features it is necessary to introduce a calcium pool that is distinct from the cytosol. We postulate a K_{ahp} -Ca_L -cluster with autonomous calcium dynamics, and used the calcium regulation module of the original Rybak model for this cluster:

$$\frac{d[Ca^{2+}]_{cl}}{dt} = \frac{I_{Ca,L}}{2Fv_{cl}}(1 - \underbrace{\frac{0.03}{[Ca^{2+}]_{cl} + 0.031}}_{Buffer}) + \underbrace{\frac{[Ca^{2+}]_{0,cl} - [Ca^{2+}]_{cl}}{17.7exp(V/35)}}_{Transport,Leak}$$

Where $[Ca^{2+}]_{cl}$ is the actual calcium concentration in the cluster, $[Ca^{2+}]_{0,cl}$ the basal level, $I_{Ca,L}$ the current of the L-type Ca^{2+} channel, F the Faraday constant, v_{cl} the volume of the cluster and V the membrane potential.

The here presented version of the integrated model combines the signalling model and the HH-model through the phosphorylation of K_{dr} by PKC and CaMKII as described in the previous chapter and the described couplings arising from the membrane potential dependency. It was tuned to a basal firing frequency of approximately 1 Hz by adapting the equilibrium

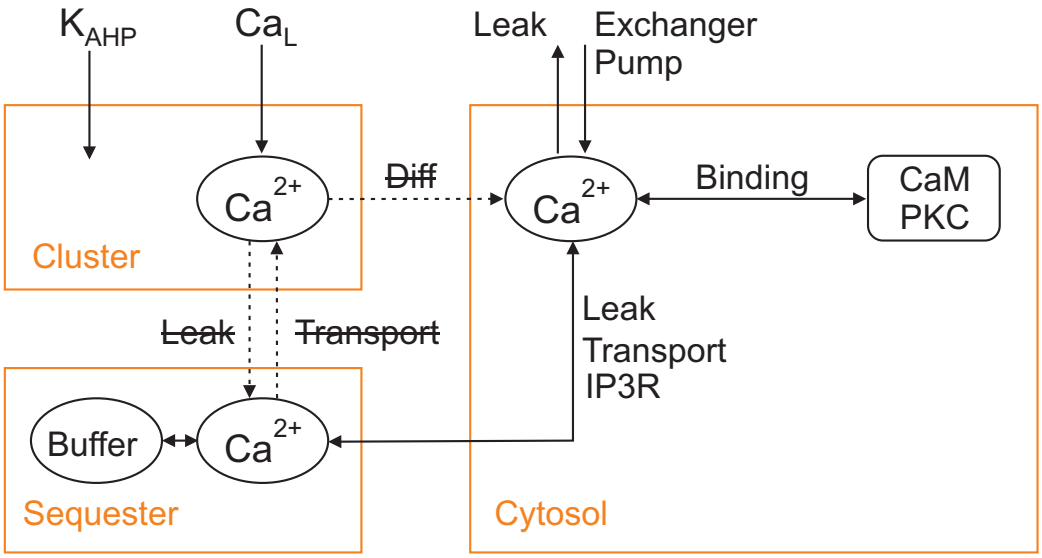

Figure 6.2: Scheme of the internal structure of the integrated model. The Ca^{2+} dynamics of the K_{AHP}-Ca_L -cluster is modelled separately, using the Ca^{2+} regulation module of the original Rybak model. This means there is no diffusion nor any kind of transport between the cluster and the sequester or cytosol.

potential of the leak channel E_{leak}. Like the original Rybak model, it shows frequency adaptation after current injection (see figure 6.3).

6.2.1 AngII effect on firing frequency (figures)

Simulating an AngII pulse of 1 μM for 60 seconds results in an increase of the firing rate starting at approximately 30 s, raising to a fast peak at 100 s and slowly decaying afterwards. This is in very good accordance with experiments in Li and Guyenet [1996] (compare figure 2.1 with 6.4). Continuous application of 10 nM increases the firing rate about 0.6 Hz (60%).

A comparison of the model response for receptor non-saturating (10 nM) and saturating (100 nM) AngII dosages showed no significant difference in the steady state phosphorylation by PKC, but a big difference in phosphorylation by CaMKII, indicating the increasing influence of CaMKII phosphorylation for higher AngII dosages. In both cases the transient behavior was accelerated (see Figure 6.5).

6.2.2 Effect of different phosphorylation kinetics (figures)

Further analysis of the fully integrated model revealed an effect of non-voltage activated transport modulation on the firing rate. In response to AngII treatment, the Ca^{2+} pump, the leak channels and the Na-Ca^{2+} exchanger are modulated, regulating the intracellular Ca^{2+} concentration. The resulting changes of the corresponding ionic currents lead to a transient decrease of the firing frequency prior to a slight increase, if the phosphorylation of the voltage activated K_{dr} channel is blocked (see Figure 6.4).

Separately blocking the phosphorylation by PKC and CaMKII by set-

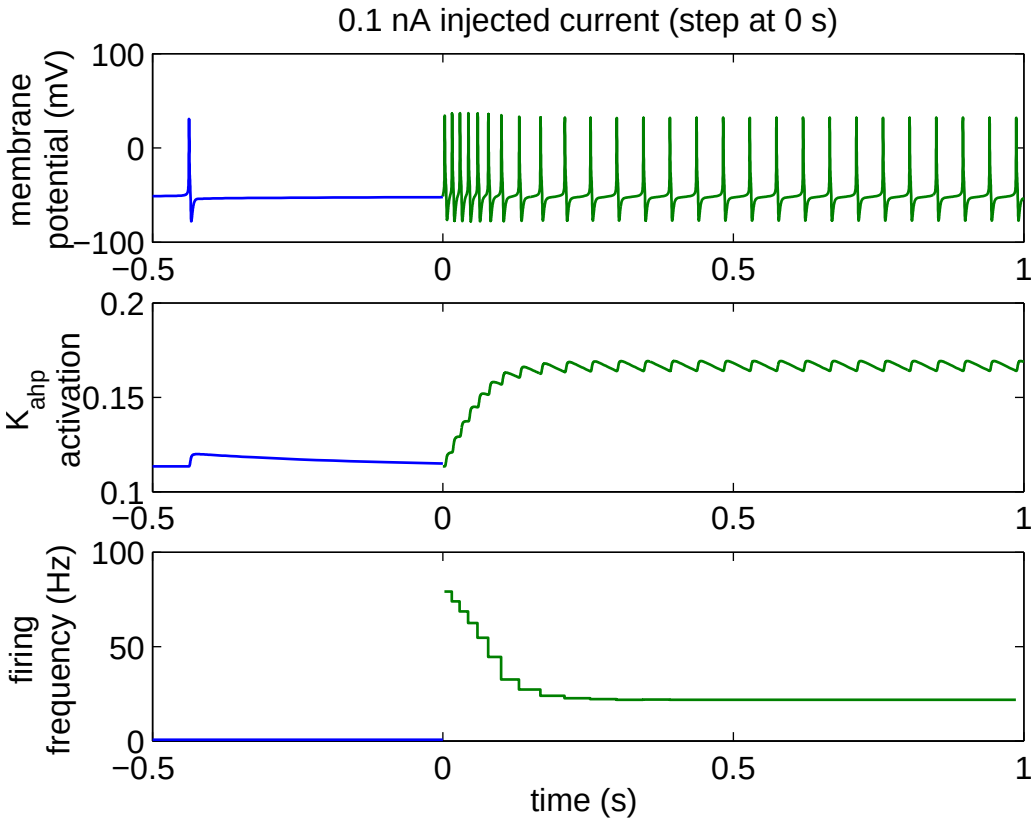

Figure 6.3: The integrated model shows frequency adaptation, after current injection, caused by the slow K_{ahp} activation due to rapidly following Ca^{2+} peaks in the Ca_L -K_{ahp} -cluster. A current of 0.1 nA at t = 0 s was injected at the basal firing rate of 0.68 Hz.

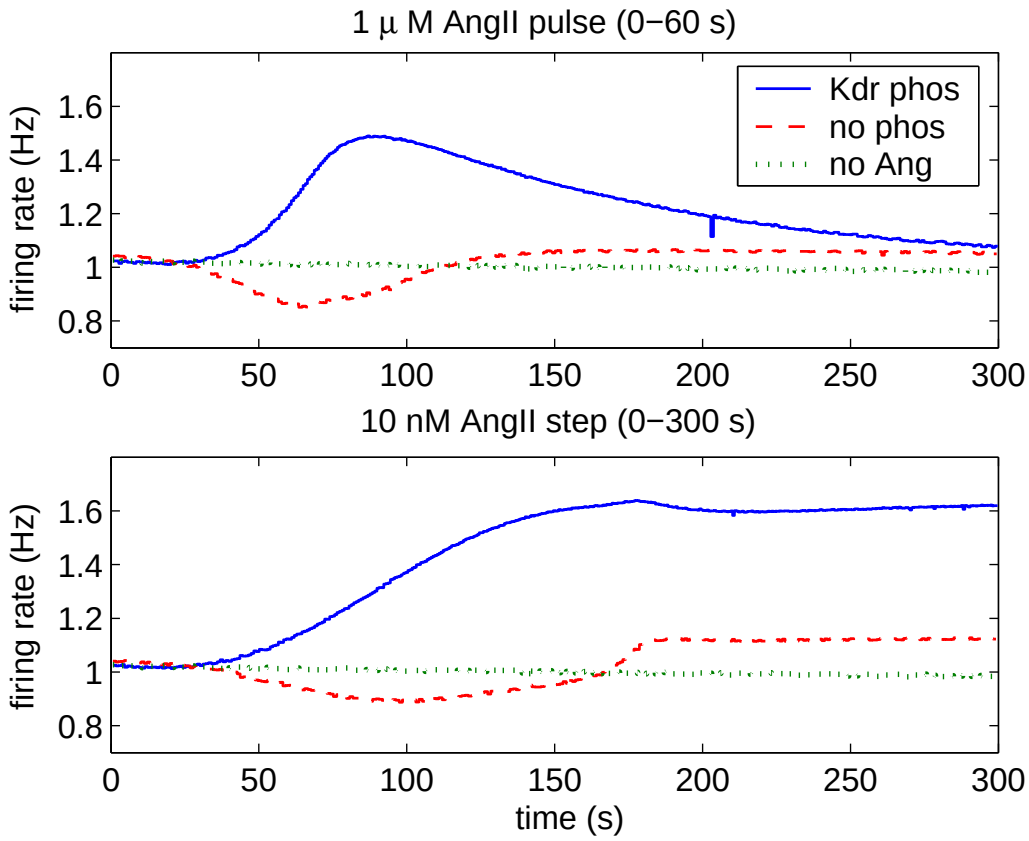

Figure 6.4: Simulation of the integrated model possessing a basal firing rate of 1.07 Hz. Stimulation with AngII increases the firing rate as observed experimentally. Upper plot: Firing frequency after application of 1 micro M AngII for 1 min (Li and Guyenet [1996] data). Lower plot: after application of 10 nM Ang II continuously (Sumners and friends data). The plot shows that simulation without phosphorylation of K_{dr} results in slightly increased firing rates, though it causes slight decreases during the transition.

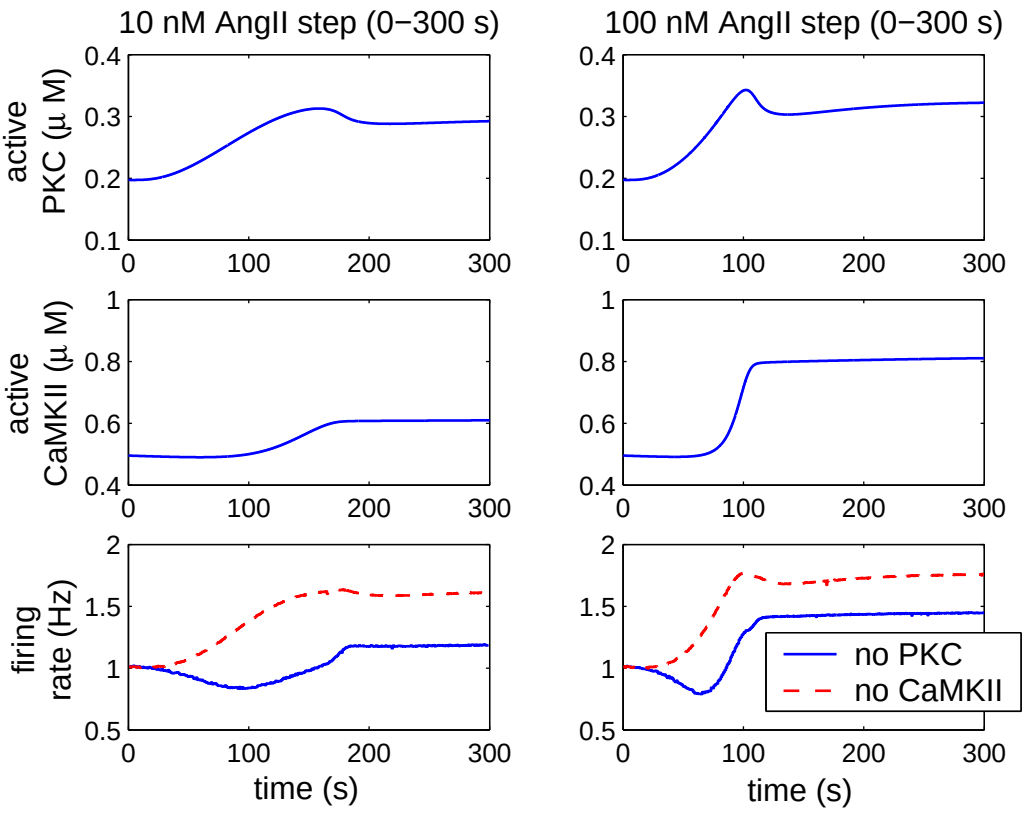

Figure 6.5: AngII response of the integrated model as above visualizing the differences of unsaturated (10 nM) and saturated (100 nM) AT1R. The steady state phosphorylation by PKC shows almost the same value, whereas phosphorylation by CaMK II is significantly higher for the saturated receptor. In both cases, the higher AngII dose accelerated the transition. PKC phosphorylation is responsible for the prevention of the transient firing rate decrease.

ting its reaction rates to zero revealed that phosphorylation by PKC alone prevents from this transient inhibitory effect (see Figure 6.6).

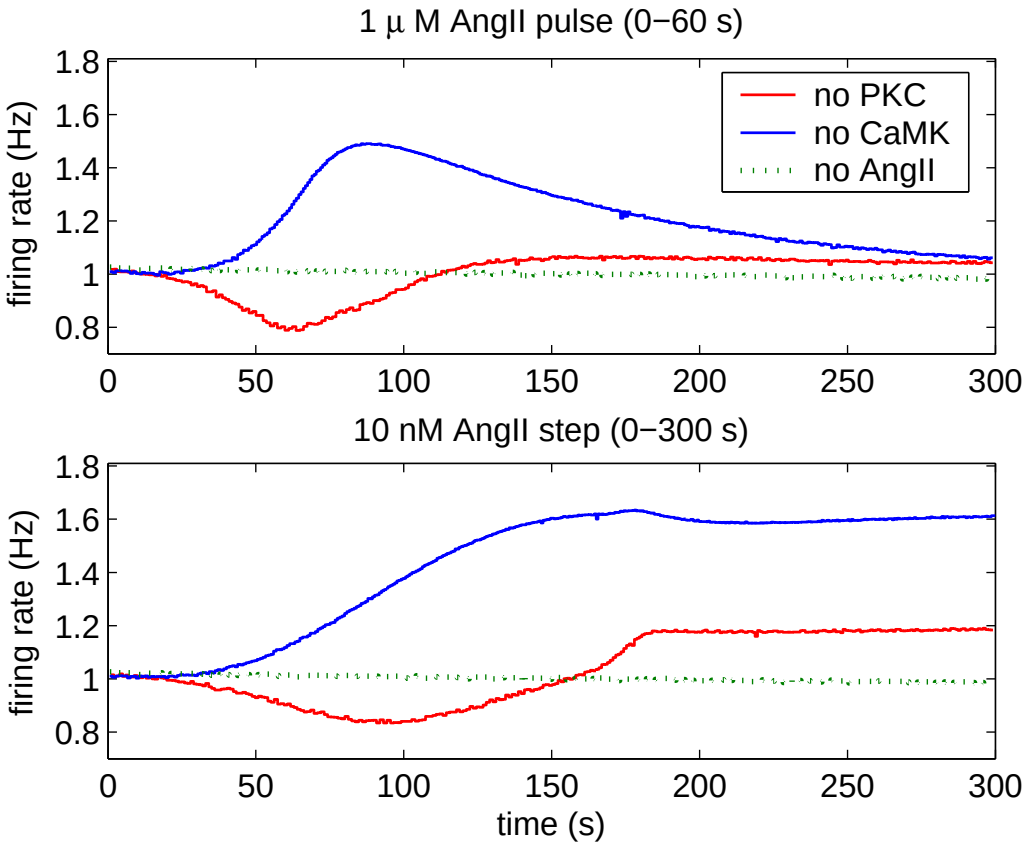

Figure 6.6: Simulation of the model only with PKC or CaMKII phosphorylation. The transient decrease of the firing frequency is prevented exclusively by the PKC phosphorylation of the K_{dr} channel.

Chapter 7

Discussion and Conclusions

This work focused on the modulation/phosphorylation of voltage activated potassium channels as immediate response of AT1R stimulation. The focus on K_{dr} and K_a was chosen because of the amount and quality of available experimental data. In order to put the work of this thesis into context, experimental studies regarding the AngII modulation of other channels as well as modeling studies regarding NTS neurons in general are briefly discussed in the following.

Modulation of other channel types

AngII modulation of the total Ca^{2+} current has been reported, however no details concerning the involved subtypes and/or voltage dependencies are currently available in the published literature. Unpublished observations suggest the inhibition due to attenuation of a negative effect of the G-protein beta-gamma subunit (mentioned in Sumners et al. [2002]). It has been proposed, that blood pressure related NTS neurons showing frequency adaptation express L-type but no T-type Ca^{2+} channels [Rybak et al. 1997]. A bimodal

effect of AngII on L-type Ca^{2+} channels in retinal ganglion cells has been reported [Guenther et al. 1997, 1996], showing a reduction of 33+-7% in 59% of all cases and an increase of 31+-6% in 41% of all experiments. An effect of PKC on L-type calcium channels has been shown in NG108-15 cells, which showed an inhibition of the Ca_L current due to bradykinin[1] application. However, introducing Ca_L activation in the HH model did not exhibit the expected results, namely the activation of firing. By this reason, we hypothize that Ca_L is not subject of AngII modulation, and the activation of the total Ca^{2+} current arises from a different channel subtype.

The inhibition of a potassium leak channel was proposed to be the underlying mechanism of AngII mediated effect on rat bulbospinal neurons [Li and Guyenet 1996]. However, the positive effect on the firing behavior in those neurons was attended by a membrane depolarization, which is not seen for hypothalamic and brain stem neurons. We did not intend to rule out these or other effects of AngII on voltage gated ion channels and their possible involvement on neuronal firing.

Electrophysiological models

Modeling of individual neurons and small networks of biological neurons has been widely used to analyze neuronal function. NTS neuron models have been published earlier, each highlighting different aspects. The first integration of multiple ion channels in a computational model for NTS neurons was published in 1993 [Schild et al. 1993; Schwaber et al. 1993]. Different firing patterns as ramp firing and frequency adaptation were explained by different

[1]Bradykinin activates a pathway very similar to that of Angiotensin, however its effect seem to be opposite. The factor responsible for this behavioral change is still unknown

functional expression of T-Type and L-type Ca^{2+} channels in combination with a Ca^{2+} dependent potassium channel [Rybak et al. 1997]. Closed loop neuronal regulation of blood pressure was studied by connecting HH models together to neuronal networks mimicking realistic NTS brain activity [Vadigepalli et al. 2001; Rogers et al. 2000]. Neurotransmitter release and related processes were modeled to analyze synaptic function [Schild et al. 1995]. Also an immense set of data was used to parameterize a very detailed NTS model to the quantitatively best possible result [Athanasiades et al. 2000]. Further minimalistic models have been analyzed, to clarify theoretical principles and mathematical necessaries of repetitive firing and bursting [Butera et al. 1999].

7.1 Summary of own results

The intend of this study was to discuss AngII mediated changes of neuronal conductances in NTS neurons and its effects on neuronal firing and excitability by means of mathematical and computational modeling, and provide an exemplary case study of electrophysiological and signal-transductional model integration.

Our modeling results led us to the hypothesis of the K_{dr} channel acting as a dual regulator, thereby distinguishing between high and low firing frequencies. This hypothesis could be easily validated by performing patch clamp experiments including current injections and pharmacological channel blocking.

Further we hypothesize that regulation of non-voltage activated transmembrane ion transport plays a role in neuropeptid induced alterations of neuronal firing activity. In our simulation this regulation led to a transient

decrease in the firing frequency, when the PKC phosphorylation of the K_{dr} channel was blocked. This is a result that is also easily testable experimentally by obtaining time-course data of the AngII response in combinations with PKC blocking.

It was demonstrated, that the separate regulation of the cytosolic and the K_{ahp} -Ca_L -cluster related Ca^{2+} dynamics is necessary to integrate experimental results of neurophysiology and quantitative signaling related molecular biology. This indicates the importance of spatial phenomena and specific local Ca^{2+} regulation. The ability of Ca^{2+} to act as dual encoder distinguishing signals locally has been presented in Naoki et al. [2005].

7.2 Conclusions

In this study, the neuron was considered as an electrical signal processing unit. The output, the firing frequency, is generated from the input, synaptic excitation received from upstream neurons, through the 'physiological transfer function'. The modulation of this transfer function is an important component of nearly all (higher) brain functions.

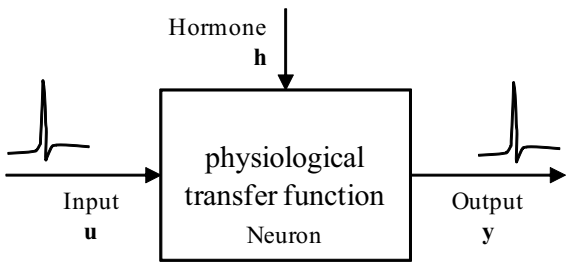

Dynamic mathematical modeling was used to explain and analyze such modulation on two levels: The electrophysiology and the signal transduction. We provided a first case study for such a modeling process, and succeeded

in a fully integrated model of AngII AT1R related intracellular signaling and electrophysiological membrane behavior. The key aspect of this integration is the link of a Hodgkin Huxley like model of the neuronal firing behavior and a detailed reaction kinetic model of the intracellular signaling pathway. This link is the change of the the maximal conductance of the delayed rectifier potassium channel upon its phosphorylation by the signaling kinases CaMKII and PKC.

The process of such model integration and its difficulties were discussed exemplarily, and our proposed solutions were presented. Systems theoretical methods as for instance sensitivity analyses, revealing the regulatory principles of voltage-gated ion channel modulation, or parameter exploration studies have shown to be useful, if not even necessary tools, to achieve a successful model integration.

The resulting model combines the features of the signaling and the electrophysiological model, and is capable of explaining the highly nonlinear AT1 receptor mediated Ca^{2+} response of neurons in the mammalian brain, as well as frequency adaptation related to synaptic-excitation. Most importantly, the integrated model is able to explain neuropeptid induced neuronal plasticity, and revealed an effect of transmembrane Ca^{2+} transport regulation on the firing frequency. This is a result that could only be obtained by a complete model integration as presented here.

There are longer term actions of AngII involving effects on noadrenalin synthesis as well as modulation of substance P and glutamatergic pathways, not only mediated by the AT1 but also the Angiotensin Type 2 (AT2) receptor. Despite the variety and abundance of AngII mediated effects in neurons, our integrated model is the first step towards wholistic understanding of neuropeptid induced neuronal plasticity.

The presented integrated model forms the basis for developing a multi-scale neuronal adaptation model that integrates electrophysiology, signaling and gene regulation. The particular system considered is of special medical importance for hypertension, since the NTS and AngII are involved in the blood pressure regulation.

7.3 Suggestion for future work

Since there are still some unanswered questions, we suggest further experiments, theoretical analysis and modeling. The phosphorylation site of Kv2.2 responsible for the AngII induced modulation of K_{dr} could not been identified and involvement of additional molecules as for instance beta subunits is possible. Also the processes involved in the total Ca^{2+} current modulation are still unclear, and it is not known which type of Ca^{2+} current is modulated and which subunits are responsible. The activation of the L-type Ca^{2+} channel in the model showed an effect opposite to the observed AngII responsive behavior, which is explained by the increased Ca^{2+} peaks leading to activation of K_{ahp} and a decrease in neuronal firing. It is therefore likely that other channel types as for example N- or T-type are responsible for the increased Ca^{2+} current. In the presented model, the Ca^{2+} current across the membrane are altered, due to AngII mediated regulation of the Na-Ca^{2+} exchanger and the Ca^{2+} leak channels, presenting examples of modulation of non-voltage-gated transport.

In order to verify and refine the phosphorylation model, quantitative measurements of channel phosphorylation, as well as time-series data of the frequency change or crucial intracellular signaling molecules (as for instance PKC and CaMKII) are necessary. Detailed analyses of different phosphory-

lation mechanisms (direct (see Chapter 5.3) and through intermediate complexes (see Appendix C) have been analyzed, so that the integration of experimental data on this topic would be most beneficial.

In addition, further modeling is required, to include the shift of the voltage dependency of the K_a activation and its maximal conductance modulation. Our findings suggest however, that this has minor effect on the firing frequency. It would be interesting to investigate the influence of this and other channel modulations on the shape of the action potential.

Modulation of the Ca^{2+} current can be included in the model as soon as experimental data becomes available. Although our computational experiments suggested that the time constants or kinetics of the channel activation and inactivation have minor effects on the frequency, experimental data concerning their modulation would be interesting, especially to investigate possible alterations of the action potential's shape.

Further the signaling model is very complex, composed of about 170 states, which arises from the fact that it is based on detailed reaction kinetic data. The integrated model is very stiff, since the time constants of the signalling model are about 1000 fold bigger than these of the channel kinetics. Both, the complexity and the stiffness make computational studies very expensive. It is therefore advisable to investigate the possibilities of model reduction for the signalling model. Less complexity of the model would also easy its validation and parametrization, since the data it relies on is obtained from several cell-lines and even cell types.

In addition to the discussed immediate actions, the AT1R pathway involve Janus kinase 2 (JAK2) association in a G-protein independent manner and the subsequent activation of transcription (STAT) molecules, as well as transactivation of tyrosine kinase pathways (e.g. Ras, MAPK) which involves

the transcription factors c-Jun c-Fos and NF-kappaB [Sumners et al. 2002; Richards et al. 1999; Huang et al. 1998; Lu et al. 1998; Marrero et al. 1996]. All these effects can be included in future modeling studies.

Bibliography

Alberi, S., Boeijinga, P. H., Raggenbass, M., and Boddeke, H. W. (2000). Involvement of calmodulin-dependent protein kinase II in carbachol-induced rhythmic activity in the hippocampus of the rat. *Brain Res*, 872(1-2):11–19.

Alberts, B., Johnson, A., Lewis, J., Raff, M., Roberts, K., and Walter, P. (2002). *Molecular Biology of the Cell*. Garland Publishing.

Athanasiades, A., Clark, J. W., Ghorbel, F., and Bidani, A. (2000). An ionic current model for medullary respiratory neurons. *J Comput Neurosci*, 9(3):237–257.

Barnes, K. L., DeWeese, D. M., and Andresen, M. C. (2003). Angiotensin potentiates excitatory sensory synaptic transmission to medial solitary tract nucleus neurons. *Am J Physiol Regul Integr Comp Physiol*, 284(5):R1340–R1353.

Boland, L. M. and Jackson, K. A. (1999). Protein kinase C inhibits Kv1.1 potassium channel function. *Am J Physiol*, 277(1 Pt 1):C100–C110.

Brown, A. (2001). *Nerve cells and nervous system - an introduction to neuroscience, 2nd edition*. Springer London Berlin Heidelberg, 2nd edition.

Butera, R. J., Rinzel, J., and Smith, J. C. (1999). Models of respiratory rhythm generation in the pre-Btzinger complex. I. Bursting pacemaker neurons. *J Neurophysiol*, 82(1):382–397.

Carlo, B. D., Pellegrini, M., and Pellegrino, M. (2003). Modulation of Ca2+-activated K+ channels of human erythrocytes by endogenous protein kinase C. *Biochim Biophys Acta*, 1612(1):107–116.

Coetzee, W. A., Amarillo, Y., Chiu, J., Chow, A., Lau, D., McCormack, T., Moreno, H., Nadal, M. S., Ozaita, A., Pountney, D., Saganich, M., de Miera, E. V.-S., and Rudy, B. (1999). Molecular diversity of K+ channels. *Ann N Y Acad Sci*, 868:233–285.

Cooper, G. M. (2000). *The Cell - A Molecular Approach*. Sinauer Associates, Inc, Sunderland (MA), 2 edition.

Fernandez, S. F., Huang, M.-H., Davidson, B. A., Knight, P. R., and Izzo, J. L. (2003). Modulation of angiotensin II responses in sympathetic neurons by cytosolic calcium. *Hypertension*, 41(1):56–63.

Gelband, C. H., Warth, J. D., Mason, H. S., Zhu, M., Moore, J. M., Kenyon, J. L., Horowitz, B., and Sumners, C. (1999). Angiotensin II type 1 receptor-mediated inhibition of K+ channel subunit kv2.2 in brain stem and hypothalamic neurons. *Circ Res*, 84(3):352–359.

Gubitosi-Klug, R. A., Mancuso, D. J., and Gross, R. W. (2005). The human Kv1.1 channel is palmitoylated, modulating voltage sensing: Identification of a palmitoylation consensus sequence. *Proc Natl Acad Sci U S A*, 102(17):5964–5968.

Guenther, E., Hewig, B., Zrenner, E., and Kohler, K. (1997). Angiotensin

II-induced inhibition and facilitation of calcium current subtypes in rat retinal ganglion cells. *Neurosci Lett*, 231(2):71–74.

Guenther, E., Schmid, S., Hewig, B., and Kohler, K. (1996). Two-fold effect of Angiotensin II on voltage-dependent calcium currents in rat retinal ganglion cells. *Brain Res*, 718(1-2):112–116.

Hagiwara, K., Nunoki, K., Ishii, K., Abe, T., and Yanagisawa, T. (2003). Differential inhibition of transient outward currents of Kv1.4 and Kv4.3 by endothelin. *Biochem Biophys Res Commun*, 310(2):634–640.

Henke, G., Maier, G., Wallisch, S., Boehmer, C., and Lang, F. (2004). Regulation of the voltage gated K+ channel Kv1.3 by the ubiquitin ligase Nedd4-2 and the serum and glucocorticoid inducible kinase SGK1. *J Cell Physiol*, 199(2):194–199.

HODGKIN, A. L. and HUXLEY, A. F. (1952). A quantitative description of membrane current and its application to conduction and excitation in nerve. *J Physiol*, 117(4):500–544.

Huang, X. C., Deng, T., and Sumners, C. (1998). Angiotensin II stimulates activation of Fos-regulating kinase and c-Jun NH2-terminal kinase in neuronal cultures from rat brain. *Endocrinology*, 139(1):245–251.

Huguenard, J. R. and McCormick, D. A. (1992). Simulation of the currents involved in rhythmic oscillations in thalamic relay neurons. *J Neurophysiol*, 68(4):1373–1383.

Huguenard, J. R. and Prince, D. A. (1991). Slow inactivation of a TEA-sensitive K current in acutely isolated rat thalamic relay neurons. *J Neurophysiol*, 66(4):1316–1328.

Hwang, P. M., Glatt, C. E., Bredt, D. S., Yellen, G., and Snyder, S. H. (1992). A novel K+ channel with unique localizations in mammalian brain: molecular cloning and characterization. *Neuron*, 8(3):473–481.

Iwamoto, T., Pan, Y., Wakabayashi, S., Imagawa, T., Yamanaka, H. I., and Shigekawa, M. (1996). Phosphorylation-dependent regulation of cardiac Na+/Ca2+ exchanger via protein kinase C. *J Biol Chem*, 271(23):13609–13615.

Iwamoto, T., Wakabayashi, S., and Shigekawa, M. (1995). Growth factor-induced phosphorylation and activation of aortic smooth muscle Na+/Ca2+ exchanger. *J Biol Chem*, 270(15):8996–9001.

Jerng, H. H., Pfaffinger, P. J., and Covarrubias, M. (2004). Molecular physiology and modulation of somatodendritic A-type potassium channels. *Mol Cell Neurosci*, 27(4):343–369.

Jiang, Y., Lee, A., Chen, J., Ruta, V., Cadene, M., Chait, B. T., and MacKinnon, R. (2003a). X-ray structure of a voltage-dependent K+ channel. *Nature*, 423(6935):33–41.

Jiang, Y., Ruta, V., Chen, J., Lee, A., and MacKinnon, R. (2003b). The principle of gating charge movement in a voltage-dependent K+ channel. *Nature*, 423(6935):42–48.

Kitano, H. (2002). Computational systems biology. *Nature*, 420:206 210.

Kubo, T. (2005). Protein kinase c activation-induced increases of neuronal activity are enhanced in the hypothalamus of spontaneously hypertensive rats. *Brain Research*, 1033:157–163.

Li, Y. W. and Guyenet, P. G. (1996). Angiotensin II decreases a resting K+ conductance in rat bulbospinal neurons of the C1 area. *Circ Res*, 78(2):274–282.

Lledo, P. M., Hjelmstad, G. O., Mukherji, S., Soderling, T. R., Malenka, R. C., and Nicoll, R. A. (1995). Calcium/calmodulin-dependent kinase II and long-term potentiation enhance synaptic transmission by the same mechanism. *Proc Natl Acad Sci U S A*, 92(24):11175–11179.

Lodish, H., Berk, A., Zipursky, S. L., Matsudaira, P., Baltimore, D., and Darnell, J. E. (2000). *Molecular Cell Biology*. W. H. Freeman & Co, New York, 4 edition.

Lu, D., Yang, H., Lenox, R. H., and Raizada, M. K. (1998). Regulation of angiotensin II-induced neuromodulation by MARCKS in brain neurons. *J Cell Biol*, 142(1):217–227.

Marrero, M. B., Paxton, W. G., Schieffer, B., Ling, B. N., and Bernstein, K. E. (1996). Angiotensin II signalling events mediated by tyrosine phosphorylation. *Cell Signal*, 8(1):21–26.

McCormick, D. A. and Huguenard, J. R. (1992). A model of the electrophysiological properties of thalamocortical relay neurons. *J Neurophysiol*, 68(4):1384–1400.

Mishra, J. and Bhalla, U. S. (2002). Simulations of inositol phosphate metabolism and its interaction with InsP(3)-mediated calcium release. *Biophys J*, 83(3):1298–1316.

Misonou, H., Mohapatra, D. P., Park, E. W., Leung, V., Zhen, D., Misonou, K., Anderson, A. E., and Trimmer, J. S. (2004). Regulation of ion chan-

nel localization and phosphorylation by neuronal activity. *Nat Neurosci*, 7(7):711–718.

Misonou, H., Mohapatra, D. P., and Trimmer, J. S. (2005). Kv2.1: a voltage-gated k+ channel critical to dynamic control of neuronal excitability. *Neurotoxicology*, 26(5):743–752.

Mohapatra, D. P. and Trimmer, J. S. (2006). The Kv2.1 C terminus can autonomously transfer Kv2.1-like phosphorylation-dependent localization, voltage-dependent gating, and muscarinic modulation to diverse Kv channels. *J Neurosci*, 26(2):685–695.

Monck, J. R., Williamson, R. E., Rogulja, I., Fluharty, S. J., and Williamson, J. R. (1990). Angiotensin II effects on the cytosolic free Ca2+ concentration in N1E-115 neuroblastoma cells: kinetic properties of the Ca2+ transient measured in single fura-2-loaded cells. *J Neurochem*, 54(1):278–287.

Murakoshi, H., Shi, G., Scannevin, R. H., and Trimmer, J. S. (1997). Phosphorylation of the Kv2.1 K+ channel alters voltage-dependent activation. *Mol Pharmacol*, 52(5):821–828.

Murakoshi, H. and Trimmer, J. S. (1999). Identification of the Kv2.1 K+ channel as a major component of the delayed rectifier K+ current in rat hippocampal neurons. *J Neurosci*, 19(5):1728–1735.

Naoki, H., Sakumura, Y., and Ishii, S. (2005). Local signaling with molecular diffusion as a decoder of Ca2+ signals in synaptic plasticity. *Mol Syst Biol*, 1:2005.0027.

Nitabach, M. N., Llamas, D. A., Thompson, I. J., Collins, K. A., and Holmes, T. C. (2002). Phosphorylation-dependent and phosphorylation-

independent modes of modulation of shaker family voltage-gated potassium channels by SRC family protein tyrosine kinases. *J Neurosci*, 22(18):7913–7922.

Pan, S., Sumners, C., and Gelband, C. (2000). Kv1.4 underlies angiotensin ii-mediated inhibition of neuronal a-type k+ current. *Biophys J*, 78(1):450A–450A.

Pan, S. J., Zhu, M., Raizada, M. K., Sumners, C., and Gelband, C. H. (2001). ANG II-mediated inhibition of neuronal delayed rectifier K+ current: role of protein kinase C-alpha. *Am J Physiol Cell Physiol*, 281(1):C17–C23.

Pedarzani, P. and Storm, J. F. (1996). Evidence that Ca/calmodulin-dependent protein kinase mediates the modulation of the Ca2+-dependent K+ current, IAHP, by acetylcholine, but not by glutamate, in hippocampal neurons. *Pflugers Arch*, 431(5):723–728.

Peretz, T., Levin, G., Moran, O., Thornhill, W. B., Chikvashvili, D., and Lotan, I. (1996). Modulation by protein kinase C activation of rat brain delayed-rectifier K+ channel expressed in Xenopus oocytes. *FEBS Lett*, 381(1-2):71–76.

Philipson, K. D., Nicoll, D. A., Ottolia, M., Quednau, B. D., Reuter, H., John, S., and Qiu, Z. (2002). The na+/ca2+ exchange molecule. In of the New York Academy of Sciences, A., editor, *Annals of the New York Academy of Sciences 976: Cellular And Molecular Physiology of Sodium-Calcium Exchange: Proceedings of the Fourth International Conference*, volume 976, pages 1–10.

Purves, D., Augustine, G., Fitzpatrick, D., Katz, L., and LaMantia, A.-S. (2001). *Neuroscience*. Sinauer Associates, Inc, Sunderland (MA).

Richards, E. M., Raizada, M. K., Gelband, C. H., and Sumners, C. (1999). Angiotensin II type 1 receptor-modulated signaling pathways in neurons. *Mol Neurobiol*, 19(1):25–41.

Rogers, R. F., Rybak, I. A., and Schwaber, J. S. (2000). Computational modeling of the baroreflex arc: nucleus tractus solitarius. *Brain Res Bull*, 51(2):139–150.

Rybak, I. A., Paton, J. F., and Schwaber, J. S. (1997). Modeling neural mechanisms for genesis of respiratory rhythm and pattern. I. Models of respiratory neurons. *J Neurophysiol*, 77(4):1994–2006.

Sauter, T. and Bullinger, E. (2004). Detailed mathematical modeling of metabolic and regulatory networks. *BIOforum Europe*, 2:62–64.

Sauter, T. and Vadigepalli, R. (2005). Computational modeling of the angiotensin ii / at1 receptor mediated ca dynamics in neurons. *internal report*, x:1–18.

Schild, J. H., Clark, J. W., Canavier, C. C., Kunze, D. L., and Andresen, M. C. (1995). Afferent synaptic drive of rat medial nucleus tractus solitarius neurons: dynamic simulation of graded vesicular mobilization, release, and non-NMDA receptor kinetics. *J Neurophysiol*, 74(4):1529–1548.

Schild, J. H., Khushalani, S., Clark, J. W., Andresen, M. C., Kunze, D. L., and Yang, M. (1993). An ionic current model for neurons in the rat medial nucleus tractus solitarii receiving sensory afferent input. *J Physiol*, 469:341–363.

Schwaber, J. S., Graves, E. B., and Paton, J. F. (1993). Computational modeling of neuronal dynamics for systems analysis: application to neurons of the cardiorespiratory NTS in the rat. *Brain Res*, 604(1-2):126–141.

Seroussi, Y., Brosh, I., and Barkai, E. (2002). Learning-induced reduction in post-burst after-hyperpolarization (AHP) is mediated by activation of PKC. *Eur J Neurosci*, 16(5):965–969.

Sumners, C., Fleegal, M. A., and Zhu, M. (2002). Angiotensin AT1 receptor signalling pathways in neurons. *Clin Exp Pharmacol Physiol*, 29(5-6):483–490.

Sumners, C., Zhu, M., Gelband, C. H., and Posner, P. (1996). Angiotensin II type 1 receptor modulation of neuronal K+ and Ca2+ currents: intracellular mechanisms. *Am J Physiol*, 271(1 Pt 1):C154–C163.

Sun, C., Du, J., Raizada, M. K., and Sumners, C. (2003a). Modulation of delayed rectifier potassium current by angiotensin II in CATH.a cells. *Biochem Biophys Res Commun*, 310(3):710–714.

Sun, C., Du, J., Sumners, C., and Raizada, M. K. (2003b). PI3-kinase inhibitors abolish the enhanced chronotropic effects of angiotensin II in spontaneously hypertensive rat brain neurons. *J Neurophysiol*, 90(5):3155–3160.

Sun, C., Sumners, C., and Raizada, M. K. (2002). Chronotropic action of angiotensin II in neurons via protein kinase C and CaMKII. *Hypertension*, 39(2 Pt 2):562–566.

Sundaram, K., Johnson, S. M., and Felder, R. B. (1997). Altered expression of delayed excitation in medial NTS neurons of spontaneously hypertensive rats. *Neurosci Lett*, 225(3):205–209.

Toselli, M. and Taglietti, V. (2005). L-type calcium channel gating is modulated by bradykinin with a PKC-dependent mechanism in NG108-15 cells. *Eur Biophys J*, 34(3):217–229.

Vadigepalli, R., Doyle, F. J., and Schwaber, J. S. (2001). Analysis and neuronal modeling of the nonlinear characteristics of a local cardiac reflex in the rat. *Neural Comput*, 13(10):2239–2271.

Wang, D., Gelband, C. H., Sumners, C., and Posner, P. (1997a). Mechanisms underlying the chronotropic effect of angiotensin II on cultured neurons from rat hypothalamus and brain stem. *J Neurophysiol*, 78(2):1013–1020.

Wang, D., Sumners, C., Posner, P., and Gelband, C. H. (1997b). A-type K+ current in neurons cultured from neonatal rat hypothalamus and brain stem: modulation by angiotensin II. *J Neurophysiol*, 78(2):1021–1029.

Welsby, P. J., Wang, H., Wolfe, J. T., Colbran, R. J., Johnson, M. L., and Barrett, P. Q. (2003). A mechanism for the direct regulation of T-type calcium channels by Ca2+/calmodulin-dependent kinase II. *J Neurosci*, 23(31):10116–10121.

Wolfe, J. T., Wang, H., Perez-Reyes, E., and Barrett, P. Q. (2002). Stimulation of recombinant Ca(v)3.2, T-type, Ca(2+) channel currents by CaMKI-Igamma(C). *J Physiol*, 538(Pt 2):343–355.

Wu, J. (2001). *Introduction to Neural Dynamics and Signal Transmission Delay by - - 2001 - 182 pages The purpose of this book is to give an introduction to the mathematical modeling.* Walter de Gruyter Berlin New York, Berlin New York.

Zhu, M., Gelband, C. H., Posner, P., and Sumners, C. (1999). Angiotensin II decreases neuronal delayed rectifier potassium current: role of calcium/calmodulin-dependent protein kinase II. *J Neurophysiol*, 82(3):1560–1568.

Zhu, M., Neubig, R. R., Wade, S. M., Posner, P., Gelband, C. H., and Sumners, C. (1997). Modulation of K+ and Ca2+ currents in cultured neurons by an angiotensin II type 1a receptor peptide. *Am J Physiol*, 273(3 Pt 1):C1040–C1048.

Appendix A

Review: Modulation of ion channels

A.1 Modulation of delayed rectifier potassium currents

Kv2.1 is widely expressed in brain and composes the majority of delayed rectifier K+ current in pyramidal neurons in cortex and hippocampus [Murakoshi and Trimmer 1999], and is also widely expressed in interneurons. Dynamic modulation of Kv2.1 localization and function by a mechanism involving activity-dependent Kv2.1 dephosphorylation dramatically impacts intrinsic excitability of neurons [Misonou et al. 2005].

Whole-cell patch-clamp studies of Murakoshi et al. [1997] provided direct evidence that the voltage-dependent activation of the delayed-rectifier K+ channel Kv2.1 can be modulated by direct phosphorylation of the channel protein, shifting the activation to more negative membrane potentials without differences in macroscopic kinetics.

Immunocytochemical, biochemical, and biophysical analyses of chimeric Kv channels show that the Kv2.1 cytoplasmic C-terminal domain can act as an autonomous domain sufficient to transfer Kv2.1-like clustering, voltage-dependent activation, and cholinergic modulation to diverse Kv channels Mohapatra and Trimmer [2006].

Kv1.1 current is inhibited by PKC activation without effecting channel activation-inactivation kinetics, conductance-voltage relationship or the number of Kv1.1 molecules on the membrane and involves its N-terminus, however not via direct phosphorylation. Activation of PKC by PMA or OAG resulted in 90% [Boland and Jackson 1999] and 50%-90% [Peretz et al. 1996] inhibition, whilst membrane protein was remains unchanged. None of the ten classical PKC phosphorylation sites on the channel molecule could account, by itself or in combination with others, for the inhibition.

A.2 Modulation of fast activating potassium current

Hagiwara et al. [2003] used the Oocytes expression system showing that stimulation of the endothelin receptor ET(A) decreases the transient outward current of Kv1.4 by about 85% after 10(-8)M ET-1, while that of Kv4.3 was decreased by about 60%. By mutagenesis experiments he identified two phosphorylation sites of PKC and CaMKII in Kv1.4 responsible for the decrease in I(Kv1.4) by ET-1.

Nitabach et al. [2002] found that Src binding and tyrosine phosphorylation are each able to modulate Kv1 family macroscopic channel currents independently. SH3-dependent binding of Src leads to the suppression of both Kv1.5 and Kv1.4 (modified to contain proline-rich SH3 domain bind-

ing sites) macroscopic currents even in the absence of Src-catalyzed tyrosine phosphorylation, whereas binding-independent tyrosine phosphorylation by Src leads to the suppression of Kv1.5 macroscopic currents and the modulation of Kv1.4 inactivation kinetics.

A.3 Regulation of Ca^{2+} activated potassium channels

Carlo et al. [2003] showed that activation of PKC inhibits single IK(Ca) channel activity of human erythrocytes, which is mainly due to changes the opening frequency without significantly affecting mean channel open time and conductance.

Muscarinic (carbachol) and metabotropic (t-ACPD) glutamate receptor agonists increase the excitability of hippocampal and other cortical neurons by suppressing IAHP. CaMKII, but not PKA, is involved in mediating the muscarinic suppression of IAHP [Pedarzani and Storm 1996] , although other pathways may also contribute.

Alberi et al. [2000] showed the involvement of CaMKII in carbachol-induced (muscarine receptor) suppression of the slow I(AHP) and the induction of plateau potentials in CA1 neurons of the rat hippocampus in vitro, suggesting the activation of I(AHP) by CaMKII.

A.4 Modulation of Ca channels

Wolfe et al. [2002] showed the regulation of Ca(v)3.2 alpha(1)-subunits (alpha1H) by CaMKII, whereby CaM (2 microM) increases T-type channel activity selectively at negative potentials, evoking an 11 mV hyperpolariz-

ing shift in the half-maximal potential (V(1/2)) for activation. The V(1/2) of channel inactivation is not altered by Ca(2+)/CaM. CaMKII-dependent potentiation of channel opening resulted in significant increases in apparent steady-state open probability and sustained channel current at negative voltages. Under identical conditions, CaMKII activation did not regulate the activity of Ca(v)3.1 channels.

Welsby et al. [2003] defined a molecular mechanism underlying the dynamic regulation of alpha1H channels (Cav3.2) responsible for a T-type Ca current by CaMKII. He showed that channel regulation is selective for the LVA alpha1H Ca2+ channel subtype, depends on determinants in the alpha1H II-III intracellular loop, and requires the phosphorylation of a serine residue absent from unregulated α1G (Cav3.1) channels.

Guenther et al. [1997] showed a bimodal effect of AngII on L-type Ca channels. Whole cell patch-clamp recordings were performed on freshly dissociated rat retinal ganglion cells to determine the action of Angiotensin II (AngII) on voltage-activated calcium current subtypes in this cell type. AngII had no effect on a toxin-resistant calcium current component; N-type currents were reduced by 27 +/- 5% in all retinal ganglion cells (RGCs) tested; L-type currents were reduced by 33 +/- 7% in 59% of the RGCs but increased by 31 +/- 6% in 41% of the cells. AngII effects were reversible within a few seconds through reperfusion with bath solution and calcium current kinetics and current-voltage relations remained unaffected. The net effect of AngII in a single RGC is either a reduction or an enhancement of the total calcium current, dependent on (1) the number of L-type channels compared to N-type channels and (2) on the kind of action AngII exerts on L-type channels.

Toselli and Taglietti [2005] showed that L-type voltage-gated Ca(2+)

channels in NG108-15 are inhibited by Bradykinin[1] (BK), involving activation of PKC and resulting in a significant reduction of the probability of channel opening.

A.5 Neurological significance

A.5.1 PKC and K_{ahp} involvement in learning

Seroussi et al. [2002] studied the role of PKC in mediating learning-related long lasting reduction of the post-burst after-hyperpolarization (AHP) in cortical pyramidal neurons. that pyramidal neurons in the rat piriform (olfactory) cortex from trained rats have reduced post-burst AHP for three days after odour-discrimination learning, and that this reduction is due to decreased conductance of calcium-dependent potassium current K_{ahp} .

A.5.2 CaMKII involvement in long-term potentiation

Lledo et al. [1995] proposed that CaMKII alone is sufficient to augment synaptic strength and that this enhancement shares the same underlying mechanism as the enhancement observed with long-term potentiation[2] (LTP). Application of active CaMKII directly injected into CA1 hippocampal pyramidal cells mimicked several features of LTP in that it caused a decreased incidence of synaptic failures, an increase in the size of spontaneous excitatory postsynaptic currents (EPSCs), and an increase in the amplitude of responses to iontophoretically applied alpha-amino-3-hydroxy-5-methyl-

[1]Bradykinin has effects on neuronal firing activity opposite to these of AngII.

[2]Long-term potentiation is the continues increase of neuronal firing due to lasting excitation. This means that with stimulation of a neuron by synaptic input increases its sensitivity for this input slowly with time.

4-isoxazolepropionate. The enhancing action of CaMKII was greatly diminished by prior induction of LTP. In addition, following the increase in synaptic strength by CaMKII, tetanic stimulation failed to evoke LTP.

A.5.3 K_{dr} involvement in excitability

Misonou et al. [2004] finding that neuronal activity modifies the phosphorylation state, localization and function of Kv2.1 suggests an important link between excitatory neurotransmission and the intrinsic excitability of pyramidal neurons. In cultured rat hippocampal pyramidal neurons, glutamate stimulation rapidly causes dephosphorylation of Kv2.1, translocation of Kv2.1 from clusters to a more uniform localization, and a shift in the voltage-dependent activation of the potassium current. An influx of Ca^{2+} leading to calcineurin activation is both necessary and sufficient for these effects.

Appendix B

Electrophysiological model

B.1 K_{dr} channel kinetics

Hodgkin-Huxley like neuron models as described in Rybak et al. [1997] and Schwaber et al. [1993], and mainly based on the channel data of Huguenard and McCormick [1992] and McCormick and Huguenard [1992] for thalamic relay neurons, were used to simulate the firing behavior, and to determine the significances of the ion channels, especially of the delayed rectifier potassium channel.

The change of excitability depends highly on the activation of the channel at resting potential and in between spike formation, i.e. voltages about -50 mV. The ionic currents in between the spikes present the driving force for the formation of the following spike, and thus determine the firing rate. They are relatively small ($I_K < 0.5$ nA)compared with the maximal potassium or sodium currents at constant voltages ($I_K > 100$ nA) or during spike formation ($I_K \approx 10$ nA). Consequently currents that significantly influence the excitability or firing frequency must be activated at these negative voltages resulting in currents about $10^{-}1$ nA, which equals an K_{Kv} activation of

around 0.1%.

B.1.1 HH-like: Comparison of channel parameters influence

The original Rybak NTS model possesses a HH-like K_{dr} channel model. The influence of the activation (α) and deactivation (β) rates on the activation variable m, the time variable τ and the current is shown in Figure B.1

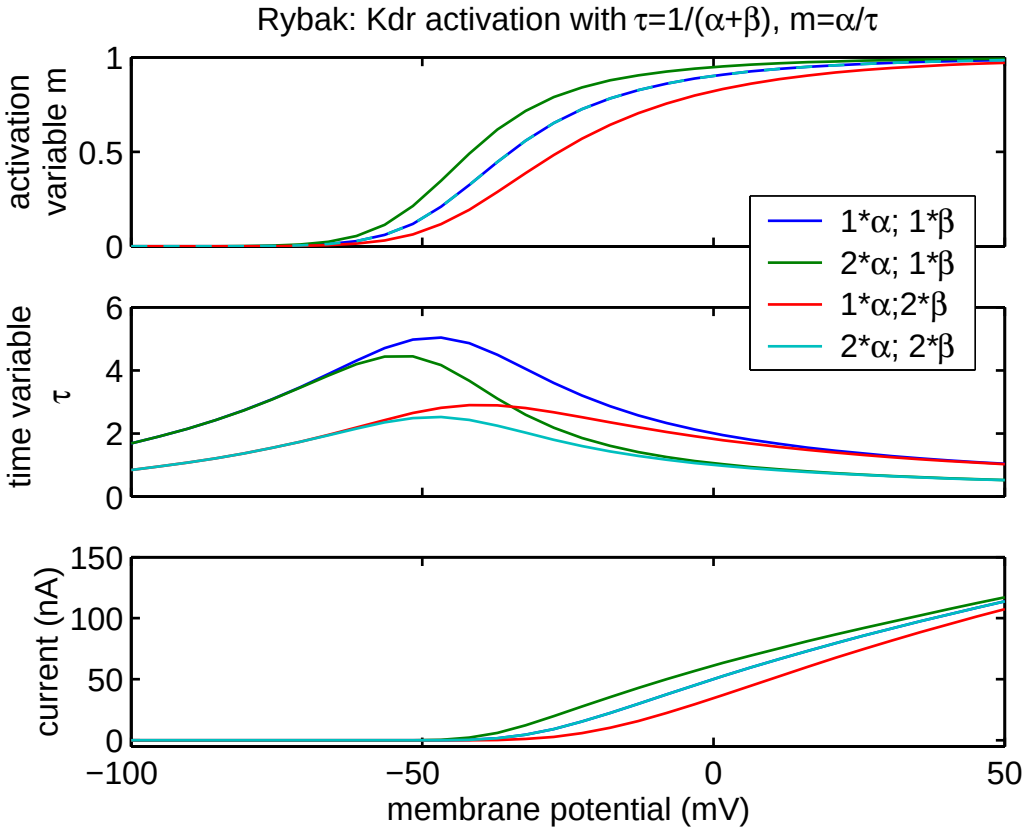

Figure B.1: Influence of α and β on the HH-like channel kinetics. The plot shows the K_{dr} model of Rybak with increased (2-fold) activation (α) and deactivation (β) rates.

B.1.2 Literature: Rybak & Huguenard

Different activation curves (empirical data) of the delayed potassium channel did not alter the shape of the action potential peaks significantly, but changed excitability and thus firing frequency. Following K_{dr} -channel kinetics have been tested: (see also figure B.2)

1. Rybak: Hodkin-Huxley like channel $m_\infty = \frac{\alpha(V)}{\tau(V)}, \quad \tau = \frac{1}{\alpha(V)+\beta(V)}$
2. Huguenard: 4. order Bolzmann function $m_\infty = (\frac{1}{1+e^{(V_{12}-V)/k}})^4$
3. Sumners: 1. order Bolzmann function $m_\infty = \frac{1}{1+e^{(V_{12}-V)/k}}$

	half activation	slope factor	time constant
1. [Rybak et al. 1997]	-11mV	NA	1 to 4 ms
2. [Huguenard and Prince 1991]	2.3mV	-17	15 to 80 ms
3. [Gelband et al. 1999]	2.3mV	-10.2	NA

B.2 Equations

Membrane potential:

$$\frac{dV}{dt} = (I_{Na} + I_{Kdr} + I_{Ka} + I_{Kahp} + I_{CaL} + I_{leak} + I_{SynE})/Cm$$

Fast sodium channel (Na):

$$I_{Na} = \bar{g}_{Na} m_{Na} h_{Na} (E_{Na} - V)$$

$$\begin{array}{rclrcl} \alpha_{m,Na} & = & \frac{0.091(V+38)}{1-exp(-(V+38)/5)} & \alpha_{h,Na} & = & 0.016exp(-(V+55)/15) \\ \beta_{m,Na} & = & \frac{0.062(V+38)}{1-exp((V+38)/5)} & \beta_{h,Na} & = & \frac{2.07}{1-exp(-(V-17)/21)} \\ \tau_{m,Na} & = & 1/(\alpha_{m,Na} + \beta_{m,Na}) & \tau_{h,Na} & = & 1/(\alpha_{h,Na} + \beta_{h,Na}) \\ m_{\infty,Na} & = & \alpha_{m,Na}/(\alpha_{m,Na} + \beta_{m,Na}) & h_{\infty,Na} & = & \alpha_{h,Na}/(\alpha_{h,Na} + \beta_{h,Na}) \end{array}$$

Delayed rectifier potassium channel (K_{dr})

$$I_{K,dr} = \bar{g}_{K,dr} m_{K,dr}^n (E_K - V)$$

1. Rybak: Hodkin-Huxley like channel, $n = 4$

$$\begin{array}{rclrcl} \alpha_{K,dr} & = & \frac{0.01(V+45)}{1-exp(-(V+45)/5)} & \beta_{K,dr} & = & 0.17exp(-(V+50)/40) \\ \tau_{K,dr} & = & 1/(\alpha_{K,dr}+\beta_{K,dr}) & m_{\infty,K,dr} & = & \alpha_{K,dr}/(\alpha_{K,dr}+\beta_{K,dr}) \end{array}$$

2. Huguenard: 4. order Bolzmann function, $n = 4$

$$\begin{array}{rcl} \tau_{K,dr} & = & 1/(exp((V-81)/25.6)+exp((V+132)/-18))+9.9 \\ m_{\infty,K,dr} & = & (1+exp((V_{12}-V)/k))^{-4} \end{array}$$

3. Sumners: 1. order Bolzmann function, $n = 1$

   τ not determined, $m_{\infty,K,dr} = (1+exp((V_{12}-V)/k))^{-1}$

4. Integrated model, $n = 4$, $V_{12} = 2.3$, $k = 17$

$$\begin{array}{rcl} \tau_{K,dr} & = & 1/(exp((V-81)/25.6)+exp((V+132)/-18))+9.9 \\ m_{\infty,K,dr} & = & (1+\underbrace{(2^{1/n}-1)}_{I\sim m^n}exp((V_{12}-V)/k))^{-1} \end{array}$$

Fast activating potassium channels (K_a)

$$I_{K,a} = \bar{g}_{K,a}m_{K,a}^4 h_{K,a}(E_K - V)$$

$$\begin{array}{rcl} m_{\infty,K,a} & = & 1/(1+exp(-(V-V_{1/2})/8.5)), \quad h_{\infty,K,a} = 1/(1+exp((V+78)/6)) \\ \tau_{m,K,a} & = & 1/(exp((V+35.82)/19.69)+exp(-(V+79.69)/12.7)+0.37) \\ \tau_{h,K,a} & = & 1/(exp((V+46.05)/5)+exp(-(V+238.4)/37.45)+0.37) \end{array}$$

1. Rybak: $I_{K,a} = g_{K,a}(0.6m_{K,a,1}^4 h_{K,a,1} + m_{K,a,2}^4 h_{K,a,2})(E_K - V)$

$$\tau_{h,K,a,1} = \begin{cases} 19 & if\ V \geq -63 \\ \tau_{h,Ka} & else \end{cases}, \quad V_{1/2,Ka1} = -60$$

$$\tau_{h,K,a,2} = \begin{cases} 60 & if\ V \geq -73 \\ \tau_{h,Ka} & else \end{cases}, \quad V_{1/2,Ka2} = -36$$

2. Integrated model: $I_{K,a} = g_{K,a}m_{K,a}^4 h_{K,a}(E_K - V)$

$$\tau_{h,K,a} = \begin{cases} 60 & if\ V \geq -73 \\ \tau_{h,Ka} & else \end{cases}, V_{1/2,Ka} = -36$$

After hyperpolarization related calcium dependent potassium channel (K_{ahp})

$$I_{K,ahp} = \bar{g}_{K,ahp}m_{K,ahp}^2(E_K - V)$$

$\alpha_{K,ahp} = 1.25 \cdot 10^{-8}[Ca^{2+}]^2, \quad \tau_{K,ahp} = \frac{1000}{\alpha_{K,ahp}+2.5}, \quad m_{\infty,K,ahp} = \frac{\alpha_{K,ahp}}{\alpha_{K,ahp}+2.5}$

High threshold calcium channel (Ca_L)

$$I_{Ca,L} = g_{Ca,L} m_{Ca,L}^2 (E_{Ca}([Ca^{2+}]) - V)$$

$$\begin{array}{rclrcl} \alpha_{Ca,L} & = & \frac{1.6}{exp(-0.072(V-5))} & \beta_{Ca,L} & = & \frac{0.02(V-1.31)}{exp((V-1.31)/5.36)-1} \\ \tau_{Ca,L} & = & 1/(\alpha_{Ca,L} + \beta_{Ca,L}) & m_{\infty,Ca,L} & = & \alpha_{Ca,L}/(\alpha_{Ca,L} + \beta_{Ca,L}) \end{array}$$

Leak channel

$$I_{leak} = g_{leak}(E_{leak} - V)$$

Calcium regulation in the cluster ($[Ca^{2+}]_{cl}$)

$$\frac{d[Ca^{2+}]_{cl}}{dt} = \frac{I_{Ca,L}}{2Fv_{cl}}\left(1 - \frac{0.03}{[Ca^{2+}]_{cl} + 0.031}\right) + \frac{[Ca^{2+}]_{0,cl} - [Ca^{2+}]_{cl}}{17.7 exp(V/35)}$$

B.3 Analysis of the original Rybak model

Different ion channels were reduced and activated as indicated in the literature [Sumners et al. 1996, 2002] to determine the influence on the firing frequency. The results are presented in Figure B.3

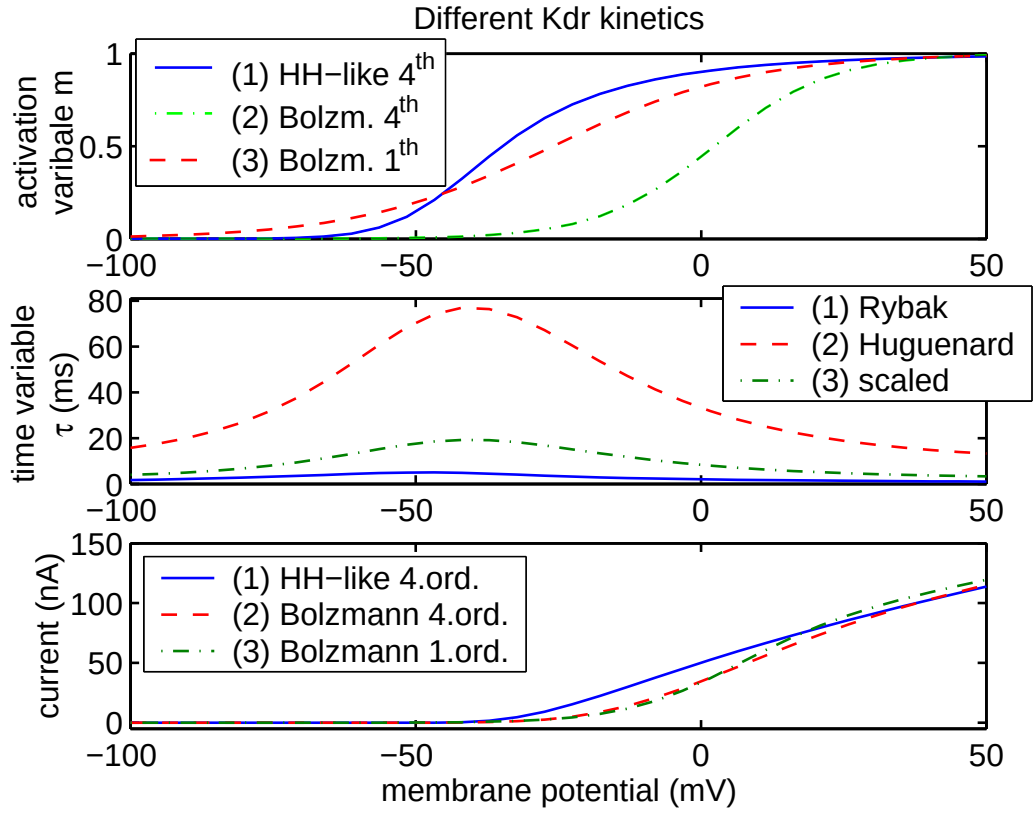

Figure B.2: Comparison of different K_{dr} channel kinetics taken from the literature. Top & bottom: Activation variables & steady-state currents (1) The Rybak K_{dr} model, (2) A forth order Bolzmann function as used in Huguenard and Prince [1991], (3) A first order Bolzmann function as used in Gelband et al. [1999]. Middle: Time variables (1) Rybak K_{dr} model, (2) Huguenard and Prince [1991], (3) Huguenard and Prince [1991] scaled to a maximum of 20ms.

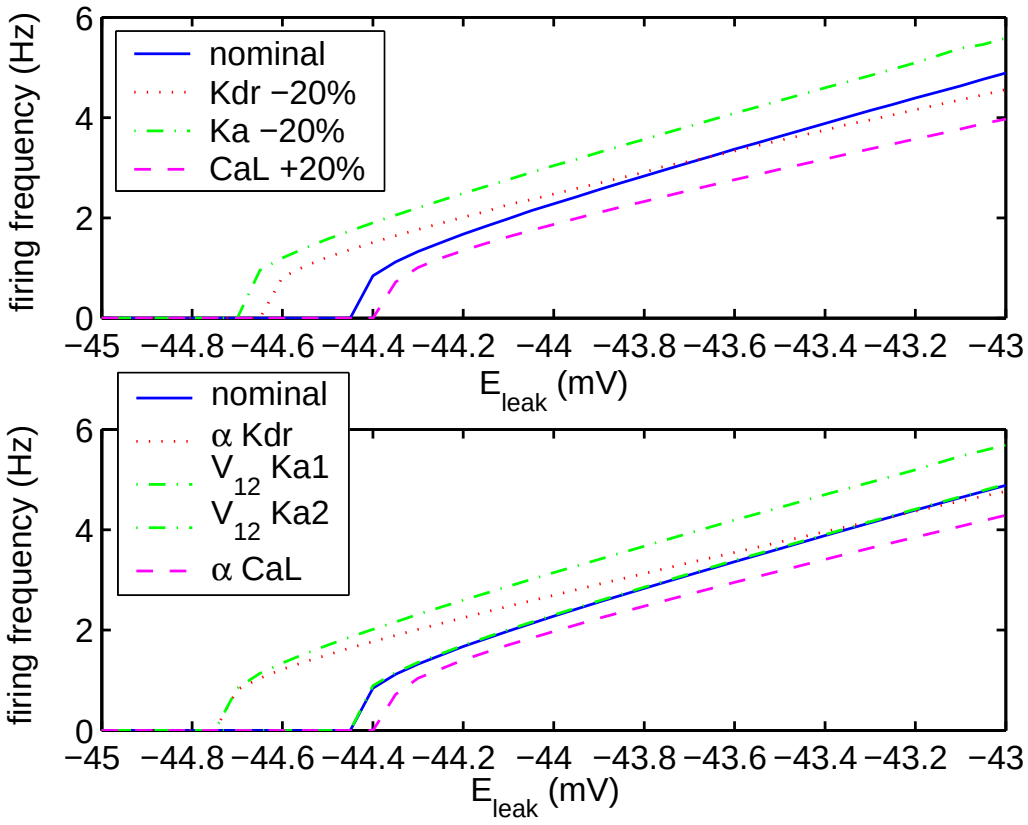

Figure B.3: Sensitivity analysis of the original Rybak model showing the firing frequency as function of E_{leak} for altered channel parameters. Top: altered maximal conductance, Bottom: altered half activation (for parameterized channel models) or activation variable (for HH-like channel models).

Appendix C

Phosphorylation kinetics

In addition to the model of direct phosphorylation as presented in the main text (see Chapter 5) the kinase binding to the channel and the phosphorylation afterwards have been modeled in two steps, similar to Michaelis Menten enzyme kinetics. For the integrated model the simpler model of direct phosphorylation was used, because it was sufficient to explain the experimental data, thereby using less parameters. However, for completeness and a detailed understanding of the process, the phosphorylation model using an intermediate complex is presented briefly.

C.1 Phosphorylation through intermediate complex

To phosphorylate the ion channel, The PKC attaches to it building a Kv-PKC complex. After the separation the ion channel phosphorylated and therewith inactive.

Reaction scheme

$$\begin{array}{ccccc} Kv^* + PKC & \overset{kp1}{\rightleftharpoons} & Kv^*\text{-}PKC & \overset{k_{p2}}{\rightarrow} & Kv + PKC \\ Kv & \overset{k_{phosphatase}}{\longrightarrow} & Kv^* & & \end{array}$$

Reaction rates

$$\begin{aligned} r_1 &= k_{p1} \cdot Kv^* \cdot PKC - k_{-p1} \cdot Kv^*\text{-}PKC \\ r_2 &= k_{p2} \cdot Kv^*\text{-}PKC \\ r_3 &= k_{phosphatase} \cdot Kv \end{aligned}$$

The total number of channels remains constant:

$$Kv^* = Kv_0 - Kv^*\text{-}PKC - Kv$$

Forming the intermediate complex happens very fast, r_1 quasi steady state:

$$\begin{aligned} 0 &= k_{p1} \cdot (Kv_0 - Kv^*\text{-}PKC - Kv) \cdot PKC - k_{-p1} \cdot Kv^*\text{-}PKC \\ \Longrightarrow \quad Kv^*\text{-}PKC &= \frac{k_{p1} \cdot PKC \cdot (Kv_0 - Kv)}{k_{p1} \cdot PKC - k_{-p1}} \\ &= \frac{PKC \cdot (Kv_0 - Kv)}{PKC - K_M} \quad \text{with } K_M = \frac{k_{-p1}}{k_{p1}} \end{aligned}$$

Differential equation for the phosphorylated channel

$$\begin{aligned} \frac{d}{dt} Kv &= k_{p2} \cdot Kv^*\text{-}PKC - k_{phophatase} \cdot Kv \\ &= k_{p2} \cdot (Kv_0 - Kv) \cdot \frac{PKC}{PKC + K_M} - k_{phosphatase} \cdot Kv \end{aligned}$$

unphosphorylated, active channel is $Kv_{active} = Kv_0 - Kv$, and with $h_p = \frac{KV_{active}}{KV_{total}}$ we get the inactivation by phosphorylation.

$$\frac{d}{dt} h_{phos} = k_{p2} \frac{PKC}{PKC + K_M} \cdot h_{phos} - k_{phosphatase} \cdot (1 - h_{phos})$$

Steady state:

$$\begin{aligned} h_{phos} &= \frac{k_{phostase}}{k_{p2} \frac{PKC}{PKC + K_M} + k_{phostase}} \\ &\overset{PKC \rightarrow \inf}{\mapsto} \frac{k_{phostase}}{k_{p2} + k_{phostase}} \end{aligned}$$

Higher order:

$$\begin{array}{lll} Kv^* + nPKC & \overset{kp1}{\rightleftharpoons} & Kv^*\text{-}PKC_n \overset{k_{p2}}{\rightarrow} Kv + PKC \\ Kv & \overset{k_{phosphatase}}{\longrightarrow} & Kv^* \end{array}$$

Differential equation:

$$\frac{d}{dt}h_{phos} = -k_{p2}\frac{PKC^n}{PKC^n + K_M^n} \cdot h_{phos} + k_{phosphatase} \cdot (1 - h_{phos})$$

Steady state:

$$\begin{array}{lll} h_{phos} & = & \dfrac{k_{phostase}}{k_{p2}\frac{PKC^n}{PKC^n + K_M^n} + k_{phostase}} \\ & \overset{PKC \to \inf}{\mapsto} & \dfrac{k_{phostase}}{k_{p2} + k_{phostase}} \end{array}$$

C.2 Kinase activity: Proof sum of species

Let us assume that two active form of a kinase A and B can phosphorylate the channel Kv^*. The reaction scheme is:

$$\begin{array}{lll} A + Kv^* & \rightharpoonup & A + Kv \\ B + Kv^* & \rightharpoonup & B + Kv \end{array}$$

Applying the law mass action, the reaction rate is calculated to

$$r_{phos} = k_A A Kv^* + k_B B Kv^*$$

With the assumption of equal activity for both active forms $k_A = k_B = k_p$, this can be simplified.

$$r_{phos} = k_p(A + B)Kv^*$$

Consequently, the corresponding reaction for this simplification can be written as

$$[A + B] + Kv^* \rightharpoonup [A + B] + Kv.$$

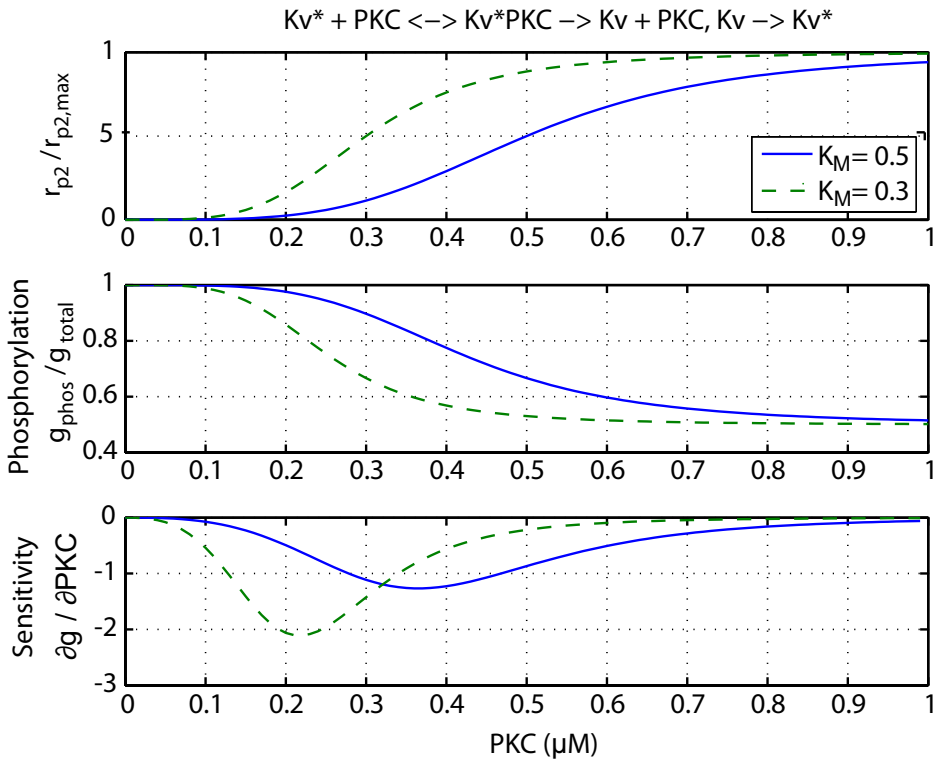

Figure C.1: Phosphorylation after PKC-channel assembly. The channel activity is minimal for PKC $\mapsto \infty$, but not zero. Decreasing K_M (half activation of $k_{p2}(PKC)$ [complex formation]) increases the sensitivity to PKC, and deactivates the channel for lower PKC levels.

Appendix D

Model integration

D.1 Cell size and cytosolic volume

The membrane surface in the Rybak HH-model is $\Omega = 0.0025mm^2$ which leads to a somata radius of $r = \sqrt{\frac{\Omega}{4\Pi}} = 1.41 \cdot 10^{-4}dm$ and a somata volume v_{cyt} of

$$v_{cyt} = \frac{4}{3}\Pi r^3 = 11.7 \cdot 10^{-12}l.$$

The Ca^{2+} concentration right underneath the membrane is modeled separately in the volume $v_{cluster}$.

$$v_{cluster} = d * \Omega = 0.25 \cdot 10^{-15}l$$

The Ca^{2+} concentration in this volume influences the Ca^{2+} dependent potassium channels K_{ahp} .

D.2 Notes: Channel concentrations

Single channel conductances:

CA1 pyrimidial neurons	channel	single conductance
	K_{dr}	19 + 0.6 pS
	K_M	11 + 0.8 pS
	K_D	18 + NA pS
	K_A	6 + 0.6 pS

For $g_{Kdr} = 1\mu S$ and $g_{Ka} = 0.15\mu S$ (40% K_D, 60% K_A) the number of channels are

$$\begin{aligned} n_{Kdr} &= \frac{g_{Kdr}}{g_{Kdr,single}} = 52,632 \\ n_{KD} &= \frac{0.4 \cdot g_{Ka}}{g_{KD,single}} = 3,333 \\ n_{KA} &= \frac{0.6 \cdot g_{Ka}}{g_{KA,single}} = 15,000 \end{aligned}$$

The conversion-factor from cytosolic to membrane concentrations is:

$$c_{mem} = \frac{v_{cyt}}{\Omega} c_{soma} \quad \text{with } \frac{v_{cyt}}{\Omega} = 4.7 \cdot 10{-}5$$

The membrane concentrations of the channels are $\frac{n_{channel}}{N_A \Omega}$: [1]

Membrane:	channel	concentration
	K_{dr}	$3.510^{-10} \mu mol/dm^2$
	K_D	$2.210^{-11} \mu mol/dm^2$
	K_A	$9.910^{-11} \mu mol/dm^2$

[1] $N_A = 6,0221415 \cdot 10^{23} mol^{-1}$